Summer 9-1-2024

Coastal flood risk in the context of climate change and urbanization in northeastern South Carolina

Hongyuan Zhang
Coastal Carolina University

Coastal flood risk in the context of climate change and urbanization in northeastern South Carolina

By

Hongyuan Zhang

Submitted in Partial Fulfillment of the

Requirements for the Degree of Doctor of Philosophy in

Marine Science: Coastal and Marine Systems Science in the

School of the Coastal Environment

Coastal Carolina University

2023

Dr. Shaowu Bao
Major Advisor

Dr. Len Pietrafesa
Committee Member

Dr. Xiaofeng Li
Committee Member

Dr. Varavut Limpasuvan
Committee Member

Dr. Paul Gayes
Committee Member

Dr. Erin Hackett
CMSS Graduate Programs Director

Dr. Chad Leverette
Dean, Gupta College of Science

Acknowledgments

First and foremost, I wish to express my deepest appreciation to my beloved parents for their unwavering encouragement and support in the pursuit of my dreams. Their love and belief in me have been the foundation upon which I have built my academic journey.

I would like to extend my sincere gratitude to my advisor, Professor Shaowu Bao, for his guidance, continuous support, and patience throughout the course of my doctoral studies. His expertise and insights have been instrumental in deepening my understanding of the intricacies of the climate system and the dynamics of the coastal and marine system processes.

I am also deeply grateful to Dr. Len Pietrafesa and Dr. Xiaofeng Li for their profound knowledge, astute guidance, and constructive input on my research over the past seven years. Their contributions have been integral to the success of my work. I would like to extend my heartfelt thanks to my dissertation committee members, Dr. Varavut Limpasuvan and Dr. Paul Gayes, for their valuable feedback and thoughtful comments on my research. Their expertise and critical evaluation have been essential in shaping the direction and quality of my work.

I would like to acknowledge the Coastal Carolina University cyberinfrastructure project for providing the resources necessary for model simulations and data processing. I am grateful for the opportunity to study at Coastal Carolina University, which has been a nurturing and conducive environment for my academic growth. I would also like to express my gratitude to the faculty and staff within the Department of Coastal and Marine Systems Science for their support and assistance.

Abstract

Researchers and the public now widely recognize the seriousness of coastal flood risks. Various changes in natural processes, such as altered rainfall patterns, increased tropical cyclone intensities, and sea-level rise, are consequences of global warming induced by heightened greenhouse gas concentrations. To comprehensively understand coastal compound flooding, it is crucial to consider multiple processes and their interactions. Moreover, the growth of coastal cities and the concentration of people and assets in these areas make them increasingly vulnerable to flooding events. Accurately estimating the future flood risks faced by coastal communities necessitates addressing the compounding effects on coastal flood risk, taking into account not only natural driving factors like storms, sea-level rise, and rainfall, but also human factors, such as population and economy. This study aims to investigate the hypothesis that human factors can influence present and future coastal flooding risks as much as natural factors, and to advance the understanding of coastal compound flood hazards. A coupled modeling framework was developed to simulate coastal compound flooding, incorporating both inland river systems and coastal processes. An indicator was devised to estimate coastal flood risk that accounts for the impact of both natural processes and human activities. The results indicate that coastal compound flooding is a localized, coincidental issue, with the timing of various factors' convergence playing a critical role in flood occurrence. The severity of coastal floods depends on the interaction of natural factors and their compounded effects, as well as the extent of vulnerability associated with population growth and GDP increase. In northeastern South Carolina, the interplay between sea-level rise and

upstream discharge significantly intensifies compound coastal flooding, thereby exacerbating potential flood hazards in the future. Over the past 20 years, flood risk has consistently increased due to the escalating vulnerability of coastal communities to coastal floods.

Table of Contents

List of Tables

List of Figures

(right). Two-way coupling is used between column land surface models and terrain routing modules while one-way coupling is used between terrain routing modules and channel & reservoir routing modules.

Figure 2.3 The domain of simulation. Three rivers (the Waccamaw, Pee Dee, and Black) enter this region and flow into the Atlantic Ocean at Winyah Bay. Two USGS stations (id: 02145200 and 02110704) provided discharge as TELEMAC-2D model input. There are five USGS stations (id: 02110815, 021108125, 02110802, 02110725, and 02110777) and one NOAA station (id:8661070) in this area that can be used for water level validation. Negative topography indicates the bathymetry of river channels and coastal oceans. The path of Hurricane Matthew is shown in the inset figure. Five cross sections (aa' to ee') were selected to check the river discharges. The bathymetries of these five cross sections are shown in the right panels.

Figure 2.4 Model inputs for 2016 Hurricane Matthew event: Time series of river discharge from Waccamaw (purple line), PeeDee (red line), and Black Rivers (green line), sea level at seaside (solid blue line), storm surge (dashed blue line), tide (dotted blue line), and domain averaged rainfall (cyan line). The discharge input (dashed red, purple, and green lines) before Oct 08 shows a decreasing trend. A slight adjustment was made by removing the decreasing trend from the discharge input (solid red, purple, and green lines). This made the compound effect caused by the interaction between discharge, tide, and surge more straightforward to assess.

channel. The black lines are the constant riverbed. The blue and red lines denote the water surface height in the river channel and streamflow in m^3/s, respectively, The solid lines show the results from the simulation with normal sea level as the downstream boundary condition, while the dashed lines are those with increased sea level as the initial condition.

Figure 3.5 Accumulated flooding area distribution for (a) keeping upstream discharge (EXP3), (b) keeping tide surge (EXP5), and (c) keeping storm surge (EXP6) scenarios. Hurricane Matthew flood event (EXP1, red) and idealized steady scenario (permanent water surface, EXP2, blue) are plotted as reference.

Figure 3.6 Flooding area comparison between model result and linear combination when the compound effect reached its peak. (a) Keep upstream discharge and tide (EXP8) at time Oct 18 19:00, (b) Keep upstream and storm surge (EXP9) at time Oct 09 14:00, (c) Keep tide and storm surge (EXP12) at time Oct 7 20:00. The linear combination (green) means that the flooding area appeared in both compound modeling result and linear combination of each individual factor result. Compound effect (red) means that the flooding area was caused by the interaction between two factors.

Figure 3.7 Flooding area comparison between model result and linear combination when the compound effect reaches its peak for keeping upstream discharge, local rainfall, tide, and storm surge (EXP1). The time is Oct 7 20:00. The linear combination (green) means the flooding area appeared in both compound modeling result and linear combination of each individual factor result.

Compound flooding (red) means the flooding area appear only in compound modeling result, which means the compound flooding caused by the interaction between each two factors.

Figure 3.8 Water volume comparison between Hurricane Matthew case (control run) and linear combination of water volume result from only one factor including upstream discharge, local rainfall, tide, and storm surge (EXP3-EXP6). Since constant upstream discharge was considered in local rainfall, tide, and storm surge only simulations, three times of water volume result from reference run was removed from the linear combination.

Figure 3.9 EOF analysis for the interaction between upstream discharge and storm surge. 1st orthogonal basis functions (EOF) and its corresponding principal component (PC). Its contribution for total variation is about 29%. The correlation coefficient of this PC with storm surge is -0.66.

Figure 3.10 EOF analysis for interaction between upstream discharge and tide. 1st orthogonal basis functions (EOF) and its corresponding principal component (PC). Its contribution for total variation is about 18%. The correlation coefficients of this PC with three upstream discharge are 0.76, 0.79, and -0.09 for Waccamaw, PeeDee, and Black rivers respectively.

Figure 3.11 EOF analysis for interaction between upstream discharge and tide. 2nd orthogonal basis functions (EOF) and its corresponding principal component (PC). Its contribution for total variation is about 14%. The correlation coefficient of this PC with tide is -0.64.

List of Symbols and Abbreviations

Roman Symbols

A: flow cross-sectional area

$Area$: Flooding area

Baseflow: steady flow before a flood event

CN: curve number

D: Population density

F: the actual infiltration

FR: Flood risk

g: gravity

GDP: Gross domestic product per capita

H: hydraulic head of water in the conduit

h: Depth of water

I_a: initial abstraction

Magnitude: the peak discharge/water level value during a single flood event

P: total rainfall

$Period$: the duration of the storm surge

Q: flow rate

q_{lat}: lateral inflow rate into the channel from rainfall and surface runoff

R: direct surface runoff

S: amount of the potential maximum retention

S_f: friction slope

S_h, S_T : source/sink terms of fluid and tracer respectively

S_x, S_y : source terms representing the wind, Coriolis force, and bottom friction

T : passive (non-buoyant) tracer

t: Time

u: Velocity of water

u, v: velocity components of vector **u**

v_t, v_T : momentum and tracer diffusion coefficients

X: the time step number with a one-hour time interval

x, y: Local coordinate in horizontal direction

Y: a random variable, such as flood magnitude

Z: free surface elevation

λ : initial abstraction coefficient

μ: location parameter

ξ: shape parameter

σ: the scale parameter

Abbreviations

ADCIRC**:** ADvanced CIRCulation model

ASGS-STORM: ADCIRC Surge Guidance System, Scalable, Terrestrial, Ocean, River, Meteorological

CN: Curve Number

CUDEM: Continuously Updated Digital Elevation Model

EM-DAT: Emergency Events Database

EOF: Empirical Orthogonal Function

FR: Flood Risk

GAALFE: Global Active Archive of Large Flood Events

GCM: General Circulation Model

GDP: Gross Domestic Product

GPW: Gridded Population of the World

HL-RDHM: Hydrology Laboratory Research Distributed Hydrologic Model

HWM: High Water Mark

IPCC: Intergovernmental Panel on Climate Change

LECZ: Low-Elevation Coastal Zone

MRLC: Multi-Resolution Land Characteristics

NCEI: National Centers for Environment Information

NOAA: National Oceanic and Atmospheric Administration

NLCD: National Land Cover Database

NWM: National Water Model

PC: Principal Component

RCP: Representative Concentration Pathway

RMSE: Root Mean Square Errors

ROMS: Regional Ocean Modeling System

SCS: Soil Conservation Service

TIN: Triangular Irregular Network

UNISDR: United Nations International Strategy for Disaster Reduction

USGS: United States Geological Survey

1. Introduction

1.1 Coastal flood

1.1.1 Three types of floods

Flooding is the overflow of rising water onto normally dry land. It is a natural process caused by a series of drivers, including heavy rainfall, rapid snow and ice melt, dam breakage, groundwater rise, storm surge, and land sinking. Based on these drivers, scientists divided floods into three types: pluvial floods, fluvial floods, and coastal floods (Figure 1.1). Pluvial floods, sometimes also called flash floods or surface floods, occur when rainfall creates a flood event independent of a pre-existing water body, often in combination with fluvial and coastal flooding. Fluvial floods occur when excessive rainfall over an extended period causes a river to exceed its water storage capacity. Snow/ice melting and dam breaks can also cause fluvial floods. Coastal flooding refers to seawater inundation typically from storm surge and wave conditions caused by severe weather events (such as hurricanes). Coastal regions are the critical zone where all three types of floods can occur. In a broader definition, coastal floods can refer to any types of flooding that occurs in coastal regions. This thesis employs this broader definition to define coastal floods.

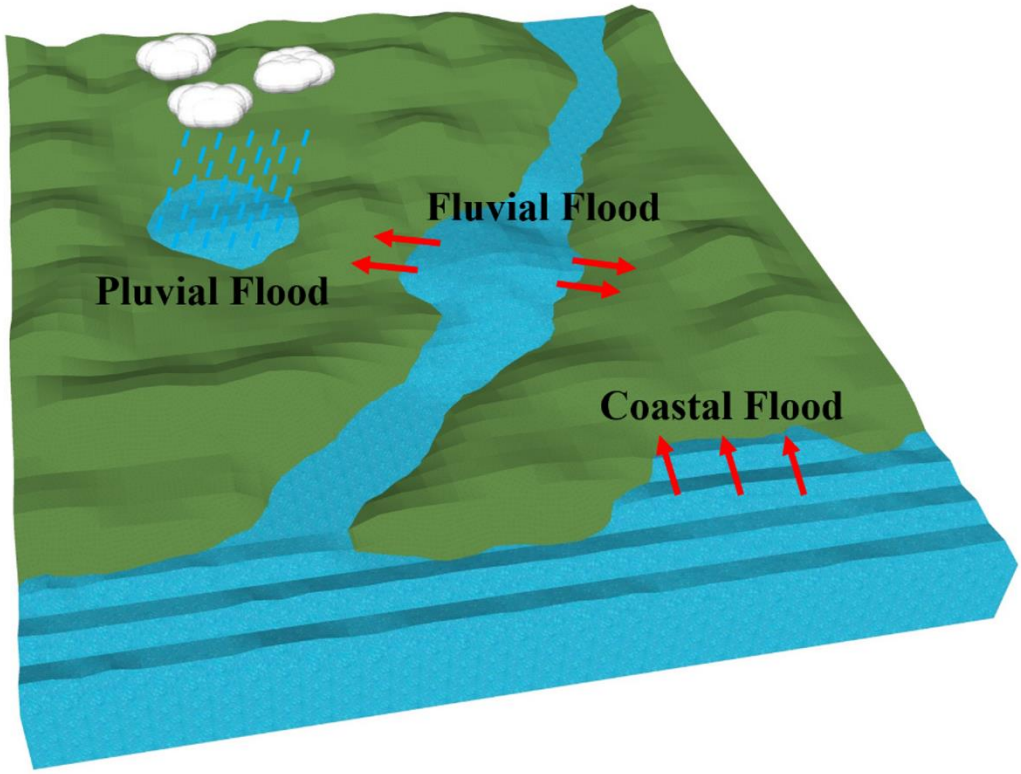

Figure 1.1. Three Types of Floods: 1) Pluvial floods, occur when rainfall creates a flood event independent of a pre-existing water body; 2) Fluvial floods, occur when excessive rainfall over an extended period causes a river to exceed its water storage capacity; 3) Coastal floods, refers to seawater inundation typically from storm surge and wave conditions caused by severe weather events. In a broader definition, coastal floods can refer to any types of flooding that occurs in coastal regions.

1.1.2 Coastal flooding as a natural process

As one of the most dynamic regions, the coast has always been at the forefront of changes in Earth's evolutionary history. The northeastern South Carolina coast exemplifies typical coastal evolution. Through flooding, rivers played a significant role in shaping South Carolina's topography. Meanwhile, interactions between the ocean and river systems affected this shaping process across multiple spatial and temporal scales. For example,

several paleochannels found offshore in Long Bay reveal the evolution of the floodplain in northeastern South Carolina. The original Pee Dee River system formed during the late Pliocene (Baldwin et al., 2006). The paleochannels formed during the glacial epoch when the sea level was below the present level. After the glacial epoch, sea-level rise from increasing global temperatures forced the shoreline to propagate landward. This propagation had two effects. One effect was that seawater inundation, caused by sea-level rise, created a series of new coastal forms such as estuaries, wetlands, barrier islands, and inlets. The other effect was that sea-level rise interrupted the original river channels, leading to frequent river flooding until a new balanced environment was established. From a historical perspective, landward migration is a natural response of the shoreline to sea-level rise, storms, and other coastal processes (Barnhardt et al., 2008). The modern coast of northeastern South Carolina is still evolving and is dominated by inland river systems and coastal processes, including tides and surges. In fact, coastal flooding in northeastern South Carolina is not a rare phenomenon associated only with extreme weather conditions, but rather a common occurrence that happens on a daily basis.

Coastal communities often overlook daily low-intensity coastal floods, as they typically do not result in significant property damage or loss of life. Coastal floods related to extreme weather conditions, such as hurricanes or tropical storms, are treated as flood risks due to the substantial damage they can inflict on coastal communities. These events can cause extensive property damage, loss of life, and long-lasting socioeconomic impacts. From this perspective, coastal floods become a flood hazard when considering their influence

on human society. This study aims to analyze coastal floods as a risk from both natural and human perspectives. It is important to note that while daily low-intensity coastal floods may not have immediate and dramatic impacts on human society, their cumulative effects can create long-term hazards for coastal communities. However, these long-term effects will not be discussed in this study.

1.1.3 Coastal flooding as a human-related hazard

Coastal regions are a small part of the land that supports a significant percentage of the total population and economy. Since 1970, the U.S. coastal population, defined as those most directly affected by the coast, has grown by about 39%. In 2010, roughly 123.3 million people (approximately 39% of the total population) lived in the U.S. coastal shoreline counties, which only account for less than 10% of the U.S. land (Crossett et al., 2013). The population density of coastal shoreline counties is roughly 446 people per km^2, which is more than three times the national average of 105 people per km^2 (Crossett et al., 2013). Globally, the population density of the low-elevation coastal zone (LECZ) is much higher than that of other regions (Neumann et al., 2015; Small & Nicholls, 2003). LECZ is defined as the contiguous and hydrologically connected zone of land along the coast and below 10 m of elevation above sea-level. In 2000, the average LECZ population density was about 241 people per km^2, which was nearly five times the global average for all land areas (Neumann et al., 2015). In addition to population density, the LECZ population growth rate in China and Bangladesh was twice the national population growth rate between 1990 and 2000 (McGranahan et al., 2007). As the population increases in coastal areas, a large amount of rural and forest land is converted into urban

land to accommodate new residents. This large amount of the population represents a significant coastal economy. A coastal economy consists of all economic activities in the coastal region and is therefore the sum of employment, wages, and output in the region (Colgan, 2003). In 2014, the coastal economy created US$7.9 trillion in Gross Domestic Product (GDP) and 54.6 million jobs in the United States (NOAA, 2017).

Since the coastal population and economy account for a large proportion of the total population and economy, it is necessary to understand coastal flooding in the context of rapid urbanization, which is the result of population and economic growth. Therefore, in addition to natural processes, human activity is another important factor to estimate compound flood risk, which is rarely mentioned in recent coastal compound flood studies (Gori et al., 2020; Moftakhari et al., 2017; Pietrafesa et al., 2019; Wahl et al., 2015). Most recent coastal compound flooding studies have focused only on natural factors, such as rainfall, sea-level changes, and river discharge (Moftakhari et al., 2017; Wahl et al., 2015). Their conclusions may lead to a misperception concerning coastal compound flooding studies: stronger natural driving factors, such as greater rainfall or stronger hurricanes, will always result in more severe flood hazards that pose a greater threat to coastal communities. Without considering human factors, the estimates of flooding hazards do not represent the true risk of flooding hazards in coastal communities. Flooding hazard is a compound natural and human-related issue, and therefore, human factors must be considered in order to assess the flooding hazard risk that coastal communities face in the context of human activities such as urbanization, population, and economic growth as while as anthropogenic climate change. To make the situation worse, the compounding

effect among the natural processes is not addressed adequately. After reviewing a series of recent studies about floods, rainfall, sea-level, and hurricanes, it is still difficult to conclude whether climate change will cause more flooding (as a natural process)/rainfall/hurricanes at a local scale. These results conflict with the awareness of increasing flood risk in previous studies (Ezer & Atkinson, 2014; Wahl et al., 2015; Wdowinski et al., 2016).

Therefore, what are the predominate factors causing the change of the compounding coastal flooding risk at present and in the future: abnormal *natural* processes related to climate change or *human* activities related to social development, such as urbanization and population/economic growth? This question remains unanswered as most recent studies have focused only on the impact of natural processes on coastal flooding risk.

1.2 Flood, flood hazard, and flood risk

Before further analysis, the terminology needs to be clarified. Flooding is a natural phenomenon that occurs when a body of water rises to overflow land that is not normally submerged (Ward, 1978). In this study, the term "flood" is only referred to as a natural process. Not all floods are considered to be flood hazards. According to the definition of the United Nations International Strategy for Disaster Reduction (UNISDR), flood hazard is a natural process that may cause loss of life, injury or other health impacts, property damage, loss of livelihoods and services, social and economic disruption, or environmental damage (UNISDR, 2009). Flood risk is an indicator used for evaluating the potential losses, in lives, health status, livelihoods, assets, and services, which could occur to a particular community or a society over some specified future time period (UNISDR,

2009). In summary, flooding is a natural phenomenon, flood hazard is a natural phenomenon accompanied by social and economic losses, and flood risk is an estimate of the potential losses caused by floods in the future environment. Associated with flood risk, “flood exposure” is defined as the population and assets subject to flooding hazards. Because of the wide gaps in understanding between different groups, the simple word “flood” has different meanings for different people, but those meanings are often used interchangeably, which can cause confusion. Most theoretical researchers only consider flooding as a natural process, whereas the public is more concerned about floods in terms of social and economic losses. When designing infrastructure and buildings, engineers pay attention to flood risk. In fact, natural processes and social/economic losses are two partial views of a flooding event. Flood researchers with different backgrounds often use floods, flood hazards, and flood risks without distinction. As a result, these unintentional conflations in terminology can sometimes cause inefficient information dissemination from scientific communities to the public. For example, most scientific publications show that “flood risk” is increasing. However, the threat of floods to the public is unclear because in scientific publications, the term “flood risk” typically refers to the probability of a certain magnitude floods occurrence. According to the above terminology clarification, flooding does not necessarily pose a significant flood risk. This study makes a clear distinction between these terms.

1.3 Coastal flood risk

1.3.1 Factors affecting coastal flood risk

Researchers and the public have reached a consensus that coastal flood risk is serious at

present (IPCC, 2015; Vitousek et al., 2017; Wahl et al., 2015; Wdowinski et al., 2016). Based on the information in above section 1.1.2 and 1.1.3, factors that affect coastal flood risk can be roughly classified into two classes (Figure 1.2). One class is the factors connected to natural flood processes, including sea level (Mousavi et al., 2011), precipitation/evaporation (Xu et al., 2019), discharge (Bevacqua et al., 2020), soil moisture (Cao et al., 2020). These factors are influenced by climate change. The other class is the factors related to social communities, such as population growth (Ibrahim et al., 2017), economic development (Jevrejeva et al., 2018), and land use/cover change (Baky et al., 2020). Especially, land use/cover change also has an effect on natural flood processes by changing the generation of surface runoff.

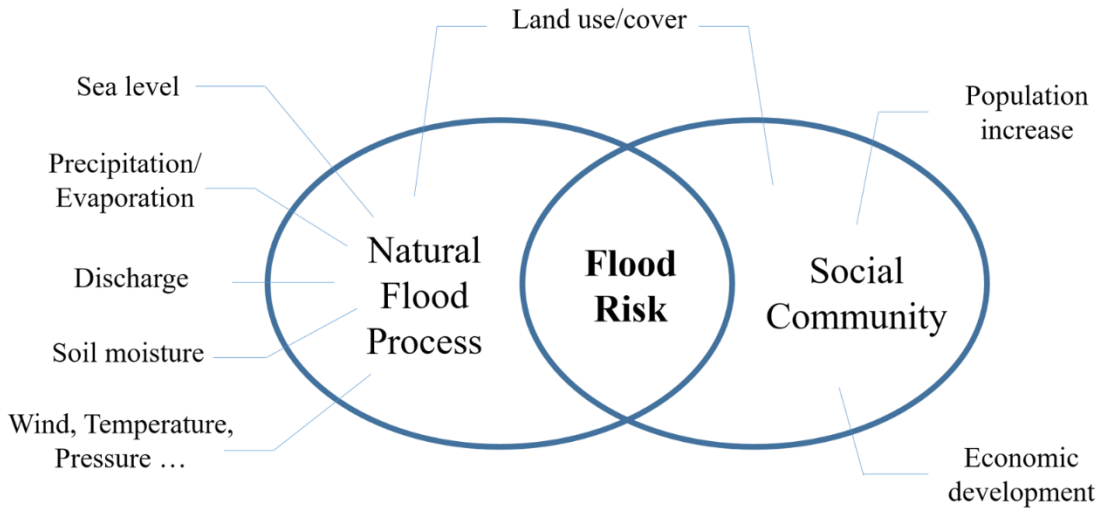

Figure 1.2. Factors affecting coastal flood risk. 1) Natural flood process, including sea level, precipitation/evaporation, discharge, soil moisture and so on, 2) Social community factors, including population increase, economic development, and land use/cover change. In addition, land use/cover change also has effect on natural flood process.

1.3.2 Effect of Climate change on coastal flood

Several important coastal flooding driving factors can be affected by climate change. The scientific community and the public have become increasingly aware that global warming caused by increased concentrations of greenhouse gases may result in a series of changes in natural processes, like rainfall patterns, tropical cyclone intensities, and sea-level (IPCC, 2001; 2008; 2015). General Circulation Models (GCMs) have been employed to analyze climate change under different CO_2 concentration scenarios. The results of these models and related downscale studies have suggested increased rainfalls due to enhanced hydrological circulation, more frequent high-intensity tropical cyclones, and higher sea-level rise rates than in the past (Emanuel, 2005; Hirabayashi et al., 2008; Horton et al., 2008). A series of extreme natural disasters in the new century has made the general public aware of ongoing climate change (Figure 1.3). According to records from the Emergency Events Database (EM-DAT) (Guha-Sapir, 2017), the average annual natural hazards after 2000 have more than doubled compared with that between 1950 – 1999. Increases in all three of these natural disasters: increased rainfalls, more frequent high-intensity tropical cyclones, and higher sea-level rise rates than in the past, indicate an environment sensitive to climate change. In addition, meteorological and hydrological processes are also affected by climate change. Based on the latest EM-DAT records, annual storms (including tropical cyclones, extra-tropical cyclones, and convective storms) and annual floods (including flash floods, riverine floods, and coastal floods), which are indirectly affected by global warming, have increased by almost two times and more than three times since 2000, respectively.

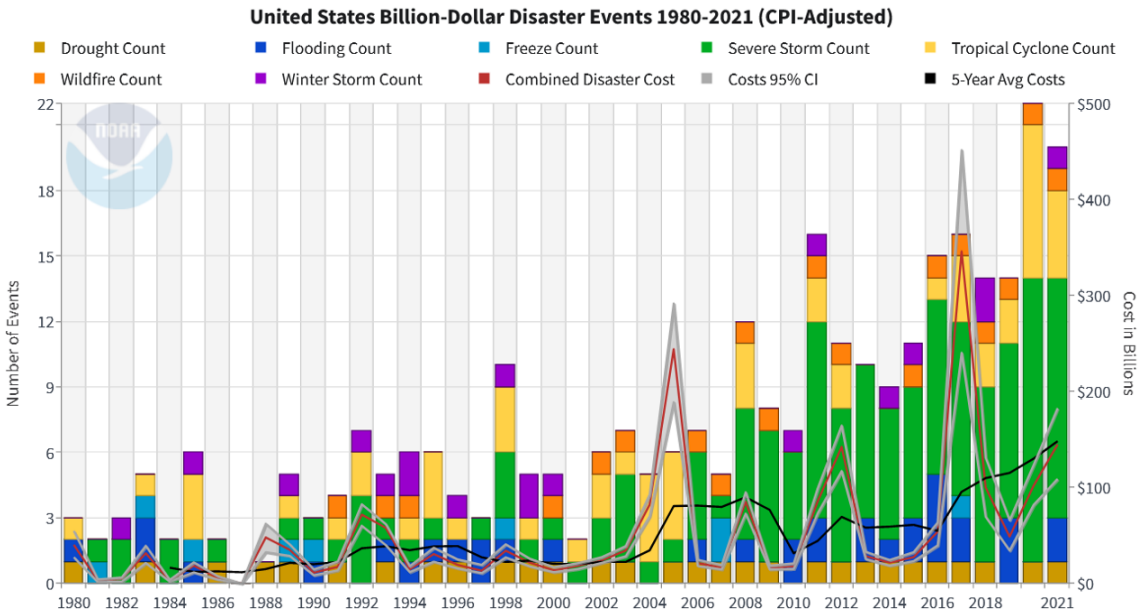

Figure 1.3. The history of billion-dollar disasters in the United States each year from 1980 to 2021, showing event type (colors), frequency (left-hand vertical axis), and cost (right-hand vertical axis.) The number and cost of weather and climate disasters is rising due to a combination of population growth and development along with the influence of human-caused climate change on some type of extreme events that lead to billion-dollar disasters. NOAA NCEI.

Although uncertainties still exist in the studies of flood trends (detail in Section 1.4.2), researchers have reached a consensus that climate change will affect coastal zones and coastal flooding. Past studies have examined several important factors related to climate change to estimate future coastal flooding hazards and risks faced by coastal communities. Among the factors, sea-level rise and storm intensity/pattern changes are considered to be the two main factors affecting coastal flooding in the future.

1.3.2.1 Sea-level rise

Since the last glacial period ended about 15,000 years ago (Severinghaus & Brook, 1999),

sea-level rise has been one of the causes of global flooding. When the glacial period ended, global temperature increase caused thermal expansion of seawater and glacial ice melting, which led to increase in sea-level and land-surface runoff, respectively (Marshall & Clarke, 1999; Lambeck & Chappell, 2001). Although studies on exact sea-level trends are subject to uncertainty (Oppenheimer et al., 2016; Santamaría-Gómez et al., 2017), there is no doubt that most coastal areas in the world have experienced sea-level rise periods. According to IPCC report, the global average sea-level rise in 2100 is projected to vary under three different scenarios (IPCC, 2019). Under RCP2.6, the sea-level rise may be 0.43m, with a likely range of 0.29m to 0.59m. In the RCP4.5 scenario, the projected rise is 0.55m, with a range of 0.39m to 0.72m. The most severe scenario, RCP8.5, predicts a rise of up to 0.84m, with a likely range between 0.61m and 1.10m. RCP means the Representative Concentration Pathway (RCP) and is a greenhouse gas concentration trajectory used by IPCC to evaluate climate change. Different RCPs describe different climate futures depending on the volume of greenhouse gases emitted in the years to come (van Vuuren et al., 2011). For example, RCP2.6, RCP4.5, and RCP8.5 are labeled according to a possible range of radiative forcing values in the year 2100 (2.6, 4.5, and 8.5 W/m^2, respectively). Ninety percent of the coastal areas will experience a sea-level rise of more than 0.2 meters if global warming reaches two degrees higher than the pre-industrial period (Jevrejeva et al., 2017).

Current studies show that long-term sea-level rise is the main reason for accelerated coastal flooding in the United States. Ezer and Atkinson (2014) used the duration of annual minor tidal flooding (defined as 0.3 m above the average higher high water level)

to evaluate the flooding conditions on the east coast of the United States. They found that this duration increased by 20 hours per year from pre-1970 to 1971-1990, and further increased by 50 hours per year from 1971-1990 to 1991-2013. The spatial variations of these increases resembled those of sea-level rise (Ezer & Atkinson, 2014). Similarly, Sweet and Park (2014) also found that the relative sea-level rise has caused the water level to increase above the thresholds of minor coastal flooding elevation in the U.S. that were set by the National Weather Service (Sweet & Park, 2014). It should be noted that the above studies are mainly based on hydrodynamic model simulations; therefore, in these studies, flooding was treated as a natural process, and the rising trends found do not imply increased coastal flooding hazards or flooding risks. Nonetheless, sea level changes related to climate change is an important factor need to be considered in coastal flood simulations.

1.3.2.2 Hurricane pattern change

At present, the link between global warming and its effects on hurricanes is still unclear (Anthes et al., 2006; IPCC, 2015; Pielke Jr et al., 2005). This uncertainty is due to the following three reasons: (1) No direct connection has so far been established between greenhouse gas emissions and the behavior of hurricanes (Walsh, 2004; Walsh et al., 2016; Watson & Albritton, 2001); (2) The change in hurricane intensity in the future may be small in the context of the observed variability (Henderson-Sellers et al., 1998; Knutson et al., 2010; Knutson & Tuleya, 2004); (3) The future damage to society caused by hurricanes could be much less than the wealth and population that will grow in the future (Pielke Jr et al., 2005). In this situation, studies currently focus mainly on whether

hurricane patterns, including hurricane frequency and intensity, will change in the future and how to describe these changes.

Landsea et al. (1996) investigated a five-decade hurricane record in the North Atlantic basin and found that the frequency of intense hurricanes continued to decrease from 1944 to 1995. Chan and Shi (1996) studied hurricanes in the western North Pacific basin and found that the number of tropical cyclones experienced a period of decrease and then an increase, showing an obvious second-order variation such that the activity had been on a generally upward trend since the late 1980s. There has been no observable trend in hurricane frequency in the following decades based on records. The inconsistencies in hurricane frequency for different ocean basins have been confirmed in a series of recent studies (Knutson et al., 2010; Landsea & Franklin, 2013; N. Lin & Emanuel, 2016; K. J. E. Walsh et al., 2016).

Compared with the uncertain frequency, researchers have reached consensus on future changes in hurricane intensity. Theoretically, the heat stored in the upper ocean near the sea surface provides the energy that fuels the development of hurricanes. Therefore, the increase in sea surface temperature caused by greenhouse gases provides a more favorable environment for the formation and growth of hurricanes. Emanuel (2005) created an index of the potential destructiveness of hurricanes to evaluate the hurricane changes. This index is based on total power dissipation, which means that it is integrated over the entire lifetime of a cyclone. Emanuel used this index to investigate hurricanes in the past 30 years and found that the index has increased significantly since the mid-1970s. Webster et al. (2005) examined the intensity of tropical cyclones for more than 35 years

in the context of increasing sea surface temperature. They found that the number of category-4 and -5 hurricanes increased different levels in the North Pacific, India, Southwest Pacific, and North Atlantic. Emanuel used a Carnot cycle model to estimate the maximum intensity of future tropical cyclones under the increased atmospheric CO_2 content. The results show that twice the present CO_2 content will increase the destructive potential of hurricanes by 40% to 50% (Emanuel, 1987). Yet, based on past studies, there is still low confidence in any robust long-term changes in tropical cyclone activity and there is low confidence in the attribution of global changes to any particular cause under climate-change scenarios (IPCC, 2015).

The potential impact of high-intensity hurricanes has been examined in several studies based on hurricane pattern change. Mousavi et al. (2011) projected that flood elevations caused by catastrophic hurricane surge in the Gulf of Mexico will rise by 0.5 m and 1.8 m by the 2030s and 2080s, respectively. Due to these uncertainties in future hurricane patterns, the future impact of climate change on landfalling tropical cyclones is also unclear (Woodruff et al., 2013). Even though uncertainty exists in hurricane pattern change studies, there is no doubt that hurricanes can be an important trigger of coastal flooding. Extreme rainfall and storm surge, which affects coastal flood, are usually accompanied by hurricanes. Under this situation, it is necessary to estimate the impact of hurricanes, especially extreme hurricanes, on the entire coastal compound flood process. In order to simulate the extreme weather event, extreme rainfall, extreme storm surge, and extreme discharge are simplified as indexes to represent and describe the extreme weather conditions in this study.

1.3.3 Effect of urbanization on coastal flood risk

Urbanization, particularly population growth and GDP increase, has significant effects on coastal flood risk. The expansion of coastal cities and the increasing concentration of people and assets in these areas make them more vulnerable to the impacts of flooding events. Additionally, urbanization alters natural landscapes, disrupts ecosystems, and contributes to climate change, exacerbating the frequency and severity of coastal flooding.

As dynamic and critical zones of human civilization, coastal regions have experienced significant land use/cover changes in the past two hundred years since the Industrial Revolution. Even though coastal regions only account for 23% of the contiguous land of the United States, the changes that have taken place in the last 50 years in the coastal regions account for approximately 50% of all land-cover changes and 43% of all urbanization in the contiguous land of the United States (Reidmiller et al., 2018). Between 1996 and 2010, approximately 8% of the coastal region changed, including the loss of more than 40,000 square kilometers of forest and more than 4,000 square kilometers of wetlands (Reidmiller et al., 2018). Nearly 15,000 square kilometers of other land-use types have become urban, which is a rate three times that of the interior of the U.S (Reidmiller et al., 2018). As urban areas expand along coastlines, more people and assets are exposed to the risk of coastal flooding. The high population density in coastal regions, combined with the concentration of critical infrastructure and economic activity, increases the potential for substantial damage and loss of life during flood events (Hallegatte et al., 2013; Neumann et al., 2015).

The economic value of property loss and population in flood-prone areas are two human-related factors affecting the estimation of flood risk. It is difficult to estimate the vulnerability of social communities to coastal flooding. At present, the property value of the potential loss is a common metric for showing the level of flood risk. This study will also employ a GDP dataset to evaluate the weight of economic loss in flood risk estimation. While advances in modeling and computation have improved our ability, they do not support the analysis of flood risk for every single person. There is no doubt that a flood affecting one person is different from a flood affecting ten people. So, from a social view, a current flood affecting ten people may imply an increase in flood risk compared to a flood affecting one person ten years before. However, reasons for increased flood risk may include both population growth and climate change. This thesis aims to analyze which factor is more important for the flood risk change in the past twenty years in South Carolina. The population dataset and GDP per capita will also be employed to enrich the view of flood risk.

1.3.4 Coastal flood and flood risk in South Carolina

This thesis will focus on South Carolina as the study domain in order to leverage the high-resolution local scale model and data. However, the developed methods and conclusions will be applicable to other areas in the world. Coastal flooding usually occurs in autumn in South Carolina. According to periods of heavy rainfall, there are three types of flood regions in South Carolina shown in Figure 1.4: the mountainous region in the west with a winter maximum; the coastal plain with a distinct summer maximum; and the region in between with a summer-autumn maximum (Changnon, 1994). It is worth noting that

although heavy rainfalls usually occur during summer, coastal floods usually occur in early autumn due to the weather conditions and the soil's water storage capacity. There are four pathways for heavy rainfalls in South Carolina: (1) large-scale synoptic storms with low pressure centers and fronts, with the highest frequency in winter or early spring and lowest frequency in summer (Maddox et al., 1979); (2) isolated convective thunderstorms with highest frequency in summer and early autumn (Barnes & Newton, 1986); (3) infrequent tropical storms that occur from June through November (Cry, 1967); and (4) sea-breeze circulation along the Atlantic coast during summer (Moran, 1989). As shown in the timeline (Figure 1.5), isolated convective thunderstorms and sea-breeze circulation bring moisture to the land and saturate the soil by the end of summer. When tropical cyclones occur in autumn, it is often easy for them to trigger severe coastal floods on the soil that has already been saturated by isolated convective storms and sea-breeze circulation. Most of the recent extreme coastal floods in South Carolina occurred between September and October and were caused by tropical cyclones, such as Hurricane Matthew (Sep 28 – Oct 9, 2016) and Hurricane Florence at (Aug 31 – Sep 17, 2018).

In 1996, Hurricane Fran (Aug 23 – Sep 8) hit the coastal area of South Carolina and caused US$ 20 million in insured property losses (Mayfield, 1996a). In contrast, tropical storm Arthur (Jun 17 – Jun 21, 1996) and Hurricane Bertha (Jul 5 – Jul 14, 1996) also hit the same area at earlier times that year but did not cause coastal flooding related losses comparable to those incurred due to Hurricane Fran. The insured property damage for tropical storm Bertha was 135 million US$ (Lawrence, 1996), and no significant damage associated with Hurricane Arthur was reported (Mayfield, 1996b). There are two possible

reasons to explain this. One is that the soil in South Carolina in late summer had not been saturated yet, thus lacking a necessary condition for severe coastal flooding. The other possible reason is due to the difference between coastal flooding versus coastal flooding hazard. This uncertainty highlights the necessity of employing an integrated approach to consider high-resolution multiple natural driving factors of coastal flooding as well as human activity factors to correctly estimate the flooding risks that coastal communities face presently and in the context of future climate change. In this study, initial soil moisture before the hurricane will be considered as a factor affecting coastal flood, which will be included in the flooding simulation.

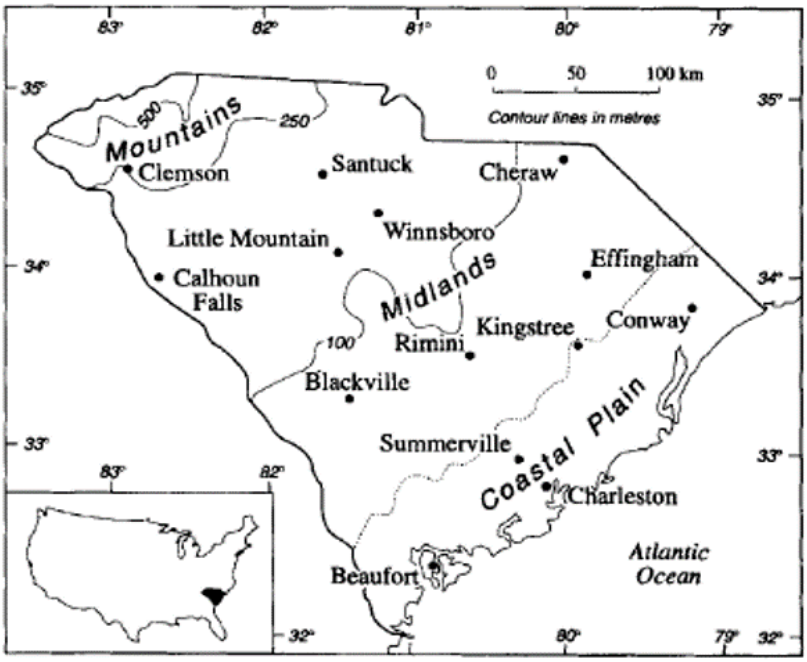

Figure 1.4. Three precipitation regions in South Carolina.1) the mountainous region with maximum precipitation in winter; 2) the midland region with maximum precipitation in summer-autumn; 3) the coastal plain region with maximum precipitation in summer. [from Changnon, 1994]

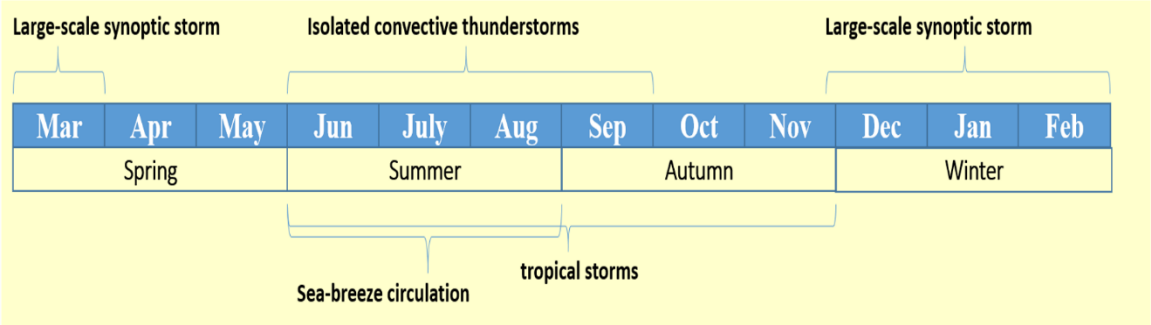

Figure 1.5. Major causes of heavy rainfall and their durations 1) large-scale synoptic storms from winter to early spring; 2) isolated convective thunderstorms from early summer to early autumn; 3) sea-breeze circulation in summer; 4) tropical storms from late summer to autumn.

1.4 Uncertainties in previous studies

Coastal flooding is critical because it can pose a risk to coastal communities. Currently, there are some uncertainties in coastal flood studies, such as: 1) how compound flooding occurs on coasts, including how different natural factors interact with each other, and 2) whether floods, as natural processes, or flood risks, as human-related issues, are increasing.

1.4.1 Coastal compound flood studies

In previous analyses of river floods, the key variable used to estimate the severity of a flood was the discharge in the river channel, as determined by observation or hydrological modeling. For sea water inundation caused by storm surges, the flooding area determined from an ocean/coastal hydraulic model is the main factor for analysis. However, neither of these two variables (discharge and flooding area) can give us a complete view of how a coastal compound flood occurs. Before moving forward, here is the review of the complete hydrological and coastal processes related to coastal flood events.

In nature, the atmosphere, river, and coastal processes work together to shape the coastal environment and influence the occurrence of coastal flooding at various temporal and spatial scales. These processes include precipitation, evapotranspiration, infiltration, overland flow, subsurface flow, ground water flow (baseflow), river channel flow, tide, wave (including storm surge) and current, all of which contribute to coastal flooding (Figure 1.6). These processes have often been studied and predicted separately by people with the expertise in this area. For example, tide, wave, and storm surge are usually simulated by coastal ocean models governed by hydrodynamic equations with wetting/drying cell capabilities. Floods in coastal ocean models mainly include seawater inundation caused by storm surge. However, hydrological processes, such as infiltration, overland flow, river channel flow, and groundwater flow, are usually simulated in hydrological models, in which pluvial floods are represented as a 1-dimensional (1D) quantity along a river channel, governed by a set of 1D Saint-Venant equations. Additionally, inland inundation in a flooding event, as a 2-dimensional (2D) process, is usually simulated by hydraulic models governed by 2D shallow-water equations. Some hydrological processes are ignored in these 2D-inundation models, such as infiltration and groundwater. The above differences between the 2D-inundation model and the hydrological model result in the discrepancies between floods represented by these models. Flooding is represented as a 2D phenomenon in the 2D-inundation model, whereas as an 1D river discharging process in the hydrological model.

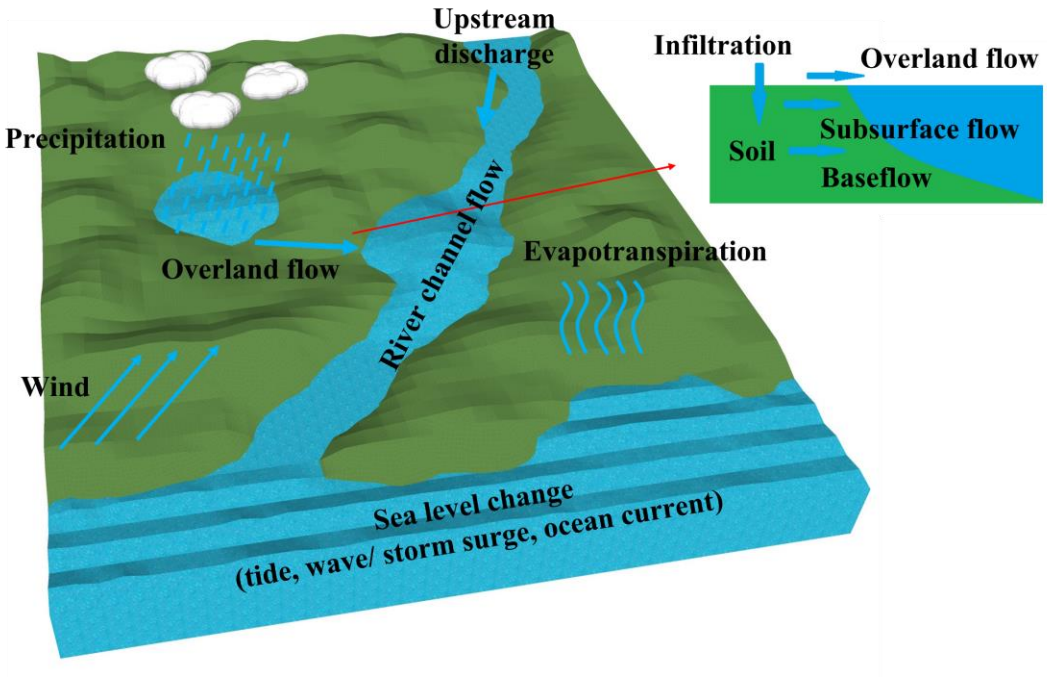

Figure 1.6. Natural process affecting coastal environments and coastal flooding: 1) Precipitation, 2) Evapotranspiration, 3) Infiltration, 4) Overland flow, 5) Subsurface flow, 6) Baseflow, 7) River channel flow, 8) Sea level change (including tide, wave/storm surge, and current).

To truly understand and accurately predict complex coastal flooding events in this context of climate change, multiple processes and their interactions must be considered simultaneously. A new term, "compound event," was first introduced in the Intergovernmental Panel on Climate Change (IPCC) report (Field et al., 2012). It has three meanings in different situations: (1) two or more extreme events occurring simultaneously or successively, (2) the combinations of extreme events with underlying conditions that amplify the impact of the events, (3) a combination of events that are not themselves extremes but lead to an extreme event or impact when combined (Field et al., 2012). In short, compound events are a combination of processes (climate drivers and

hazards) that lead to significant impacts (Zscheischler et al., 2018). Coastal flooding is a typical compound event for environmental researchers. Coastal compound flooding is a coincidence of multiple coastal processes that can contribute to the overflowing of rising water in the coastal area, including precipitation, overland routing, infiltration, sea-level change (surge, tide, and wave), and hurricanes. Globally, long-term sea-level rise, extreme rainfall, and storm surges are considered to be important drivers of coastal compound floods (IPCC, 2015; Nicholls & Cazenave, 2010; U.S. Global Change Research Program, 2009). In recent years, more intense rainfall due to more frequent extreme storms (such as hurricanes) has also been responsible for a series of coastal floods (N. Lin & Emanuel, 2016; Wahl et al., 2015). Hydrological background, including soil moisture and upstream discharge, is another important factor in causing coastal compound floods. The blocking effect of storm surge on river discharge is a typical phenomenon in compound coastal flooding (Pietrafesa et al., 2019; van den Hurk et al., 2015).

The two primary driving processes of a coastal compound flooding event are rainfall as a freshwater source and coastal water level as a seawater source. The rainfall can have a direct impact on the simulation area by falling directly into the domain, or it can have an indirect impact by generating streamflow upstream that flows into the model domain as a lateral boundary condition. Traditionally, the two types of processes have been studied by different communities: hydrologists on freshwater-related processes and oceanographers on seawater-related processes. With the increasing recognition of the compound flooding concept, efforts have been made in recent years to link river and ocean processes. Coupling method should be applied to establish the link between

hydrological model and hydraulic model.

Currently, the one-way coupling method, presently dominates coastal modeling strategies. This one-way prescribes the upstream river discharge into the study area by setting an upstream boundary condition. A coupled model named the ADCIRC Surge Guidance System, Scalable, Terrestrial, Ocean, River, Meteorological (ASGS-STORM) was developed to incorporate tides, waves, winds, rivers and surge to simulate total water level at coastal regions (Dresback et al., 2013). In ASGS-STORM, the discharges simulated by the hydrological component Hydrology Laboratory Research Distributed Hydrologic Model, (HL-RDHM) described in the User Manual v. 3.00 (*HL-RDHM User Manual v. 3.0.0*, 2009) were passed to the coastal model ADCIRC as a boundary, but the processes associated with rainfall that fell directly into the model domain were not considered. Bakhtyar et al. (2020) used a hydraulic/hydrodynamic model HEC-RAS/D-Flow FM to simulate severe historical tropical cyclones in the Delaware River Basin, with the National Water Model (NWM) providing an upstream discharge boundary condition and the ADCIRC and WW III models providing the downstream boundary condition of water levels. Similar to ASGS-STORM, the direct impact of rainfall was not represented in this model system (Bakhtyar et al., 2020). Other hydraulic/hydrodynamic models, such as Delft3D (Muñoz et al., 2022) and the Semi-implicit Cross-scale Hydroscience Integrated System Model (SCHISM) (Ye et al., 2020) were also used to simulate total water level in coastal regions with upstream discharge forcing from NWM. Given the current stage of numerical modeling development, we have also employed a one-way coupling technique for our coastal flood modeling endeavors. Thus far, the role of the non-linear interactions

between the driving forces has not been quantitatively assessed

It is intellectually anticipated that a compound flood induced by multiple driving factors (e.g. simultaneous storm surge, upstream discharge, and rainfall) may be expected to inflict greater damage than the damage induced by a single driving force. However, it is unknown whether the damage caused by a compounding flood would exceed the linear combination of the damages caused by those same driving forces, but individually and independently, rather than simultaneously as in an interactively coupled compounding flood. In other words, because the role of the non-linear interactions between the driving forces has not been quantitatively assessed, it remains unclear what the difference will be between using interactively coupled modeling methods rather than modeling the floods caused by each individual driving forces independently and then linearly combining the results.

1.4.2 Flood trend studies

Climate model simulations show that global warming has intensified the global water cycle. At the beginning of the 21st century, the IPCC synthesis report predicted that the magnitude and frequency of flooding may increase in many areas due to the increased frequency of heavy rainfall events (IPCC, 2001). It is worth noting that the increase in the magnitude and frequency of flooding is not based on actual flood records, but a projection based on increased rainfall due to global warming. Milly et al. (2002) analyzed the annual maximum monthly-mean discharge of 29 large rivers over more than 30 years of observations and global numerical simulations. The results showed that the frequency of major floods (1% annual chance flood) increased during the 20th century (Milly et al.,

2002). However, the monthly-mean discharge data used by Milly et al. (2002) is not precise enough for flood study. It is vital to use peak discharge data to analyze flood processes.

Despite the results of increasing flood shown by global-scale studies and local river basin scale case studies suggest that the frequency of flooding has not been consistently increasing. Schmocker-Fackerl and Naef（2010) used long-term (up to 105 years) discharge data on rivers in Switzerland to investigate whether the frequency of flooding has increased. The results show that the trend of flood frequency varied spatially and temporally and fluctuated due to large-scale atmospheric circulations. Delgado et al. (2010) used the annual maximum discharge from four gauge stations in the Mekong river basin (Southeast Asia) to investigate flood trends and variabilities. To reveal the trend and variability of floods with a variety of statistical measures, three statistical methods were used in their analysis, including the Mann Kendal test (MK), ordinary least squares with resampling (OLS), and non-stationary generalized extreme value function (NSGEV). The results from all three methods indicate that the likelihood of extreme flooding increased in the second half of the 20th century, but the probability of average flooding decreased (Delgado et al., 2010).

In addition to the above discharge-based studies, flood trends can also be estimated using data from insurance databases, news reports, and so on. According to the Munich RE insurance database, the number of annual floods has almost doubled since 1980 (Figure 1.7), in line with the results of the above theoretical and model studies. However, the trend of catastrophic floods seemed to occur in a random pattern (Figure 1.8). The

increase in the total number of flooding events in the database may be due to the development of the insurance industry. The number of catastrophic floods may better reflect actual trends. Since 1985, the Global Active Archive of Large Flood Events (GAALFE) has been an active program supported by the University of Colorado to record flooding events based on news, governmental, instrumental, and remote-sensing sources (Brakenridge, 2010). The database provides detailed flood information, including the location of flood-affected areas, the duration of a flood, fatalities, main cause, and severity class. The severity class is on a 1-2 scale, where class 1 indicates large flood events with a recurrence interval < 20 years; class 1.5 indicates very large flood events between 20 to 100 years; class 2 indicates extreme flood events > 100 years. No evident increase in flooding was observed from the GAALEF database records (Figure 1.9). From 1985 to 2008, coastal flooding increased significantly. After 2008, coastal flooding still increased slightly compared to the 1990s (Figure 1.9). In all coastal floods from 1985-2019, heavy rain has been the main cause, and tropical cyclones were only a minor factor (Figure 1.10).

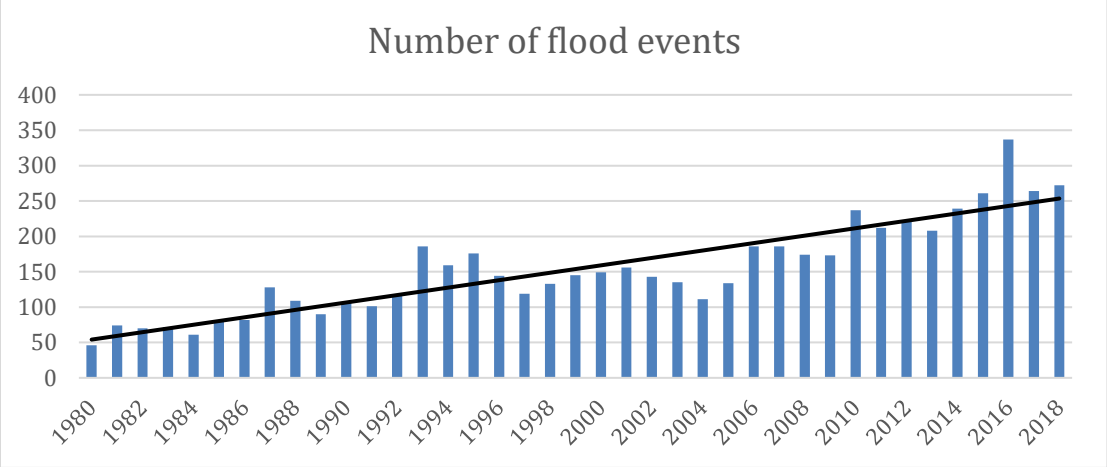

Figure 1.7. Number of flood events (1980-2018) (Data Source: Munich RE)

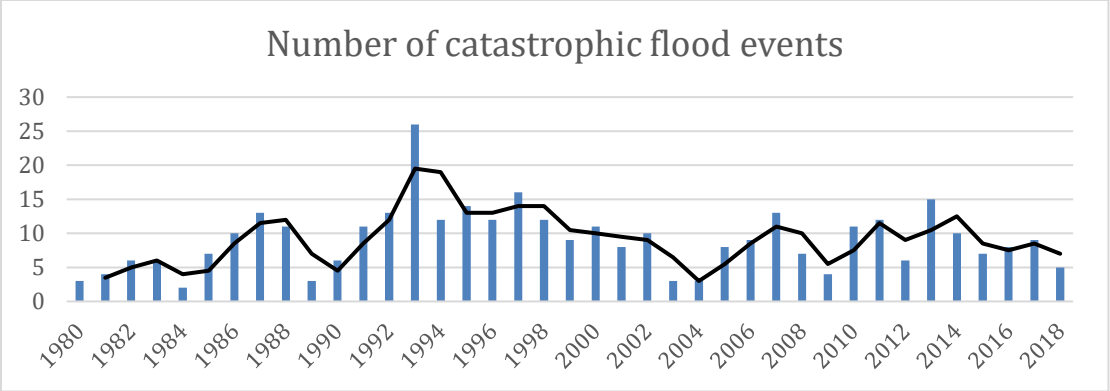

Figure 1.8. Number of catastrophic flood events (1980-2018) (Data Source: Munich RE)

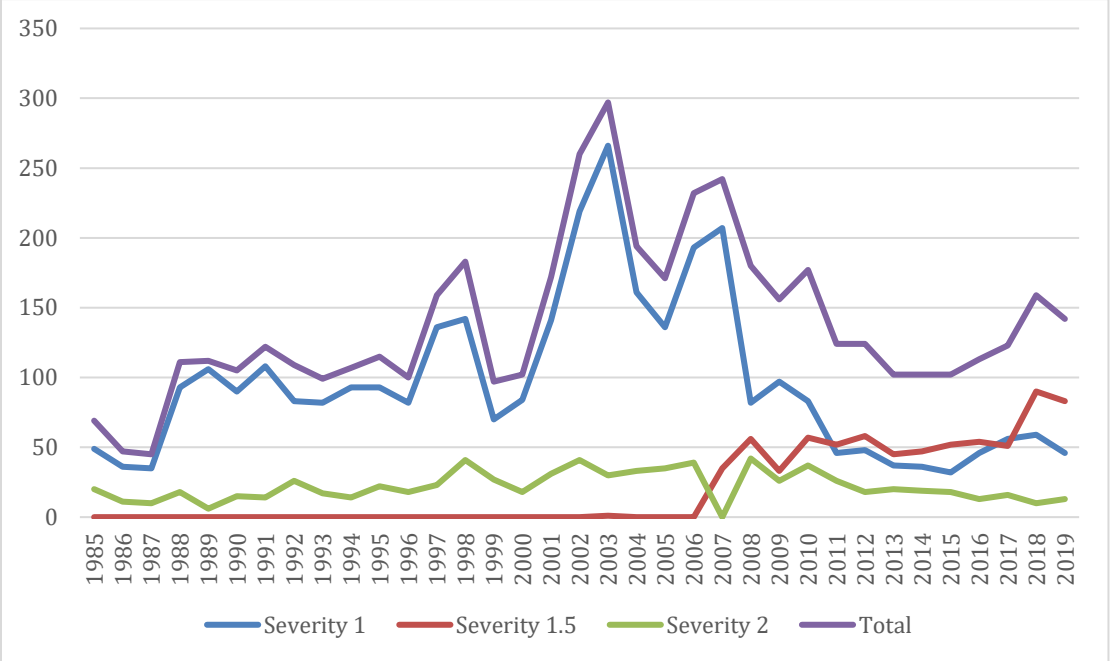

Figure 1.9. Number of reported flood events with different severities (1985-2019) (Data Source: Global Active Archive of Large Flood Events)

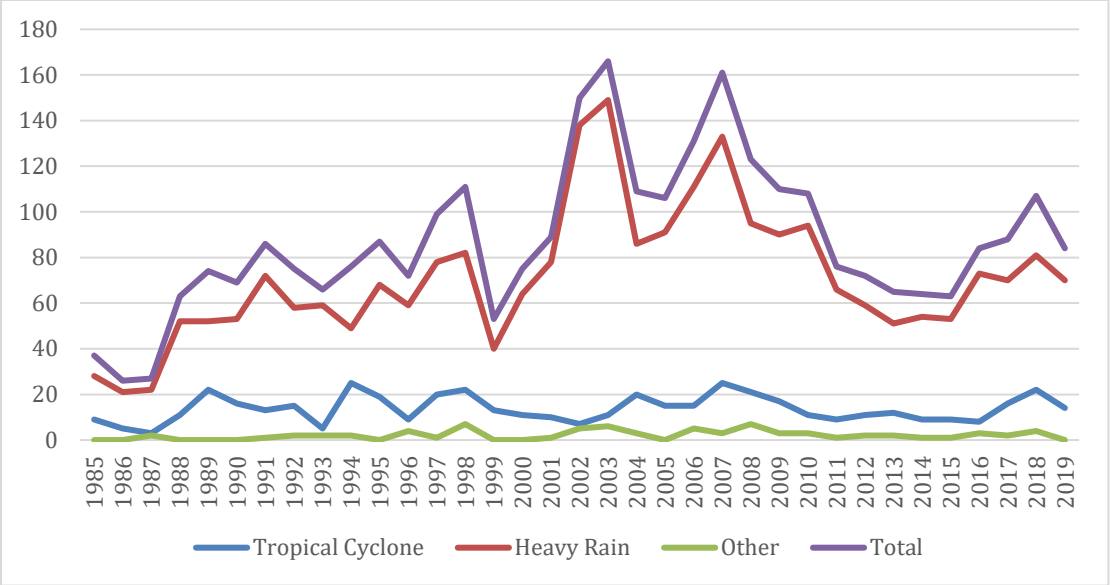

Figure 1.10. Number of coastal floods with different causes (Data Source: Global Active Archive of Large Flood Events)

By above literature review, there is no definitive evidence about increasing trend in flooding. Accompanying with the difference in representation of flood in hydrological model and hydraulic model, more detailed and multi-view study about coastal flood need to be analyzed. This study aims to answer these questions and shed light on this unresolved topic. We developed coastal compound flood modeling system that can simulate the processes of rainfall with infiltration, upstream discharge, and downstream coastal ocean water level changes as a result of tides, storm surge and sea level rise.

1.4.3 Flood risk studies

Previous studies on flood risk estimation suggest a rising trend of flood risk threatening coastal communities at present and in the future. Both natural and human factors were considered in these studies. Jongman et al. (2012) estimated the economic exposure to pluvial and coastal floods from 1970 to 2050. Exposure refers to the population and value

of assets subject to flooding hazards. Two methods based on population and land use/cover, respectively, were used to estimate a damage caused by 1% annual chance flood. The result of Jongman et al. (2012) suggests that the global economic exposure to the flood was US$46 trillion (by population) /US$27 trillion (by land use) in 2010 and will increase to US$158 trillion (by population) / US$80 trillion (by land use) in 2050. In order to gauge flood risk in the future global warming environment, Hirabayashi et al. (2013) estimated global flood risk based on 11 climate models and demonstrated that under high-concentration CO_2 scenarios, flood frequency will increase significantly in Southeast Asia, Peninsular India, Eastern Africa, and Northern Andes, but will decrease in some areas such as the Ob river basin and northern Europe. Global exposure to flooding also increases with global warming (Hirabayashi et al., 2013). They also pointed out that more attention should be paid to coastal communities in lower latitudes, where flood frequency and population are both projected to increase.

Most flood risk estimation studies are conducted on large-scale or global-scale with low resolutions. Therefore, flood-affected areas were estimated through either a simplified relationship between flood area and water depth or rough global model projection. Additionally, human activities are difficult to represent in these low resolution studies. To overcome these deficiencies, a high-resolution local-scale coupled model that can represent multiple natural driving factors, such as hydrological and inundation processes, as well as local human factors such as population and GDP data sets, will be employed in this study.

Moreover, for researchers, current global model predictions and discharge observations

provide only a partial view of flood risk as a natural process. For the public, flood information in the news and other media offers a similarly limited perspective on flood risk, which only represents flooding as a natural hazard. Although some studies indicate rising trends in flooding, these trends are often not found in other studies that use local-scale flood observational records. One of the reasons for these inconsistent and contradictory results is the interchangeable use of the key terms discussed in section 1.2. For instance, floods as natural processes are represented by discharge in model-based studies, whereas floods as hazards and risks are estimated based on observations/records involving human factors. Therefore, to accurately estimate the future flood risks that coastal communities face, it is essential to address the compounding effects on coastal flood risk by considering not only a variety of natural driving factors (such as storms, sea-level rise, and rainfall) but also human factors, such as population and economy.

1.5 Research goal and objective

This study aims to test the hypothesis that human factors can impact present and future coastal flooding risks to coastal communities as much as natural factors and to advance the understanding of coastal compound flood hazards. To achieve this goal, a comprehensive method will be developed to estimate coastal flooding risk. Both natural processes and human-related factors (such as GDP per capita and population density) will be considered and examined to address their impact on coastal flooding risk. This study will follow these three steps to achieve the research goal:

1. Design a modeling framework to simulate coastal compound flooding with representations of both inland river system and coastal processes. Analyze how a

compound flood happen through this modeling framework.

2. Create an indicator to estimate coastal flood risk that reflects the impact of both natural processes and human activities. Test the sensitivity of this indicator to changes in natural and human driving factors such as sea-level, discharge, population density and GDP per capita.

3. Model historical coastal flood events in South Carolina and estimate their flood risk by applying the above modeling framework and flood risk estimation method.

2 Methods and data

2.1 Methods

2.1.1 Flood risk calculation

To quantitatively estimate flood risk, a Flood Risk (FR) was defined based on GDP per capita, population density, and flood area as follows:

$$FR = \sum (D \times GDP \times Area) \tag{2.1}$$

where D is the population density, GDP is the gross domestic product per capita, and $Area$ is the flooding area caused by a flood at a certain magnitude (base on return period). For each model run, the flooding area is a certain output variable resulting from a series of model inputs, such as rainfall, sea-level, and discharge. The physical meaning of FR is the GDP affected by a flood event with a certain flood magnitude. As a common indicator, GDP is widely used in evaluating economic estimation. It is a convenient way to evaluate the damage of floods worldwide through GDP since GDP is relatively easy to obtain. By the definition of FR, flood risk is a result of both natural factors and human factors in a flood event.

2.1.2 Models

In this study, the National Water Model (NWM) hydrological model and the Regional Ocean Modeling System (ROMS) ocean model were coupled with an inundation model (TELEMAC-2D) to simulate discharge, water depth and flooding area in the coastal region

(Figure 2.1). TELEMAC-2D is the central component of the modeling system. Since the accuracy of the inputs is crucial for the reliability of the results, we attempted to use the discharge from United States Geological Survey (USGS) gauge stations for all the river inlets. Unfortunately, due to limited availability of observational data, we were only able to use discharge data from two USGS gauge stations for two of the river inlets, while for the remaining inlets, we had to rely on discharge simulated from the NWM.

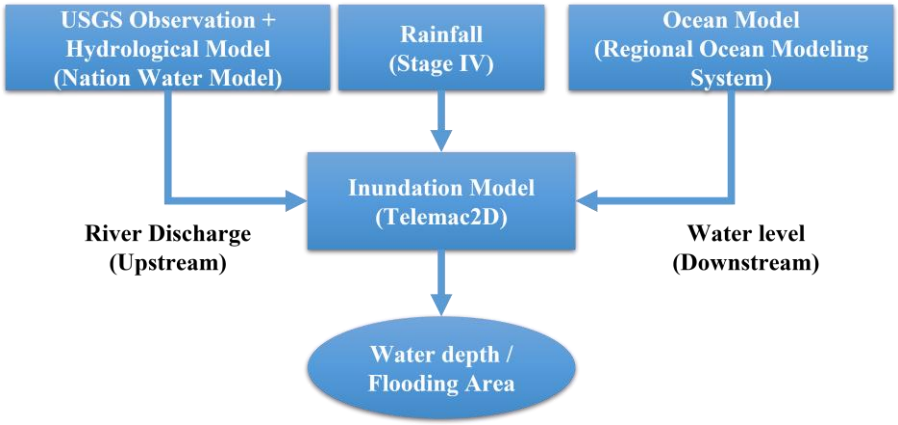

Figure 2.1. Model structure. River discharge from USGS observation and inland hydrological model NWM, water level from the coastal ocean model ROMS, and rainfall from observation were fed into the inundation model TELEMAC-2D. Discharge, water depth/level and flooding area were simulated.

2.1.2.1 Inundation model TELEMAC-2D

TELEMAC-2D is an integrated suite of solvers for studies about free-surface flow containing the modules SISYPHE, NESTOR, TOMAWAC, ARTEMIS, MASCARET, TELEMAC-2D, and TELEMAC-3D. TELEMAC-2D is a module for estimating free-surface flow with two horizontal dimensions, which is employed in the thesis for modeling 2D-inundation of coastal flooding. This module uses an unstructured finite-element mesh and two

horizontal components of velocity to calculate the depth of water at each point. Basically, the TELEMAC-2D module solves two-dimensional Navier-Stokes equations, written as:

$$\frac{\partial h}{\partial t} + \mathbf{u} \cdot \nabla h + h \cdot \nabla \mathbf{u} = S_h \quad (2.2)$$

$$\frac{\partial u}{\partial t} + \mathbf{u} \cdot \nabla u = -\mathrm{g}\frac{\partial Z}{\partial x} + \frac{1}{h}\nabla(h v_t \nabla u) + S_x \quad (2.3)$$

$$\frac{\partial v}{\partial t} + \mathbf{u} \cdot \nabla v = -\mathrm{g}\frac{\partial Z}{\partial y} + \frac{1}{h}\nabla(h v_t \nabla v) + S_y \quad (2.4)$$

$$\frac{\partial T}{\partial t} + \mathbf{u} \cdot \nabla T = \frac{1}{h}\nabla(h v_T \nabla T) + S_T \quad (2.5)$$

where h is the depth of water (unit: m); u, v are the velocity components of vector **u** (unit: m/s); T is a passive (non-buoyant) tracer, which can be water temperature (unit: g/l or ℃); g is gravity (unit: m/s^2). T, h, u, v are unknowns that need to be solved through these equations. v_t, v_T are the momentum and tracer diffusion coefficients (unit: m^2/s), which are 10^{-6} m^2/s as default constant value. Z is free surface elevation (unit: m). t is time (unit: s). x and y are the horizontal space coordinates (unit: m). S_h and S_T are the source/sink terms of fluid and tracer respectively. S_x and S_y are source terms representing the wind, Coriolis force, and bottom friction.

TELEMAC-2D uses a rainfall-runoff model developed by the US Soil Conservation Service (SCS) to calculate runoff potential, which means surface runoff. The runoff potential in the SCS model is defined by a unique parameter called Curve Number (CN), which is a function of hydrological soil groups, land use/cover, hydrologic surface condition of native pasture, and antecedent moisture conditions (Chow et al., 1988). In theory, CN values range from 0 to 100. For impervious and water surfaces, the CN value is 100, which means

all rain that falls on the ground becomes surface runoff. In my thesis, a lookup-table method, which is based on the results of a global CN number estimation using satellite and geospatial data (Hong & Adler, 2008), is applied for assigning CN value. The CN method is described as:

$$P = I_a + F + \mathrm{R} \tag{2.6}$$

$$\frac{R}{P - I_a} = \frac{F}{S} \tag{2.7}$$

$$I_a = \lambda S \tag{2.8}$$

$$\mathrm{S} = \frac{25400}{CN} - 254 \tag{2.9}$$

where P is total rainfall (mm), R is direct surface runoff (mm), F is the actual infiltration (mm), S is the amount of the potential maximum retention (mm), λ is initial abstraction coefficient, $I_a$is initial abstraction, and CN is curve number. In reality, the surface runoff is also influenced by the soil moisture condition. In my thesis, Antecedent Moisture Conditions were considered for the determination of λ in each model run.

TELEMAC-2D has supported the Soil Conservation Service Curve Number (SCS-CN) method since 2013. The SCS-CN is a widely used calculation method for determining effective rainfall formation based on precipitation and area-specific runoff factors. With this feature, runoff generation is linked to overland flow, allowing TELEMAC-2D to be extended to a Hydrodynamic Rainfall-Runoff Model.

2.1.2.2 Hydrological model WRF-Hydro (NWM)

The NWM is a hydrologic modelling framework that simulates observed and forecast streamflow over the entire continental United States. The NWM simulates the water cycle

with mathematical representations of the different processes and how they fit together. This complex representation of physical processes such as snowmelt, infiltration and movement of water through the soil layers varies significantly with changing elevations, soils, vegetation types and a host of other variables. Overall, NWM provide a relatively reasonable production of streamflow currently. The current NWM framework was established based on the Weather Research and Forecasting Model Hydrological modeling extension package (WRF-Hydro).

WRF-Hydro is a physics-based distributed hydrological model with a representation of groundwater flow processes (Gochis et al., 2015). Three main components are used in the WRF-hydro system: column land surface models, terrain routing modules, and channel and reservoir routing modules (Figure 2.2). First, the one-dimensional Noah land surface column model or Noah land surface model with multi-parameterization options (Niu et al., 2011) driven by atmospheric forcing data, calculates soil states and fluxes, including soil moisture, evapotranspiration, and vertical water motion (such as infiltration and exfiltration). Atmospheric forcing includes rain rate, shortwave, and longwave radiations, surface pressure, near-surface wind, specific humidity, and temperature. Second, the distributed terrain routing module uses output from the land surface model to calculates variables related to overland flow and subsurface flow, including stream inflow (lateral inflow), surface water depth, groundwater depth, and soil moisture. Two-way coupling is used to communicate between the land surface model and terrain routing modules. Finally, channel & reservoir routing modules calculate streamflow, flow velocity, and

other variables. One-way coupling is used to communicate from terrain routing to channel reservoir routing.

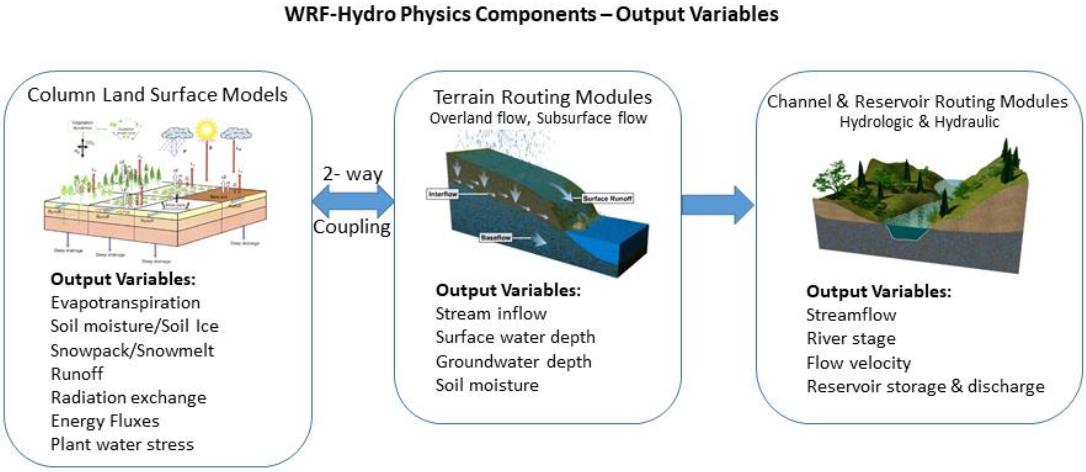

Figure 2.2. Three components of WRF-Hydro. Column land surface models (left), Terrain routing Modules (middle), Channel and reservoir routing modules (right). Two-way coupling is used between column land surface models and terrain routing modules while one-way coupling is used between terrain routing modules and channel & reservoir routing modules.

The Saint-Venant Equation, a one-dimensional simplified Navier-Stokes equation is used to govern overland routing and river channel routing as grided routing. The equation is as follows:

$$\frac{\partial A}{\partial t} + \frac{\partial Q}{\partial x} = 0 \tag{2.10}$$

$$\frac{\partial Q}{\partial t} + \frac{\partial (Q^2/A)}{\partial x} + \mathrm{gA}\frac{\partial H}{\partial x} + \mathrm{gA}S_f = 0 \tag{2.11}$$

where x is distance, t is time, A is flow cross-sectional area, Q is flow rate, S_f is friction slope, g is acceleration of gravity, and H is hydraulic head of water in the conduit. $H =$

$Z + Y$, where Z is conduit invert elevation, and Y is conduit water depth. The first two terms of Eq. 2.11 are ignored in WRF-Hydro, which makes the calculation as simple as calculating diffusive waves.

In the NWM, the Muskingum-Cunge method is applied to represent river channel routing as linked routing across the continental United States. WRF-Hydro utilizes a standard implementation of the Muskingum-Cunge method for hydrograph routing, which makes use of time-varying parameter estimates. The scheme is a practical approach to characterizing watershed runoff characteristics over large networks and extensive watershed flow integration. As a one-dimensional explicit scheme, it does not account for backwater. Channel flows are routed from upstream to downstream in a cascading routing manner, with the assumption that there are negligible backwater effects. The "no backflow" assumption may not always be appropriate, particularly for coastal regions.

Additionally, a conceptual baseflow (groundwater flow) model, usually named “bucket model,” is employed in WRF-Hydro. In this model, groundwater flow is a function of water depth in the “bucket” at each subbasin, which represents the water storage capacity of the subbasin. Due to limited knowledge, groundwater flow in the hydrological model is often treated as a black box. However, it is a crucial component that significantly contributes to river channel routing and cannot be ignored. Therefore, accurately estimating the parameter related to this bucket model is essential for obtaining reliable discharge outputs.

2.1.2.3 Ocean model ROMS

ROMS is a free-surface, terrain-following, primitive equations ocean model widely used by the scientific community for a diverse range of applications. In the vertical, the primitive equations are discretized over variable topography using stretched terrain-following coordinates. The stretched coordinates allow increased resolution in areas of interest, such as thermocline and bottom boundary layers. In the horizontal, the primitive equations are evaluated using boundary-fitted, orthogonal curvilinear coordinates on a staggered Arakawa C-grid.

2.1.3 Study Area

The Northeastern coast of South Carolina was selected as the study domain in my thesis (Figure 2.3). Three rivers enter this region and eventually reach the adjacent Atlantic Ocean. The area belongs to the coastal plain of South Carolina (as mentioned in Section 1.3.4) and is affected by hurricanes and storms from the North Atlantic Ocean almost every year during the early autumn.

Two USGS stations (id: 02145200 and 02110704) provided discharge as TELEMAC-2D model input. To validate the model, water level from five USGS stations (id: 02110815, 021108125, 02110802, 02110725, and 02110777) and one NOAA station (id:8661070) in the domain were utilized.

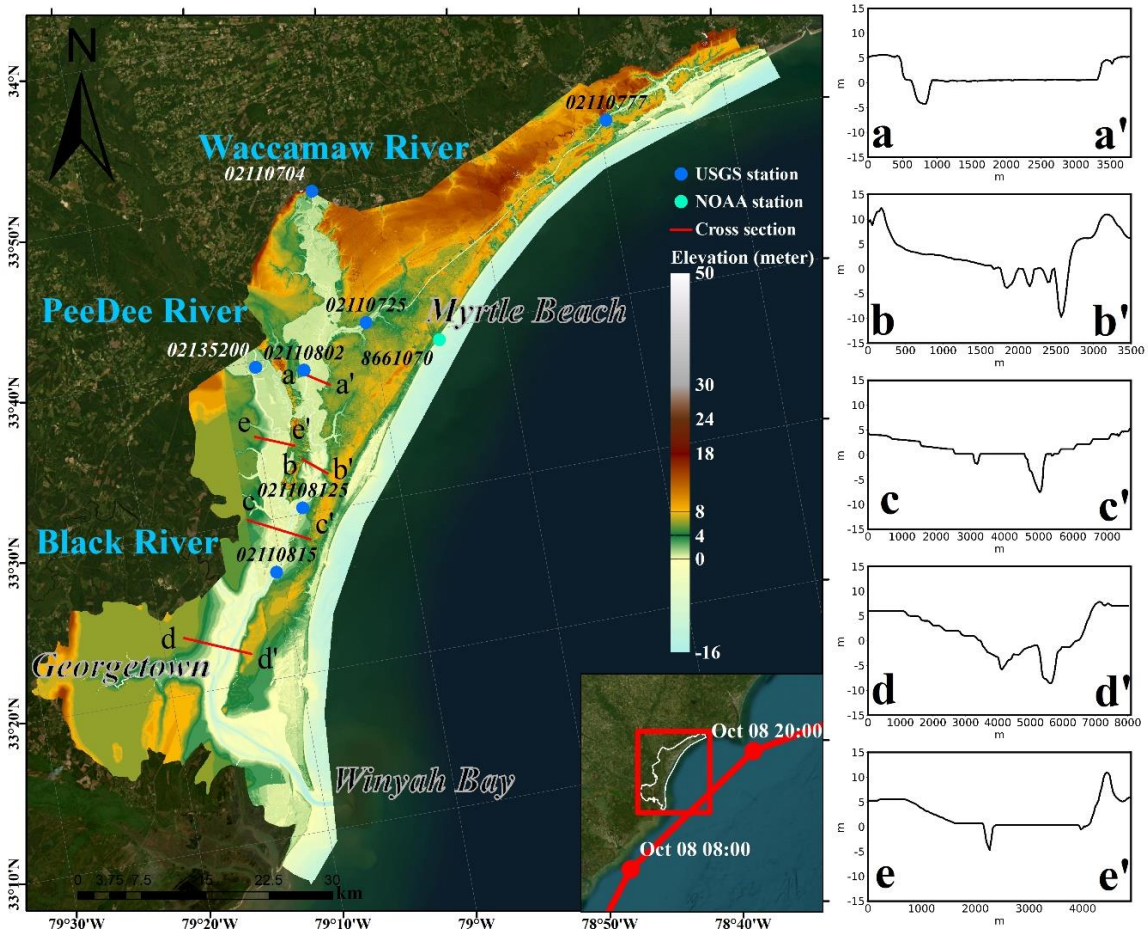

Figure 2.3. The domain of simulation. Three rivers (the Waccamaw, Pee Dee, and Black) enter this region and flow into the Atlantic Ocean at Winyah Bay. Two USGS stations (id: 02145200 and 02110704) provided discharge as TELEMAC-2D model input. There are five USGS stations (id: 02110815, 021108125, 02110802, 02110725, and 02110777) and one NOAA station (id:8661070) in this area that can be used for water level validation. Negative topography indicates the bathymetry of river channels and coastal oceans. The path of Hurricane Matthew is shown in the inset figure. Five cross sections (aa' to ee') were selected to check the river discharges. The bathymetries of these five cross sections are shown in the right panels.

2.1.4 Model validation

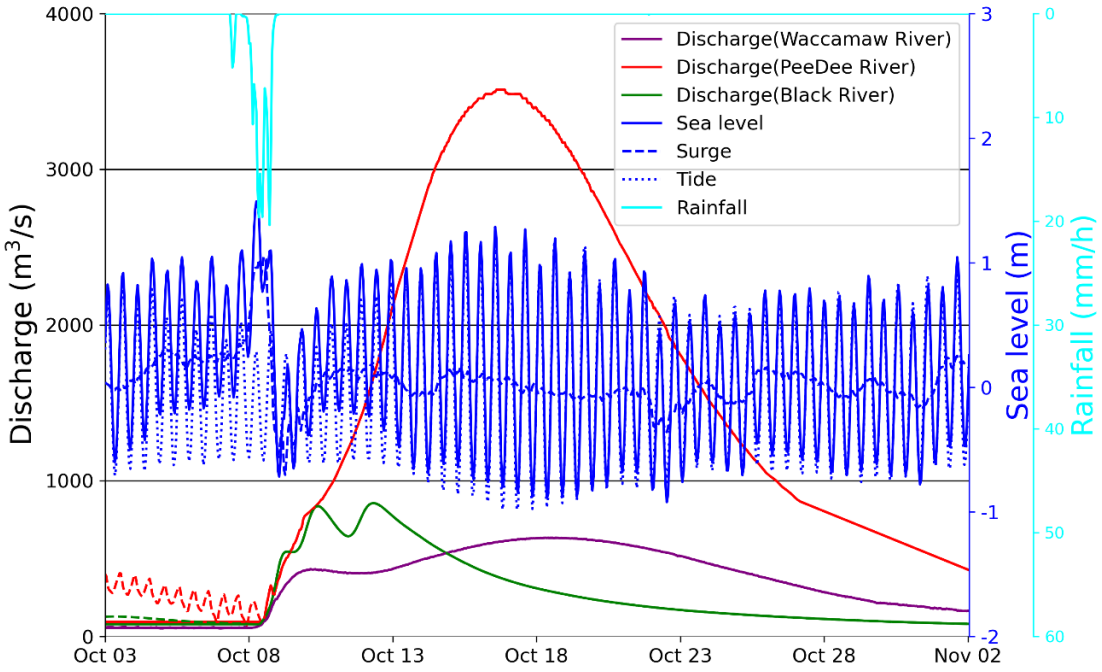

Figure 2.4. Model inputs for 2016 Hurricane Matthew event: Time series of river discharge from Waccamaw (purple line), PeeDee (red line), and Black Rivers (green line), sea level at seaside (solid blue line), storm surge (dashed blue line), tide (dotted blue line), and domain averaged rainfall (cyan line). The discharge input (dashed red, purple, and green lines) before Oct 08 shows a decreasing trend. A slight adjustment was made by removing the decreasing trend from the discharge input (solid red, purple, and green lines). This made the compound effect caused by the interaction between discharge, tide, and surge more straightforward to assess.

Hurricane Matthew, which occurred in 2016, was selected as the primary case for model validation. Hurricane Matthew was an extremely powerful hurricane that made landfall in South Carolina on October 8th, 2016 and caused widespread damage to the southeastern US. The combination of storm surge inundation and inland flooding left

more than 1 million structures damaged and cost approximately 10.3 billion US dollars. USGS recorded 112 high-water marks at flooded locations in the study area during and after Hurricane Matthew. To validate the inundation model, I assessed its performance in two aspects: flood extent and water level/depth, utilizing data from both USGS and NOAA stations in the area.

Figure 2.4 shows the characteristics of the input data to TELEMAC-2D for the 2016 Hurricane Matthew event. The storm rainfall in the study area began after October 7th, 2016 and peaked around October 08, 2016, exceeding the 10% annual chance rainfall, as estimated from the Stage IV history data. On October 9th, 2016, the abnormal sea level rise was observed due to the storm surge, which occurred slightly later than the storm rainfall. It is noteworthy that the storm surge coincided with the neap tide. The spring tide arrived around October 18th, 2016, and dominated the sea level change immediately. With regard to the upstream discharge, the peaks from the three rivers arrived about two days later compared to the storm surge and rainfall, with significant differences in their magnitudes. The PeeDee River had a much higher upstream discharge, exceeding 3500 m^3/s, which is near a magnitude of 5% of the annual chance discharge based on estimates from the USGS long term observation. The Waccamaw River had relatively smaller peak discharge than the PeeDee River, but still reached the level of discharge of 5% of the annual chance. The large upstream discharges were reasonable given that most of the storm rainfall over the period October 4th to October 25th, 2016, fell onto the PeeDee and Waccamaw River basins (Figure 2.4). In contrast, upstream discharge from the Black River was relatively small, falling between the magnitudes of its

discharge of with 10% and 5% of annual chances. The discharge input before October 8th showed a decreasing trend, which introduced uncertainty in calculating the compound effect in the discussion section. To fix the issue, a slight adjustment was made by removing the decreasing trend from the discharge input. As a result, the compound effect caused by the interaction between discharge, tide, and surge was more straightforward to assess. To clarify, the model runs without any modification to the discharge inputs were used for validation purposes (Section 2.1.4), whereas the subsequent model runs with modified discharge inputs were used to examine the individual and combined effects of various natural factors (Section 3.1).

2.1.4.1 Flood extend validation

Figure 2.5 shows the results of the model validation with high water marks (HWM) for the flooded areas. During and after the storm, USGS recorded 112 HWMs at flooded locations in the study area. However, due to the 100-meter spacing of the computation grid and the 0.01-meter water depth threshold used for extracting water surface, there were some bias in the location of the HWMs compared to the water surface area produced by the coupled model. To validate the flooding area, we applied a wider range of HWM locations. This involved considering cells within one or two cell distances of the HWMs. A '1 cell range' ('2 cell range') means considering cells near a HWM within one (two) cell distance. If at least one nearby cell was wet, we considered the HWM to be simulated. With the '1 cell range' applied, the model was able to simulate all but four of the HWMs, resulting in an accuracy of 96.4%. With a '2 cell range' applied, all HWMs except one of the HWMs were simulated as flooded by TELEMAC-2D during the study period, yielding an accuracy

of 99.1%.

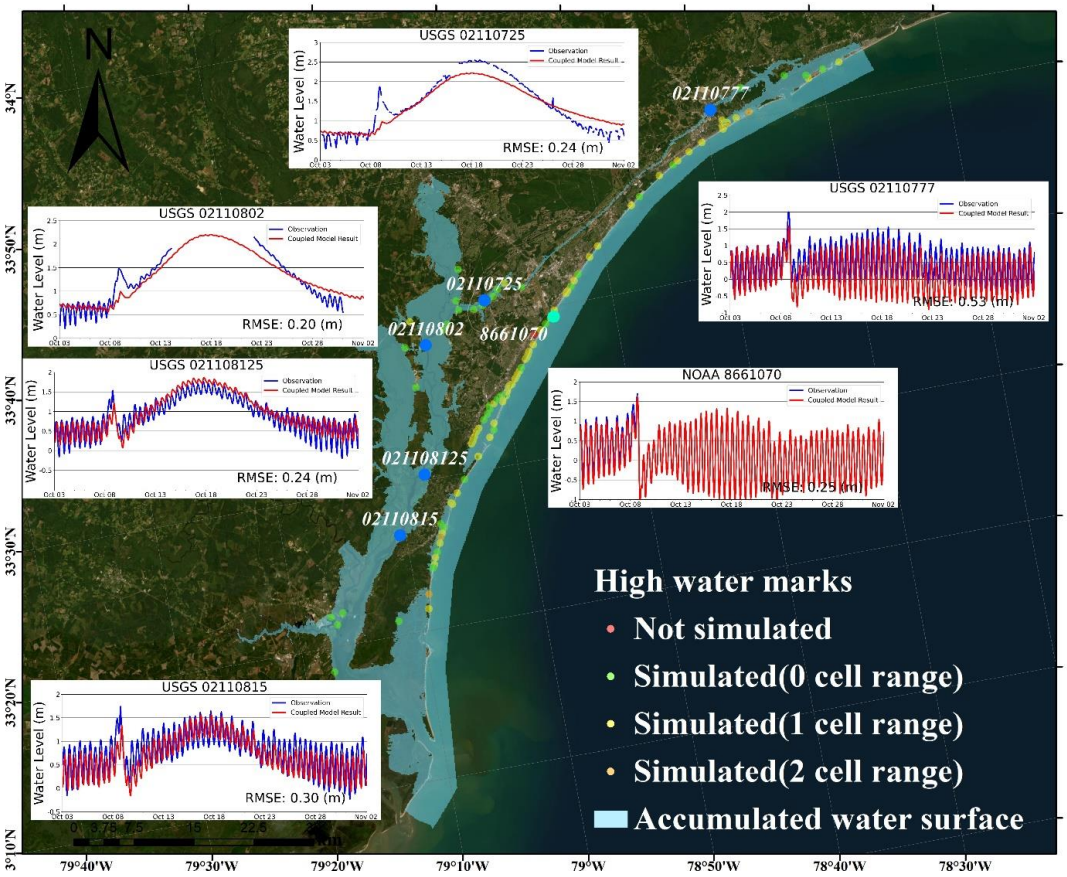

Figure 2.5. Model validation for water level and flooding area: Time series of sea level result from TELEMAC-2D (blue) and sea level observation from USGS and NOAA stations (lines). During and after Hurricane Matthew, the observed high-water marked locations compared with the model-simulated flooded areas were shown in the map. The light blue color represents the accumulated water surfaces during the simulation period, including both the flooded area and the permanent water surface. The USGS recorded high-water mark locations are indicated by dots with different meanings: green dots represent a simulated observation within 0 cell range, yellow dots represent a simulated observation within 1 cell range, orange dots represent a simulated observation within 2 cell range, and red dots represent locations that were not simulated.

2.1.4.2 Water level/depth validation

Figure 2.5 also shows the model validation with USGS and NOAA stations for the water level. The coupled model result was found to fit relatively well with the USGS and NOAA observations. The root mean square errors (RMSEs) were 0.23m, 0.18m, 0.24m, 0.29m, and 0.51m for the five USGS stations. However, the NOAA verified water level observations were missing from October 8th, 2016 to December 15th 2016, possibly due to storm damage. Hence, we only compared the water level data from October 4th, 2015, to October 8th, 2015. The TELEMAC-2D simulated water level agreed well with the NOAA observations, with an RMSE of only approximately 0.08m.

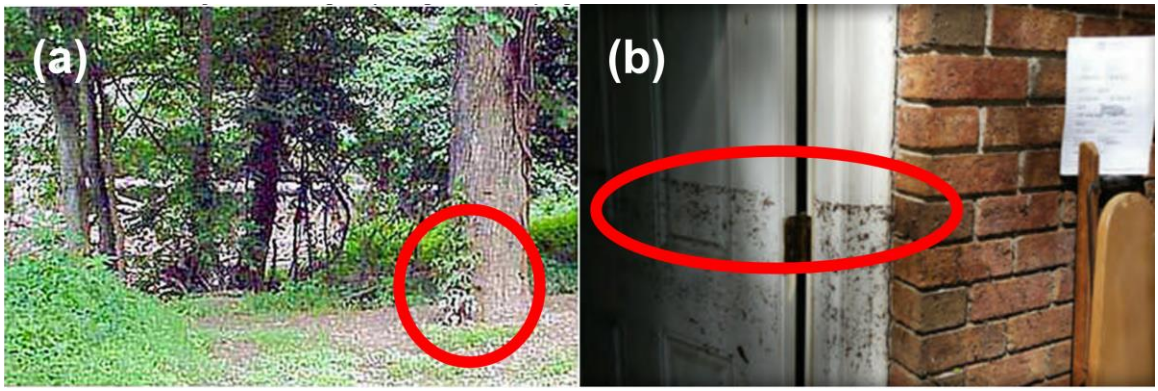

Figure 2.6. High Water Mark (HWM) example from USGS website (https://www.usgs.gov/special-topics/water-science-school/science/high-water-marks-and-flooding, accessible in March 2023). a) Line of dried mud on poison ivy; b) High-water mark from the October 2015 flooding in Columbia, South Carolina.

For the water depth validation with HWMs, the validation process is slightly more complicated. HWMs (Figure 2.6) provide physical evidence of the water level that occurred during a flood event. They are typically left by debris, stains, or damage caused

by the floodwaters. USGS conducts post-flood field investigations to document these HWMs in order to provide valuable information for floodplain mapping, calibrating flood models, and understanding the impacts of flooding. Two key features of HWMs are important for water depth validation:

1) The HWM is the minimum value of the maximum water level in one region during a flood event. The actual water level could be higher.
2) The time of flagging and surveying the HWMs is not the time when the HWMs were formed, as the HWM formation time may have occurred earlier.

Thus, to validate water depth with HWMs, the process was as follows: First, search for water depth within a 1 cell range before the HWM survey date. Then, find the highest water depth for each cell. Finally, use the cell where the highest water depth is closest to the "height above ground" provided by the HWM to validate water depth. The water depth validation with HWMs is shown in Figure 2.7, which indicates a relatively strong positive correlation between the coupled model result and HWM observations, with a correlation coefficient of 0.38. By excluding two abnormal model outputs, the correlation coefficient increases to 0.88.

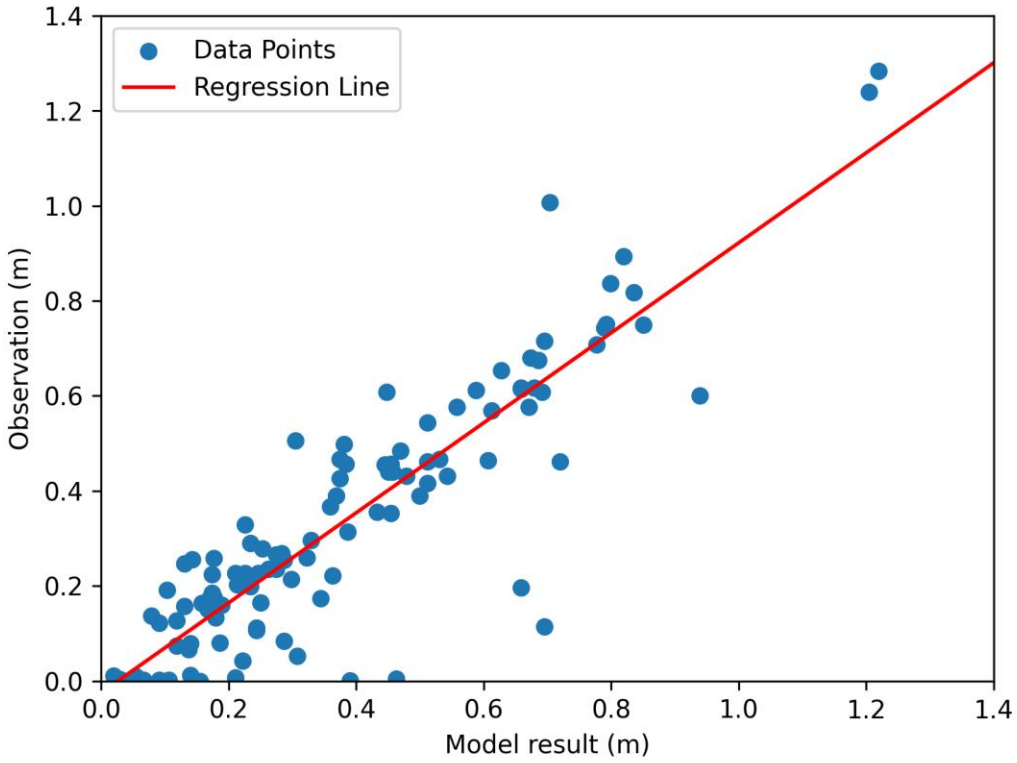

Figure 2.7. Water depth validation with HWMs.

2.1.5 Experimental design

2.1.5.1 Coastal compound flood analysis

To analyze the contributions of four natural factors - upstream discharge, local rainfall, tides, and storm surge - to coastal flooding, we designed a series of model simulations with different input settings (Table 2.1). We selected the flood event triggered by Hurricane Matthew in 2016 as our case study and used the same model inputs as those utilized for the TELEMAC-2D validation section (Figure 2.4), with one exception that the initial decrease in upstream discharge prior to its peak was modified to a constant value. This modification was crucial to reduce uncertainty in the compound effect analysis and to make the compound effect clearer.

Table 2.1 Experimental design for testing the contribution of river discharge, rainfall, and sea level to coastal flooding.

EXP	Upstream discharge	Local Rainfall	Sea level		Note
			Tide	Surge	
1	X	X	X	X	Control
2	O	O	O	O	Reference
3	X	O	O	O	Impact of individual factors
4	O	X	O	O	
5	O	O	X	O	
6	O	O	O	X	
7	X	X	O	O	Impact of 2 factors
8	X	O	X	O	
9	X	O	O	X	
10	O	X	X	O	
11	O	X	O	X	
12	O	O	X	X	
13	O	X	X	X	Impact of 3 factors
14	X	O	X	X	
15	X	X	O	X	
16	X	X	X	O	

Here were the steps to set up the model simulations (Table 2.1). Firstly, we ran a control simulation (EXP1) using the upstream discharge, local rainfall, tides, and storm surge observed during Hurricane Matthew. A five-day simulation was used as a spin-up period to establish a relatively steady initial condition, which was also applied to the rest of the model runs. The discharge inputs for the spin-up and at the beginning of EXP1 were constant. Subsequently, a reference simulation (EXP2) was run using constant discharge identical to the spin-up, zero rainfall and a constant sea level, indicating no tide or storm surge. The water surface from this idealized steady scenario (EXP2) was then be used as the permanent water surface, and the differences in water surface area between other experiments and the reference simulation were used to calculate the flooding area.

Then three groups of experiments were performed to test the individual effect of each factor and the compound effects of two or three factors. Simulations from EXP3 to EXP6 examined the impacts of single factors including upstream discharge, local rainfall, tide, and storm surge, respectively. EXP7 to EXP12 assessed the impacts of two factors in various combinations, while EXP13 to EXP16 investigated the impacts of three factors in various combinations.

2.1.5.2 Flood risk sensitivity test

The flood risk sensitivity test examines the sensitivity of flood risk to changes caused by different factors. The analysis of coastal compound flooding (elaborated in the discussion section) revealed that coastal flooding occurrence is heavily dependent on the magnitude and timing of peak upstream discharge and peak storm surge. Therefore, the flood risk sensitivity test is designed to evaluate how extreme upstream discharge and storm surge influence coastal flood inundation. Additionally, long-term sea level rise, population and GDP per capita which were used to calculate flood risk as defined in Section 2.1.1, are also considered in this sensitivity test. However, to conduct the sensitivity test, several problems need to be solved.

The first problem is how to compare different factors with different units. For example, river discharge values range from hundreds to thousands of cubic meters per second, while sea level change values, including storm surge and long-term sea level rise, are only within a few meters. By designing sensitivity with actual numbers, the result will be hard to reflect the reality. In order to make the comparison more meaningful, the annual chance, generally known as the return period, was utilized in my thesis. Extreme value

estimation was applied to obtain the extreme upstream discharge and extreme storm surge with certain annual chances, including 1% (1-in-100 years), 2% (1-in-50 years), 5% (1-in-20 years), and 10% (1-in-10 years).

The second problem is how to modify the discharge and storm surge with extreme value estimates. Based on the coastal compound flooding analysis (detailed in the discussion section), the timing of different factors is critical in producing coastal compound flooding. Multiplying the time series data by the extreme values is not appropriate due to the bias introduced by large values occurring at an early stage. For example, with upstream discharge, simple multiplication might cause a relatively large discharge to occur before the peak discharge comes. This relatively large discharge could interact with topography settings before the real discharge peaks, adding complexity to the result analysis. Therefore, a curve fitting method is used to obtain a formula to represent the time series discharge and storm surge, making the analysis of coastal flood risk more straightforward.

The last problem is about interpreting the physical meaning of each factor in the sensitivity test comparison. Upstream discharge and storm surge are addressed with different annual chances, while long-term sea level rise values correspond to potential sea level rise at the end of the 21st century with different RCP projections. For population growth and GDP increase, the yearly change rate represent the change. The detailed factors in this sensitivity test include:

1) Upstream discharge magnitude with a certain annual chance.
2) Storm surge height with a certain annual chance.
3) Sea level rise prediction by the end of this century with different RCPs projection.

4) Annual population growth rates.

5) Annual GDP increase rates.

My thesis aims to fairly compare the roles of the above five factors, avoiding bias due to their different physical meanings. As all these factors are related to a year, the comparison would be more meaningful and valuable.

2.1.5.2.1 Upstream discharge simplification

Figure 2.4 shows the model inputs for Hurricane Matthew in 2016. The Waccamaw River and the Pee Dee River inlets data is from USGS gauge stations, while the Black River inlet data is from NWM reanalysis dataset. Examining the upstream discharge patterns for the three river inlets during the hurricane, it reveals that the discharge remained at a relatively steady level before the hurricane. However, it increased rapidly to the peak value and then gradually decreased. Since the shape of these lines resembles an exponential function, the upstream discharge time series was defined as follows:

$$Discharge = Magnitude \times e^{\left(\frac{-(\log X-\mu)^2}{2\cdot\sigma^2}\right)} + Baseflow \qquad (2.12)$$

where X is the time step number (starting from 1) with a one-hour time interval, μ represents the location parameter, and σ represents the scale parameter. Magnitude is defined as the peak discharge value during a single flood event, while baseflow refers to the steady flow before a flood event. Baseflow remains fixed for the three rivers. The parameters μ and σ were used for curve fitting, and by changing the magnitude to the peak discharge with a certain annual chance, specific extreme discharge lines with a certain annual chance can be obtained.

The calculated fitting parameters for three river inlets are in Table 2.2:

Table 2.2 Fitting parameters for discharge simplification of three river inlets

	μ	σ	$Baseflow(m^3/s)$
Waccamaw River	5.11	0.85	50
Pee Dee River	5.22	-0.54	100
Black River	4.11	0.89	70

With these fitter parameters, the formulas for three river discharge time series are as follows: Waccamaw River (equation 2.13), Pee Dee River (equation 2.14), and Black River (equation 2.15).

$$Discharge = Magnitude \times e^{\left(\frac{-(\log X - 5.11)^2}{2 \cdot 0.85^2}\right)} + 50\ m^3/s \quad (2.13)$$

$$Discharge = Magnitude \times e^{\left(\frac{-(\log X - 5.22)^2}{2 \cdot 0.54^2}\right)} + 100\ m^3/s \quad (2.14)$$

$$Discharge = Magnitude \times e^{\left(\frac{-(\log X - 4.11)^2}{2 \cdot 0.89^2}\right)} + 70\ m^3/s \quad (2.15)$$

2.1.5.2.2 Storm surge simplification

As a kind of wave, storm surge was defined as:

$$Surge = Magnitude \times sin\ (2\pi X/Period) \quad (2.16)$$

where X is the time step number, starting from 1 with a one-hour time interval. The magnitude is defined as the peak water level value during a single flood event, while the period refers to the duration of the storm surge in Hurricane Matthew, which is about 80 hours. Then, the equation 2.16 were rewritten as:

$$Surge = Magnitude \times sin\ \left(\frac{X}{11.5\ \mathrm{hr}}\right) \quad (2.17)$$

2.1.5.2.3 Extreme value estimation

The Generalized Extreme Value (GEV) distribution method is often used in hydrology and climatology to model the distribution of extreme events. For example, it can be used to estimate the return period of floods or droughts, which is the expected time intervals between events of a given magnitude. In my thesis, GEV was used to estimate extreme values for upstream discharge and storm surge height. The GEV distribution is characterized by three parameters: location parameter (μ), scale parameter (σ), and shape parameter (ξ). The probability density function (PDF) of the GEV distribution can be expressed as:

$$f(Y,\mu,\sigma,\xi) = \frac{1}{\sigma}\left[\left(1+\xi\left(\frac{\mathrm{Y}-\mu}{\sigma}\right)\right)^{-1} - \frac{1}{\xi}\right] e^{-(1+\xi(\frac{\mathrm{Y}-\mu}{\sigma}))^{-\frac{1}{\xi}}} \qquad (2.18)$$

where Y represents a random variable, such as flood magnitude. The location parameter (μ) determines the peak of the distribution, while the scale parameter (σ) determines the spread of the distribution. Lastly, the shape parameter (ξ) defines the shape of the distribution.

The length of data used for extreme value estimation is critical. The record for PeeDee River inlet (USGS station 02135200) spans only 22 years, from 2001 to the present. The Waccamaw River record (USGS station 02110704) covers approximately 29 years, dating from 1994 to the present. There is no data for Black River inlet. By incorporating NWM reanalysis dataset, the data length extends to 44 years, from 1979 to the present. The sea level record form NOAA (id: 8661070) station is from 1979 to the present. Due to data gaps, especially for large surges caused by extreme weather conditions, extreme value

estimations for storm surge may be underestimated. Figures 2.8, 2.9, 2.10, and 2.11 are the results of extreme value estimation. μ, σ, and ξ for the three river inlets and storm surge are provided in Table 2.3.

Table 2.3 Fitting parameters for extreme value estimation of three river inlets and storm surge height

	μ	σ	ξ
Waccamaw River	-0.53	148.36	89.26
Pee Dee River	-0.10	1125.52	642.75
Black River	-0.54	231.77	124.86
Storm Surge	-0.07	1.58	0.13

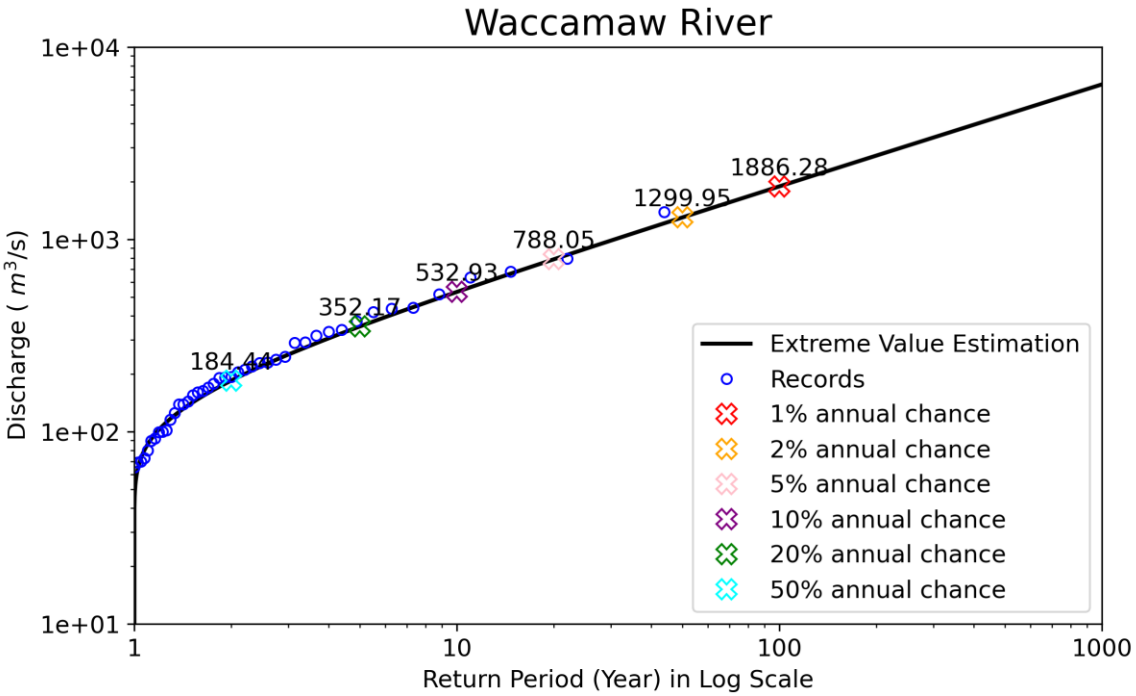

Figure 2.8. Extreme value estimation for Waccamaw River inlet. Data is from NWM and USGS station 02110704 covering a period from 1979 to 2022.

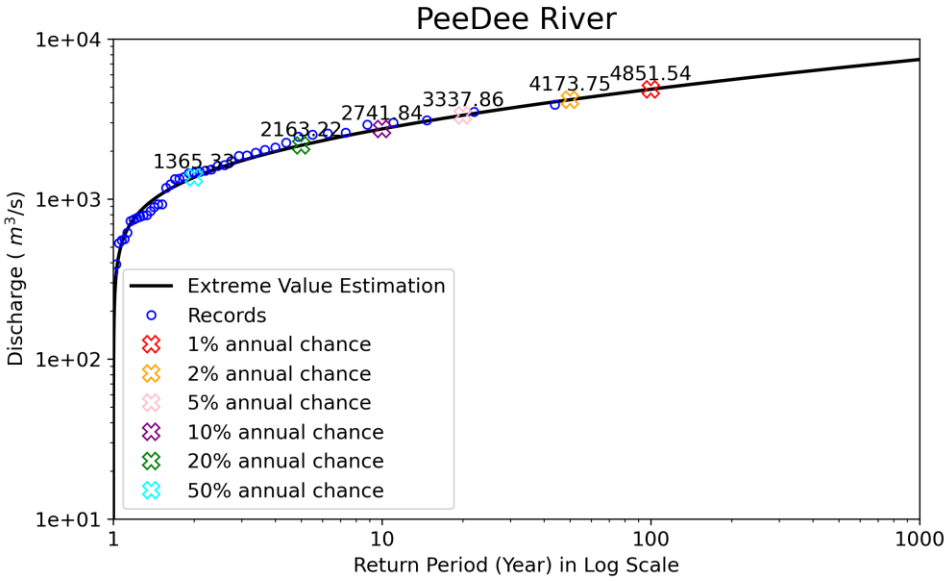

Figure 2.9. Extreme value estimation for Pee Dee River inlet. Data ranges from 1979 to 2022. Data is from NWM and USGS station 02135200.

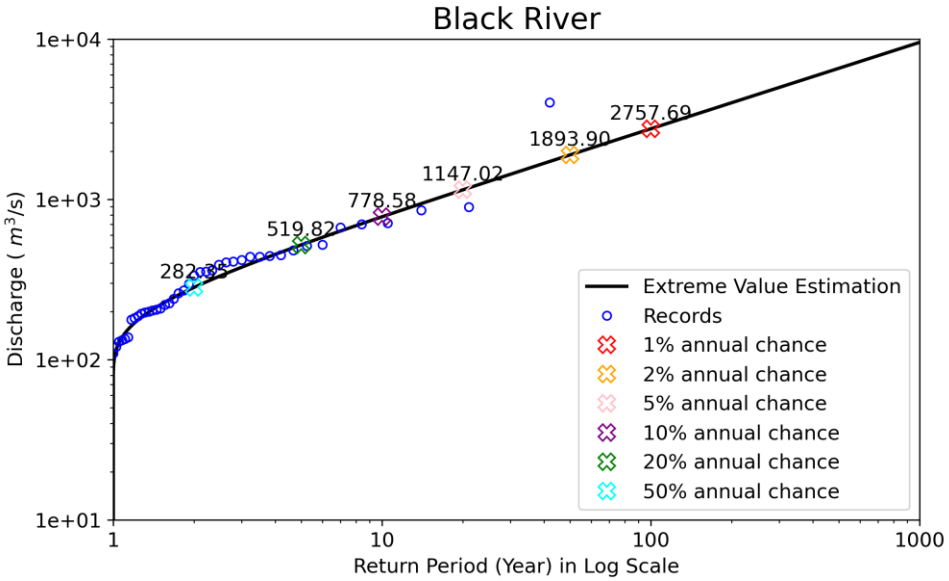

Figure 2.10. Extreme value estimation for Black River inlet. Data ranges from 1979 to 2020. Data is from NWM.

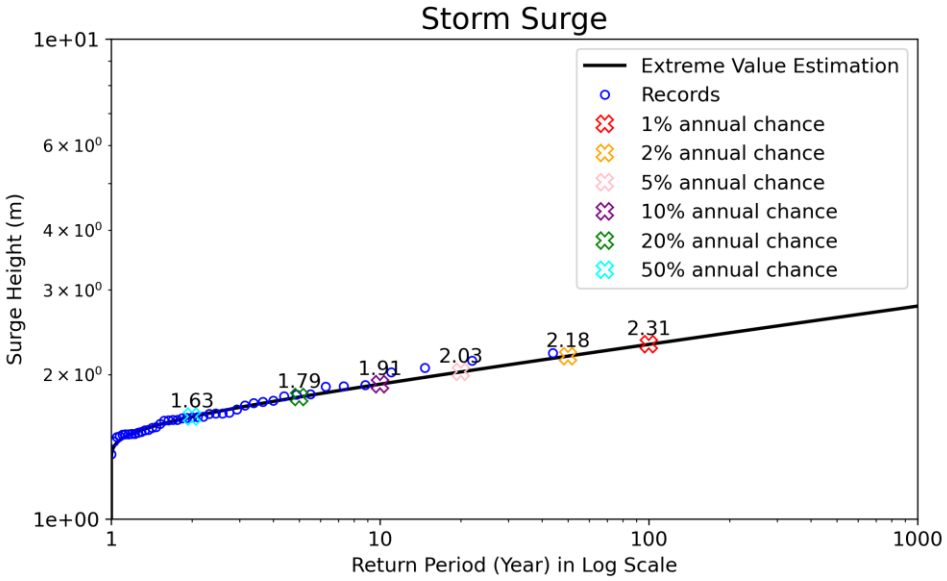

Figure 2.11. Extreme value estimation for storm surge. Data ranges from 1979 to 2022. Data are from NOAA station 8661070.

The term “return period” can be misleading when describing the frequency of flood events. For instance, a 1-in-100 year flood is often considered as a general indicator for flood magnitude. However, rather than happening just once in a 100-year span, a 1-in-100 year flood actually signifies a 1% chance of occurrence in any given year. Based on this calculation, a 1-in-100 year flood has only a 36.97% (Eq. 2.19) chance of occurring once or a 63.40% (Eq. 2.20) chance of occurring at least once in a 100-year period. For clarification, the phrase "annual chance” is used instead to describe the magnitude of a flood throughout the rest of my thesis.

$$P(X = 1) = \binom{100}{1} \times 0.01^1 \times 0.99^{99} \approx 0.3697 \qquad (2.19)$$

$$P(X = 1,2,3 \ldots 98,99,100) = 1 - 0.99^{100} \approx 0.6340 \qquad (2.20)$$

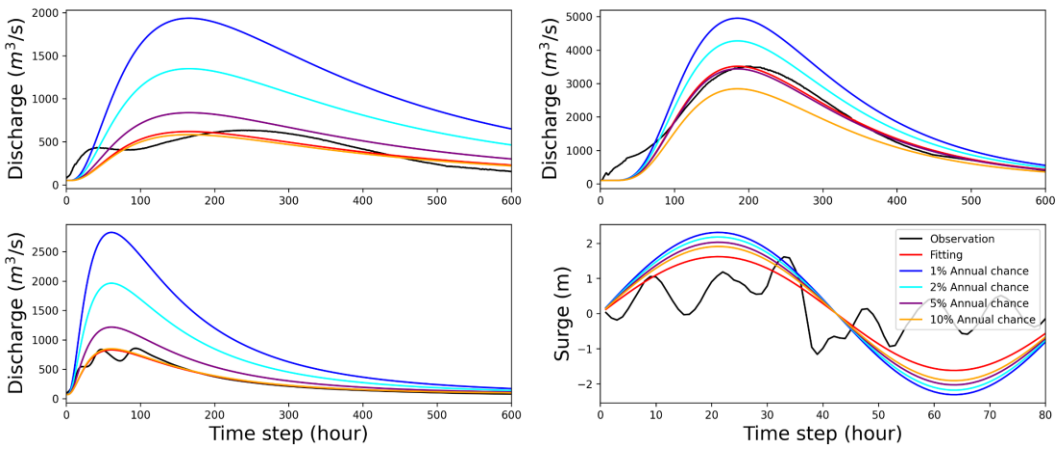

Figure 2.12. Extreme value estimation was applied to upstream discharge and storm surge (surge + tide) data by using observational data, including USGS observation for Waccamaw (a) and Pee Dee (b) Rivers, NWM reanalysis data for Black (c) River, and NOAA observation for storm surge (d), which were used for curve fitting. The black lines in the graphs represent the observational data, while the red lines show the fitting results. The magnitude equations (2.13-2.15,2.17) were modified with specific values related to specific annual chance to create time series of upstream discharge and storm surge. These time series data were used for sensitivity tests. The X axis, representing time step, is different for upstream discharge and storm surge. To ensure consistency in the sensitivity tests, additional modifications were made to align the peaks of each upstream discharge and storm surge.

The estimated extreme values mentioned above are used to set the magnitude in simplified river discharge and storm surge time series data. In this sensitivity test, only 1%, 2%, 5%, and 10% annual chances, which represent extreme events, upstream discharge and storm surge were used. Figure 2.12 shows the result of applying extreme value estimated to upstream discharge and storm surge simplified formulas.

2.1.5.2.4 Sensitivity test design

The primary objective of the sensitivity test is to examine how sensitive the flood risk related to the change in upstream discharge, storm surge, long term sea level rise, population growth, and GDP increase is. The testing process involves the following steps:

1) Set up model runs with different upstream discharge, downstream water levels (including storm surge and long term sea level rise). As summarized in Table 2.4, in total, 64 model runs are simulated.

Table 2.4 Sensitivity test design for upstream discharge, storm surge, and long-term sea level rise comparison.

	Upstream Discharge	Storm Surge	Sea level Rise
Sen_EXP001	1%	1%	0m
Sen_EXP002	1%	1%	0.43m
Sen_EXP003	1%	1%	0.55m
Sen_EXP004	1%	1%	0.84m
Sen_EXP005	1%	2%	0m
Sen_EXP006	1%	2%	0.43m
Sen_EXP007	1%	2%	0.55m
Sen_EXP008	1%	2%	0.84m
Sen_EXP009	1%	5%	0m
Sen_EXP010	1%	5%	0.43m
Sen_EXP011	1%	5%	0.55m
Sen_EXP012	1%	5%	0.84m
Sen_EXP013	1%	10%	0m
Sen_EXP014	1%	10%	0.43m
Sen_EXP015	1%	10%	0.55m
Sen_EXP016	1%	10%	0.84m
Sen_EXP017	2%	1%	0m
Sen_EXP018	2%	1%	0.43m
Sen_EXP019	2%	1%	0.55m
Sen_EXP020	2%	1%	0.84m
Sen_EXP021	2%	2%	0m
Sen_EXP022	2%	2%	0.43m
Sen_EXP023	2%	2%	0.55m

Sen_EXP024	2%	2%	0.84m
Sen_EXP025	2%	5%	0m
Sen_EXP026	2%	5%	0.43m
Sen_EXP027	2%	5%	0.55m
Sen_EXP028	2%	5%	0.84m
Sen_EXP029	2%	10%	0m
Sen_EXP030	2%	10%	0.43m
Sen_EXP031	2%	10%	0.55m
Sen_EXP032	2%	10%	0.84m
Sen_EXP033	5%	1%	0m
Sen_EXP034	5%	1%	0.43m
Sen_EXP035	5%	1%	0.55m
Sen_EXP036	5%	1%	0.84m
Sen_EXP037	5%	2%	0m
Sen_EXP038	5%	2%	0.43m
Sen_EXP039	5%	2%	0.55m
Sen_EXP040	5%	2%	0.84m
Sen_EXP041	5%	5%	0m
Sen_EXP042	5%	5%	0.43m
Sen_EXP043	5%	5%	0.55m
Sen_EXP044	5%	5%	0.84m
Sen_EXP045	5%	10%	0m
Sen_EXP046	5%	10%	0.43m
Sen_EXP047	5%	10%	0.55m
Sen_EXP048	5%	10%	0.84m
Sen_EXP049	10%	1%	0m
Sen_EXP050	10%	1%	0.43m
Sen_EXP051	10%	1%	0.55m
Sen_EXP052	10%	1%	0.84m
Sen_EXP053	10%	2%	0m
Sen_EXP054	10%	2%	0.43m
Sen_EXP055	10%	2%	0.55m
Sen_EXP056	10%	2%	0.84m
Sen_EXP057	10%	5%	0m
Sen_EXP058	10%	5%	0.43m
Sen_EXP059	10%	5%	0.55m
Sen_EXP060	10%	5%	0.84m
Sen_EXP061	10%	10%	0m
Sen_EXP062	10%	10%	0.43m
Sen_EXP063	10%	10%	0.55m
Sen_EXP064	10%	10%	0.84m

2) Combine the flooding area grid with the population density grid by

multiplication. Then, further multiply by the GDP per capita to obtain the flood risk grid. The sum of this grid represents the flood risk as defined in section 2.1.1.

3) Finally, a five-dimensional matrix of flood risk (including discharge, surge, SLR, population, and GDP per capita) is calculated. By the comparison of change rate along each dimension, the sensitivity of flood risk to each considered factor can be determined. The sensitivity indicates the extent to which flood risk is affected by upstream discharge increase, storm surge height increase, sea level rise, population growth, and GDP growth.

2.1.5.3 Historical flood event study

To evaluate the contributions of inland river systems (represented by upstream discharge) and coastal processes (represented by storm surge and tide) to coastal flooding, we conducted a series of model simulations for historical coastal flood events that occurred between 2000 to 2020 (Table 2.5). For each flood event, we designed seven simulations to assess the contributions of upstream discharge, storm surge, and tide to coastal flood risk. These seven simulations included upstream discharge only, storm surge only, tide only, upstream discharge + storm surge, upstream discharge + tide, storm surge + tide, and upstream discharge + storm surge + tide (Table 2.6).

Table 2.5. Coastal flood events happened in northeastern South Carolina (2000 to 2020).

Event Name	Simulation Start	Simulation End	Near Landing Date
KYLE	2002-10-06	2002-11-11	2002-10-11
GASTON&IVAN	2004-08-24	2004-10-02	2004-08-29 & 2004-09-17
HANNA	2008-09-01	2008-10-05	2008-09-06
MATTHEW	2016-10-03	2016-11-06	2016-10-08
FLORENCE&MICHAEL	2018-09-09	2018-11-10	2018-09-14
DORIAN	2019-08-31	2019-09-20	2019-09-05
BERTHA	2020-05-22	2020-06-25	2020-05-27

Table 2.6. Experiments design for each historical flood events

EXP	Upstream discharge	Sea level	
		Tide	Surge
discharge only	X	O	O
tide only	O	X	O
storm surge only	O	O	X
upstream discharge + tide	X	X	O
upstream discharge + storm surge	X	O	X
storm surge + tide	O	X	X
upstream discharge + storm surge + tide	X	X	X

2.2 Data

The quality of input data serves as the foundation for any modeling process. The availability of input data determines whether a modeling process is feasible. Moreover, the spatial and temporal resolution of input data determines the phenomena that can be addressed and analyzed through model results. The accuracy of input data also impacts the validity of model results. This section delves into the data used in my thesis for modeling. However, it is important to acknowledge that the scope of the results and discussions presented is limited by the constraints of the input data.

2.2.1 Topography

The topography and bathymetry data for my thesis were obtained from the Continuously Updated Digital Elevation Model (CUDEM) from National Centers for Environment Information (NCEI), which was developed to improve inundation modeling and mapping, among other purposes. With a resolution of a ninth arc-second (approximately 3 meters), it provides the most accurate topography and bathymetry available for the study area.

The spatial resolution of TELEMAC-2D computation grid used in my thesis is about 100m. We used the GIS techniques to convert CUDEM to a Triangular Irregular Network (TIN) in order to preserve more detailed topography information with fewer points. Then, the nodes of the TIN were used to interpolate the TELEMAC-2D computation grid. Through this pre-processing, the high resolution topography input improves the accuracy of TELEMAC-2D modeling, even though the model computation gird is much larger than the topography input,.

2.2.2 Atmospheric forcing

Rainfall data used in this study is from National Stage IV Quantitative Rainfall Estimates Product (Stage IV). The data is derived from regional hourly or six-hourly multi-sensor (e.g., radar and rain gauges) rainfall analyses, produced operationally by the twelve River Forecast Centers across the continental U.S. at National Centers for Environmental Prediction (Y. Lin, 2011). A domain-averaged rainfall from Stage IV was used as model input for TELEMAC-2D.

2.2.3 Land use/cover

The land use/cover data (Figure 2.13) used in this study was from the Multi-Resolution Land Characteristics (MRLC), a consortium of federal agencies that collaborate to generate consistent and relevant nationwide land use/cover data for various environmental, land management, and modeling applications. From decadal Landsat satellite imagery and other supplementary datasets, this consortium has produced the National Land Cover Database (NLCD), which is a comprehensive product of nationwide land cover and land cover change at a 30m resolution with a 16-class legend based on a

modified Anderson Level II classification system (Homer et al., 2020). Since 2001, the dataset has been updated seven times in 2001, 2004, 2006, 2008, 2011, 2013, and 2016. Figure 2.14 shows the land cover data as of 2016 the northeast coast of South Carolina. Since 2001, the areas covered by forest, wetland, and shrub land have decreased by more than 3%, while urban areas have increased by about 4% (Figure 2.14).

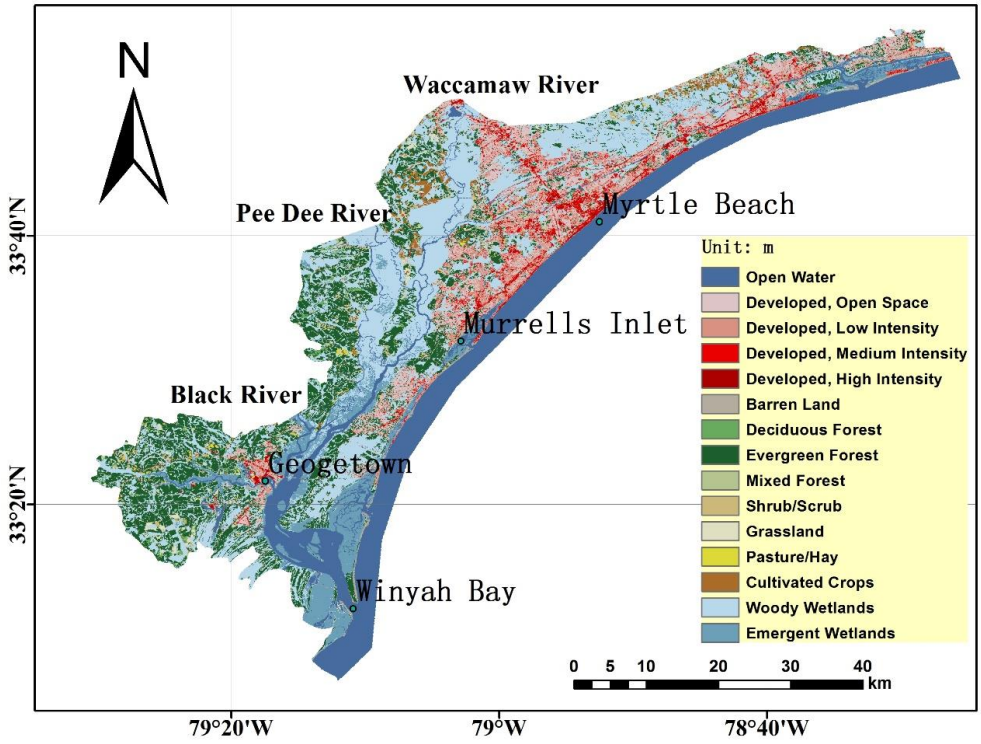

Figure 2.13. Land cover data for TELEMAC-2D domain (2016). Developed land, forest, shrubland, and wetland are four major land use/cover types in this region.

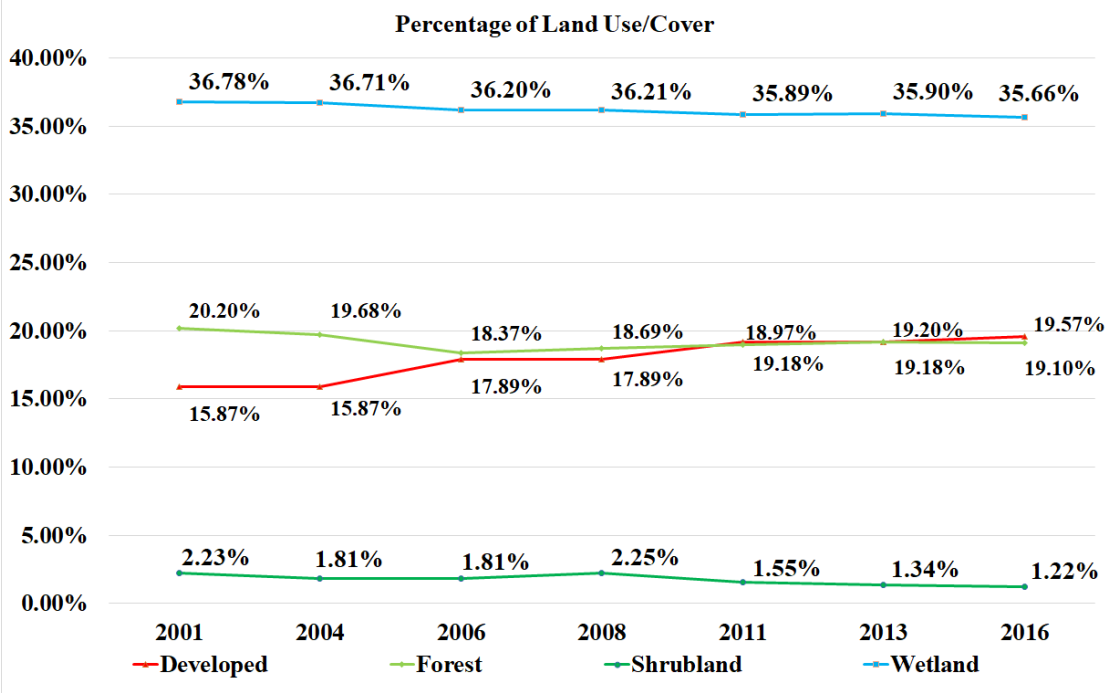

Figure 2.14. Land use/cover change of TELEMAC-2D domain since 2001. Developed areas increased by about 4%.

2.2.4 Population density

The population data used in my thesis is from the Gridded Population of the World (GPW) dataset version 4 provided by the Center for International Earth Science Information Network of Columbia University. GPW models the continuous distribution of human population (number and densities) on a grid of 30 arc-seconds (approximately 1 km at the equator). The input population in this dataset was collected based on the most detailed spatial resolution available from the 2010 Population and Housing Censuses, which took place between 2005 and 2014 (Center For International Earth Science Information Network-CIESIN-Columbia University, 2018). The input data are extrapolated to produce population estimates for the years 2000, 2005, 2010, 2015, and 2020 (Figure 2.15, 2.16). The dataset also provides a set of estimates adjusted for national-level population

predictions based on the United Nations' World Population Prospects report for the same years. These data is used as gridded population density for flood risk calculation using Eq. 2.1. A spatial interpolation method was used to interpolate the population.

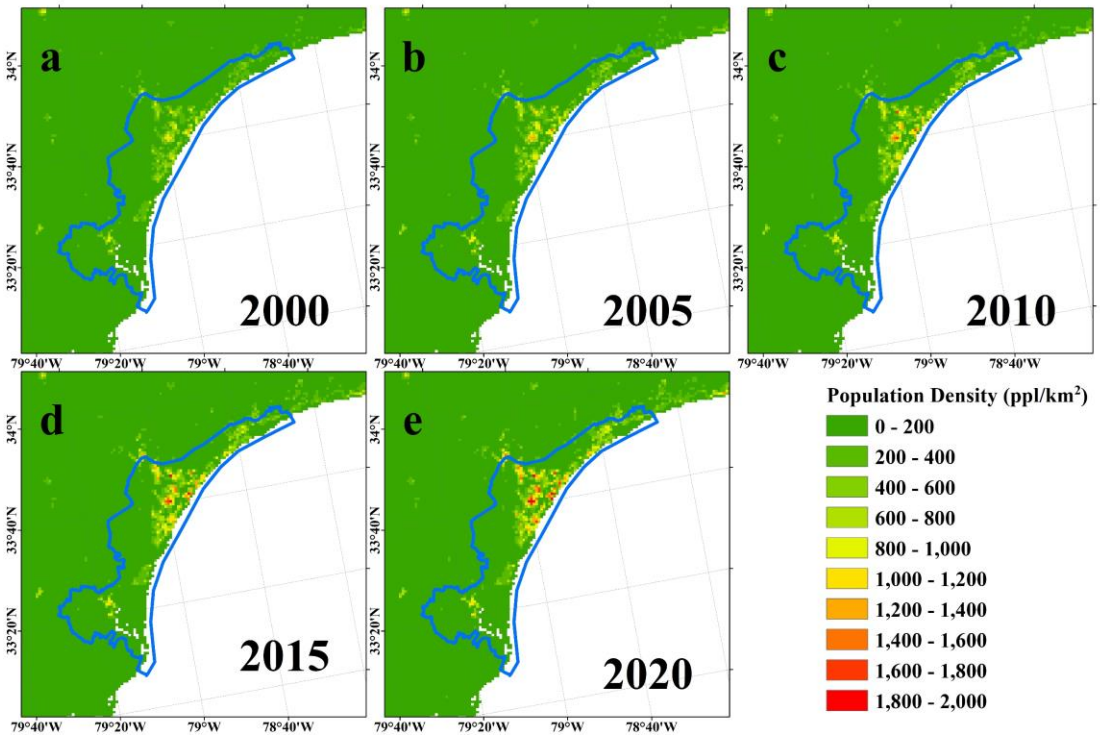

Figure 2.15. Population Density from the Gridded Population of the World (GPW) dataset version, 4: a)2000 population density distribution, b)2005 population density distribution, c)2010 population density distribution, d)2015 population density distribution, e)2020 population density distribution. Spatial resolution is 100 meters.

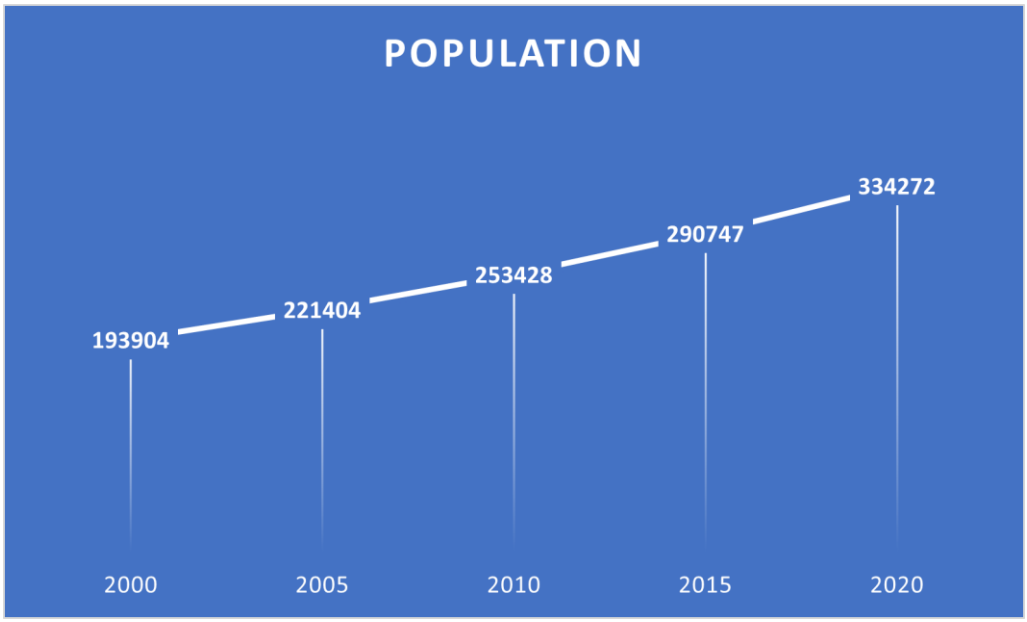

Figure 2.16. Population growth in study area since 2000.

2.2.5 GDP per capita

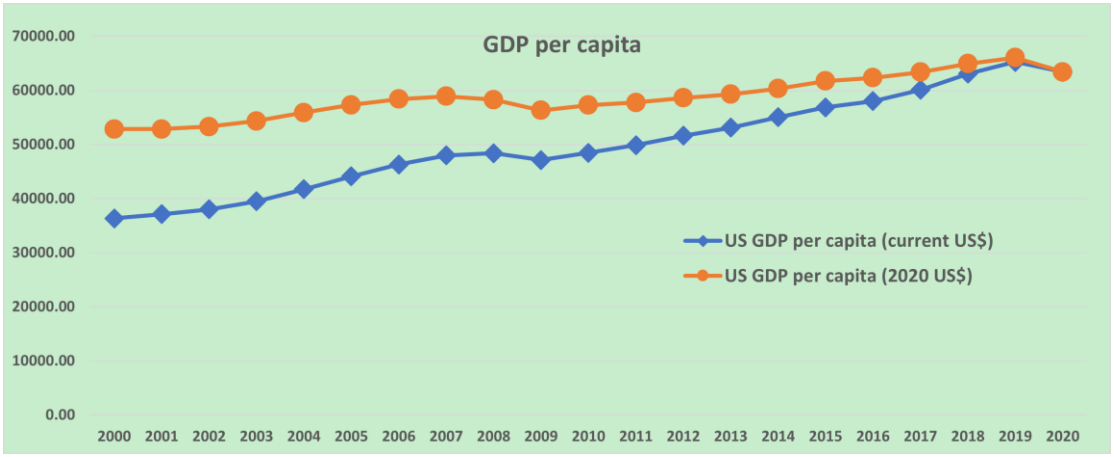

Figure 2.17. US GDP per capita in current US$ and 2020 US$

GDP per capita used in this study is from World Bank (Figure 2.17). In order to compare the flood risk without the influence of inflation, the unit of GDP per capita is unified to constant 2020 U. S. dollar. The transformation method is as follows:

$$GDP_{2020} = Nominal\ GDP \times \frac{GDP\ deflator_{2020}}{GDP\ deflator} \qquad (2.21)$$

where $Nominal\ GDP$ represents the value of the economy's output calculated using every individual year's prices and GDP_{2020} measures the value of the economy's output adjusted for price changes (inflation or deflation) with 2020 as the base year. $GDP\ deflator$ is a measure of price inflation/deflation with respect to a specific base year. GDP deflators used in this study are also from World Bank.

Table 2.7. US GDP per capita and SC GDP per capita

	US GDP per capita (current US$)	GDP deflator	US GDP per capita (2020 US$)
2000	36334.91	68.74	52854.63
2001	37133.24	70.25	52856.56
2002	38023.16	71.36	53280.53
2003	39496.49	72.69	54335.97
2004	41712.80	74.65	55880.57
2005	44114.75	76.97	57313.07
2006	46298.73	79.30	58383.66
2007	47975.97	81.43	58916.04
2008	48382.56	83.02	58281.69
2009	47099.98	83.65	56307.43
2010	48466.66	84.62	57273.89
2011	49882.56	86.39	57740.93
2012	51602.93	88.05	58608.31
2013	53106.54	89.59	59275.80
2014	55049.99	91.25	60329.03
2015	56863.37	92.12	61728.33
2016	58021.40	93.09	62331.43
2017	60109.66	94.84	63383.16
2018	63064.42	97.11	64939.64
2019	65279.53	98.85	66041.68
2020	63413.51	100.00	63413.51

Data source: World Bank

3 Results and discussion

In the previous flood studies, the discharge in the river channel was the key variable used to estimate the severity of a flood. This common understanding in the flood research field guided the development of hydrological models. However, in reality, flooding is not a one-dimensional issue, especially for coastal floods. Compared to the extreme values appearing in the discharge time series, the spatial and temporal distribution of the flooded area is more effective in reflecting the severity of a coastal flood. In my thesis, several improvements have been made by adopting a more comprehensive approach to understanding the complexity of coastal floods. These improvements include:

The main variable used for analysis was the flooding area, defined as the difference in water surface area between each model simulation and the reference run (EXP2). To better understand the dynamics of the flooding process, the real-time flooding area and the accumulated flooding area were analyzed separately.

1) Calculate total wave volume every hour to gain insights into how much water remained in the study domain.
2) Integrate discharges along 12 selected cross sections to analyze the spatial and temporal changes of water flows in the study domain.

These improvements help to provide a more accurate and comprehensive understanding of coastal floods, which could assist in the development of hydrological models and

improve the prediction of coastal floods.

3.1 Coastal compound flooding

3.1.1 Time evolution of flooding area and total water volume in the study domain

Figure 3.1 presents the time variation of flooding area and water volume as simulated by Exp 3-6. Figure 3.1(a) clearly illustrates the moments when various factors dominated the increase in flooding area. Local rainfall (green line) had minimal impact on the flooding area throughout the simulation period. The tide (purple line) was the first to have an effect, followed by storm surge (red line), and then by upstream discharge (blue line). Subsequently, tides, which transitioned from neap tides (around October 8th) to spring tides (around October 19th) with increasing amplitude (see Figure 2.7), also contributed to the increase in flooding area (purple line). However, the effect of the spring tides was not evident in the control simulation (cyan line), because it was obscured by other factors. This can be observed in the simulated spatial distribution of flooding area in Section 3.1.3. Upstream discharge, tide, and surge had greater effects than local rainfall. Upon comparing the peak flooding areas of each individual factor run, we can see that storm surge had the largest influence on flooding area, followed by upstream discharge and tide. Local rainfall had the least impact on flooding area in this case. It is important to note that this does not imply that rainfall is less important than the other factors. By further examining the accumulated rainfall in the whole Pee Dee basin (Figure 3.2), we found that most of the rainfall fell into upstream basins, including Pee Dee and Waccamaw basins, rather than directly into the study domain. Hence, the rain impacted the flooding area by contributing to the upstream discharge.

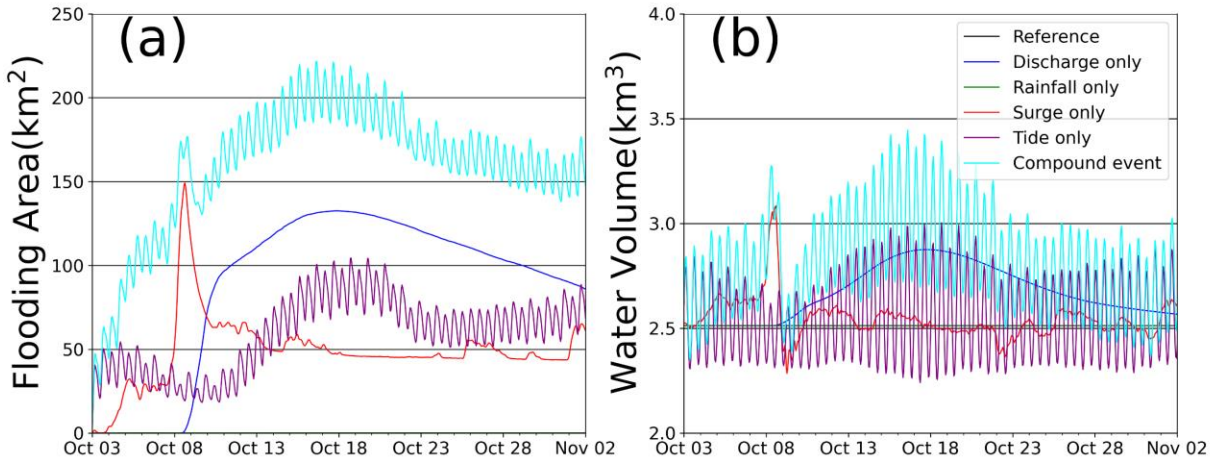

Figure 3.1 Time series of (a) flooding area and (b) total water volume for: keeping upstream discharge (EXP3, blue lines), keeping local rainfall (EXP4, green lines), keeping tide (EXP5, purple lines), and keeping storm surge (EXP6, red lines) scenarios. Hurricane Matthew flood event (EXP1, cyan lines) and idealized steady scenario (EXP2, black lines) are plotted as reference. Flooding area for rainfall and reference are similar to each other.

There was a modeling bias regarding rainfall representation which needed to be clarified. Originating from our hydrodynamic model, governed by the primitive equation - Navier-Stokes Equations, the inundation model has a weak representation of hydrological processes. In our model setting, a curve number (CN) based process was used to model surface runoff and infiltration. Thus, three hydrological processes are missing: exfiltration, baseflow, and evapotranspiration.

In reality, rainfall stops infiltrating when the soil becomes saturated. At that point, all rainfall water turns into surface runoff, which is the exfiltration in the hydrological cycle. Even though the behavior of soil when it gets saturated is an interesting question worth exploring, modeling this process is not the focus of my thesis. It is important to clarify that

this exfiltration water may not flow into the river channel all the time, especially in relatively flat regions, such as our study area. With little or no elevation gradient and thus no gravitational forcing, exfiltration water flow is impossible to flow into river channels that are kilometers away. Most of the time, the exfiltration water becomes detention water for some period and eventually be subsumed into the groundwater table. The missing exfiltration process in our model setting does not induce any biases.

The baseflow, in a typical hydrological model, is traditionally estimated via highly conceptual models. The baseflow is then added to the river channel flow as a source of lateral flow. Unfortunately, there is no pre-defined or constant river channel in a 2D inundation model. Determining how to add the baseflow to the river channel flow and understanding its contribution to the flooding area require future investigation. Besides these two hydrological processes, evapotranspiration is not represented in the current version of TELEMAC-2D. These are expected to influence the flood area by decreasing the duration.

The above discussion briefly clarifies some of the weaknesses of the current inundation model concerning modeling bias and uncertainty. In general, we admit the limitations of the inundation model that we employed. There is no doubt that current community inundation models need to be improved. However, based on the validation presented in the previous Method section, we believe that our flooding area results are reasonable and reliable.

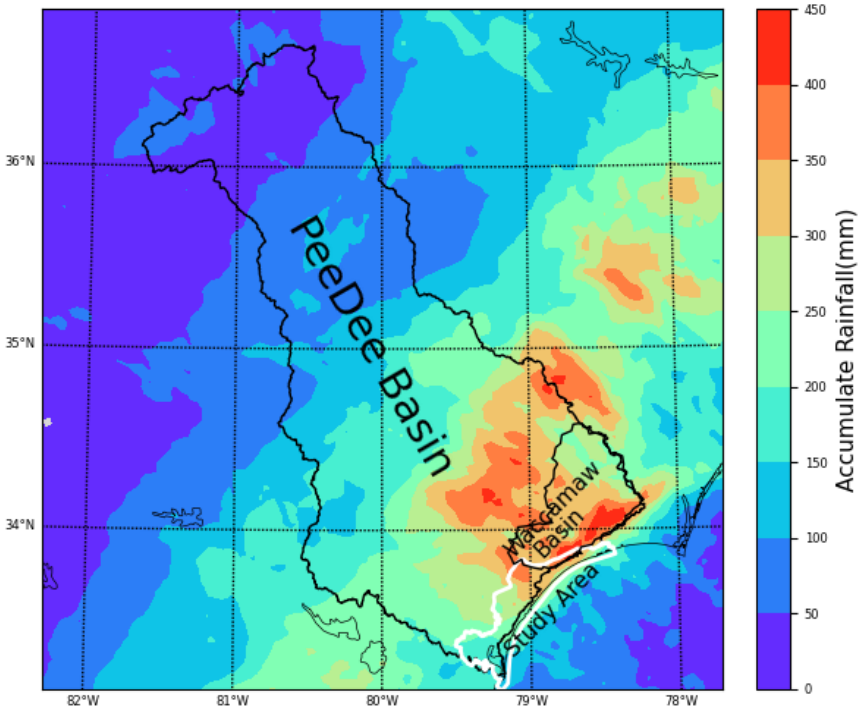

Figure 3.2. Accumulated rainfall in study area and the whole Pee Dee basin from Oct 03 to Nov 02, 2016.

The change in total water volume depicted in Figure 3.1(b) corresponded with the variation of flooding area in Figure 3.1(a). Storm surge was responsible for the large water input around October 8th, followed by a rapid retreat (red line), while after October 18th, the total water volume was mainly from upstream discharge (blue line). The tides caused semi-diurnal oscillations and the neap-spring cycle (purple line). The total water volume driven by local rainfall (green line) was close to that in the reference run (black line), indicating that local rainfall did not directly bring a significant amount of water into the study domain compared with the other factors. It is consistent with the argument that

the impact of rain on the flooding area is indirect.

3.1.2 Time evolution of river discharge

Figure 3.3 presents the time series of discharge simulated by the control, reference, and Exp 3-6 runs at five cross sections. From Waccamaw River (Pee Dee River) inlets to Winyah Bay, the cross-section order is as follows: aa' – bb' – cc' – dd' (ee' – cc' – dd'). The upstream discharge (blue lines) was the dominant driver at all cross sections. Local rainfall had little impact on the discharges. The semi-diurnal tide effect reached as far as about 50 miles inland, slightly affecting the discharge at cross-section ee' and becoming more significant as approaching the coast, ultimately dominating near Winyah Bay at cross-section dd'. When the storm surge pushed seawater onshore from October 8th to 9th, it blocked the river flow and even caused backflows visible at all cross sections aa', bb', cc', dd', and ee'. These storm surge-induced backflows (red lines) were blended with tidal oscillations (purple lines) and displayed as slightly lower low-tides in the control simulation results (cyan lines). Lateral flooding occurred when the blocked river flows exceeded the river channel capacity, coinciding with the period when the storm surge also caused a rapid increase in the flooded area (see red lines in Figure 3.1).

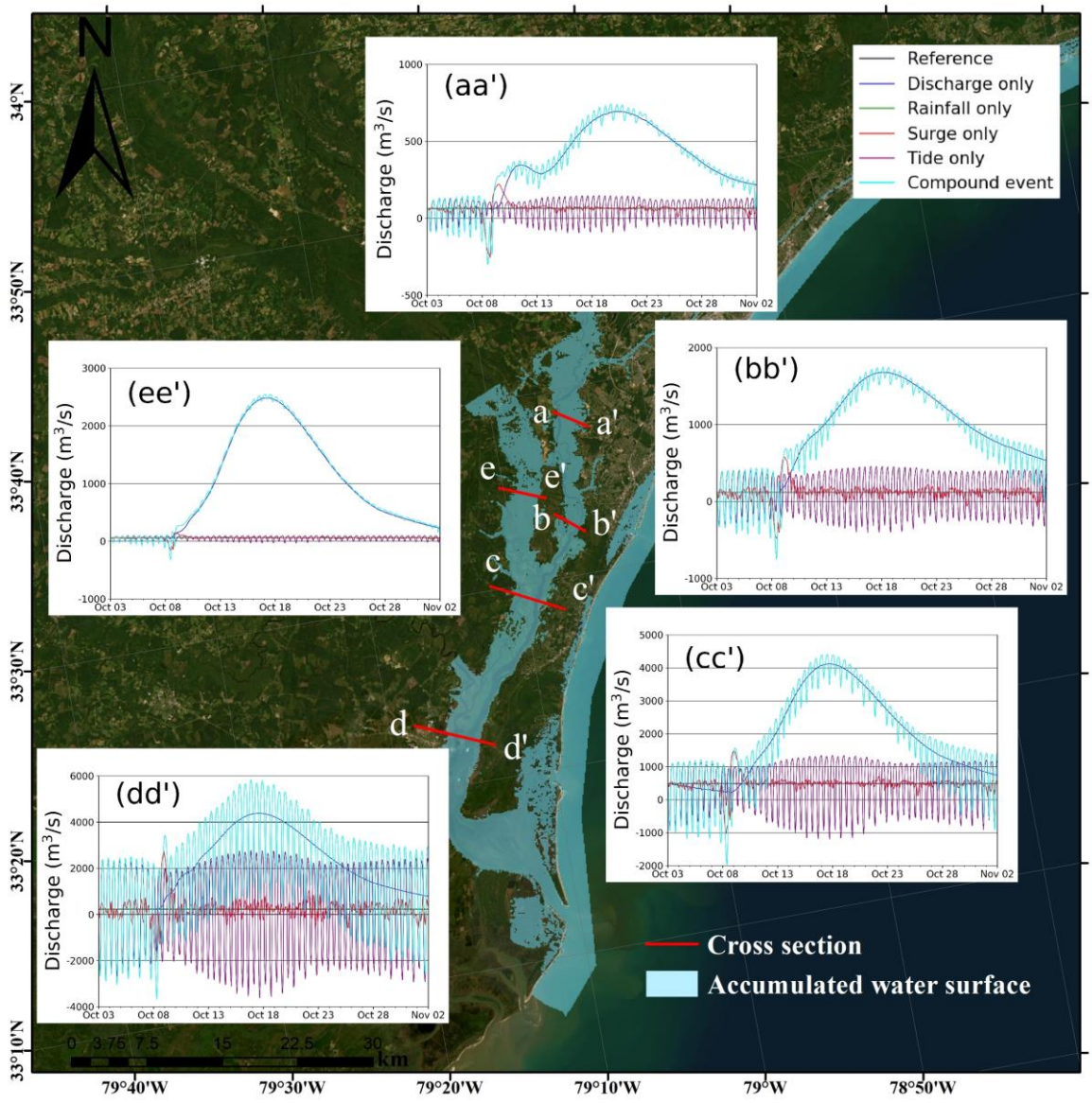

Figure 3.3 Time series of discharge at five cross sections for one group simulations: keep upstream discharge (EXP3, blue line), keep local rainfall (EXP4, green line), keep tide (EXP5, purple line), and keep storm surge (EXP6, red line) scenarios. Hurricane Matthew flood event (EXP1, cyan line) and idealized steady scenario (EXP2, black line) are plotted as reference.

To better understand the blocking effect of sea water to the upstream discharge, an idealized one-dimensional hydrological model based on the Saint-Venant (S-V) equation

(Equation 2.10, 2.11) is designed. We employ the S-V model to provide simplified, yet revealing foundational, physics to the compound flooding phenomena. The first two terms of Equation 2.11 are ignored as in WRF-Hydro, which makes the calculation as simple as calculating diffusive waves. Then the equations are:

$$\frac{\partial A}{\partial t} + \frac{\partial Q}{\partial x} = q_{lat} \tag{3.1}$$

$$\mathrm{gA}\frac{\partial h}{\partial x} + \mathrm{gA}S_f = 0 \tag{3.2}$$

where A is the flow area of cross-section, Q is the flow rate, $q_{lat}$is the lateral inflow rate into the channel from rainfall and surface runoff, and h is the water surface elevation. S_f is the friction slope, defined as $\mathrm{S_f} = (\frac{\mathrm{Q}}{\mathrm{K}})^2$, where K is the conveyance from Manning's equation, defined as $\mathrm{K} = \frac{\mathrm{C_m}}{\mathrm{n}}\mathrm{AR}^{2/3}$, where n is the Manning's roughness coefficient, R is the hydraulic radius $\mathrm{R} = A/P$, and P is the wetted perimeter.

The idealized 1-D model used a 10 km linear river channel with a bed slope of 0.0002. The initial river water depth was set at 1 m and the vertical dimension of the river channel was assumed to be effectively infinite. Two downstream sea levels were used: 1 m (Control Experiment) as the normal condition, which is the same as the normal river surface height, and 1.5 m (Δ-Sea-Level Experiment), as the condition after the hurricane-induced storm surge. An idealized rainfall amount was added to the river channel, with a lateral discharge value of 30 m^3/s to model an example of the rainfall process, lasting for 30 minutes.

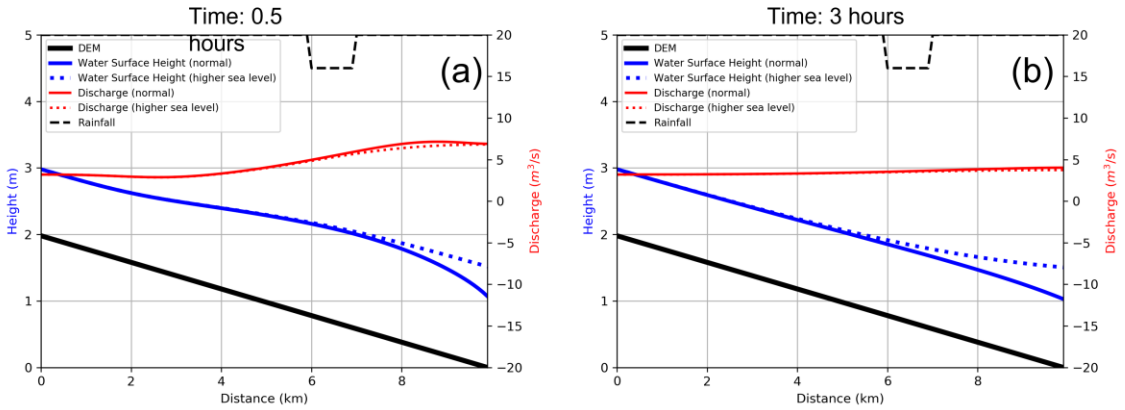

Figure 3.4. One-dimensional idealized river channel simulation results. (a) 0.5 hour after the rain event; and (b) 3 hours after the rainfall was added to the river channel. The black lines are the constant riverbed. The blue and red lines denote the water surface height in the river channel and streamflow in m3/s, respectively, The solid lines show the results from the simulation with normal sea level as the downstream boundary condition, while the dashed lines are those with increased sea level as the initial condition.

Results of this model are shown in Figure 3.4. The dashed black line suggests that the rainfall occurred 3 to 4 km from the river mouth. About half an hour after the rainfall was deposited into the river channel, the water surface height in the Δ-Sea-Level Experiment was higher than the Control Experiment up to 2 km from the downstream boundary. Three hours after the rainfall, the discharge in the Δ-Sea-Level Experiment was slightly less than the Control Experiment, and the higher water surface level intruded further toward inland, reaching up to 4 km from the downstream boundary. The surface water slope in the Δ-Sea-Level Experiment was flatter than the Control Experiment, resulting in a slower water flow speed (V). However, the higher water surface in Δ-Sea-Level also

created a large river cross-section area (A). Therefore, the simulated streamflow discharges ($Q = V \times A$) in the Control Experiment and the Δ-Sea-Level Experiment converged after 3 hours.

Note that in this idealized experiment, the vertical dimension of the river channel was assumed to be infinite, meaning that the increased water can be stored in the river channel. However, in real-world conditions, the increased water will move laterally and become flood waters.

3.1.3 Spatial distribution of accumulated flooding area

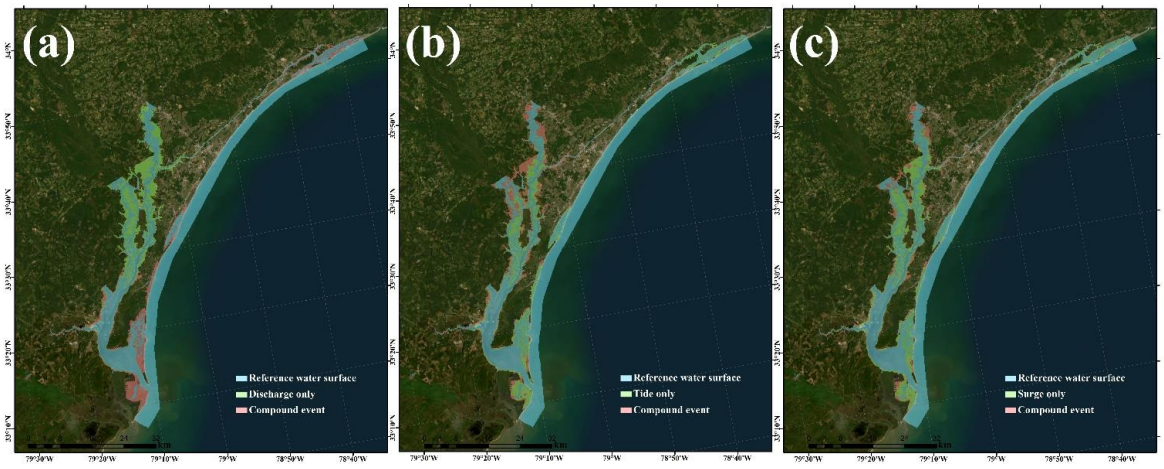

Figure 3.5. Accumulated flooding area distribution for (a) keeping upstream discharge (EXP3), (b) keeping tide surge (EXP5), and (c) keeping storm surge (EXP6) scenarios. Hurricane Matthew flood event (EXP1, red) and idealized steady scenario (permanent water surface, EXP2, blue) are plotted as reference.

Figure 3.5 displays the accumulated flooding areas simulated by the control run, reference run, and the Exp 3, 5, and 6 runs. When only the upstream discharge was considered, flooding occurred in the inland portion of the river channel (Figure 3.5a). When taking into account only the tide (Figure 3.5b) or storm surge (Figure 3.5c), flooding

occurred in coastal regions along the coastline, as well as some low-elevation areas within the inland portion of the Waccamaw River channel. Although the flooding patterns caused by tide or storm surge were similar, the extent was larger for the latter. The contributions of the three factors to the flooding area in Figure 3.5 align with the time series in Figure 3.1. Areas flooded solely due to rainfall are not depicted here, as their extent is minimal and not easily distinguishable on the maps.

Figure 3.5 also shows the water surface with a 1 cm threshold, meaning that cells with a water depth of less than 1 cm were not considered as wet (flooded) cells. The use of a threshold is a standard approach in inundation numerical modeling. In reality, 1 cm water depth on the land surface does not pose a problem for human society. As such, this 1 cm threshold is reasonable for filtering out insignificant water depths. Meanwhile, there were some near-zero water depths in the TELEMAC-2D results, caused by computational biases. This 1 cm threshold helped eliminate any misleading effects induced by the biased data.

3.1.4 Compound effect in flooding area

In the previous sections, we analyzed the individual effects of the four factors - upstream discharge, local rainfall, storm surge, and tides - on the temporal and spatial distribution of the simulated flooding area. In this section, the compound effect, or the effect of the interactions between multiple factors, was quantified as the difference between the flooding area simulated as a compound event and the linear sum of flooded areas simulated as single-factor events. In other words, the compound effect is defined as: $|(Q + R + T + S)| - (|Q| + |R| + |T| + |S|)$, where the || symbol denotes the flooding

area, and Q, R, T, and S represent upstream discharge, local rainfall, tides, and storm surge, respectively. The results are shown in Table 3.1 and Figure 3.6. Due to the relatively small effect of rainfall, it was not considered in the assessment of the compound effect.

Table 3.1 Flooding area comparison between linear combination and compound modeling at the time when compound effect is the largest.

	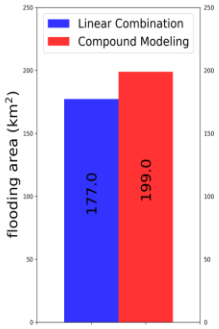	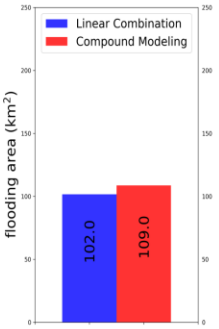	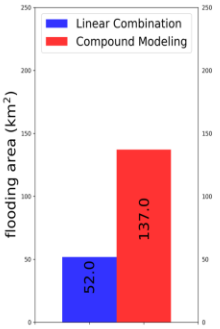	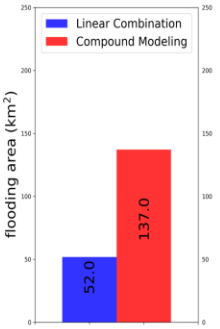
Compound Effect/Coupled Model	11%	7%	62%	62%
Upstream Discharge	X	X		X
Tide	X		X	X
Storm Surge		X	X	X

The compound effect caused by the interactions between upstream discharge and tide resulted in more flooding along the river channel from inland to the coast (Figure 3.6a). The values in Table 3.1 imply that the interaction between upstream discharge and tide created a larger flooding area (in number) than the interaction between upstream discharge and storm surge. This was mainly due to the peak storm surge arrival time, which was about 2 days apart from the arrival time of the upstream peak discharge (Figure 2.4). The interaction between upstream discharge and tide caused an 11% increase in compound flooding (Table 3.1) near October 18th at 19:00. In fact, when large upstream discharges occur, some inland areas along the river channel are flooded regardless. Since

all upstream input water flow cannot be discharged into the ocean instantaneously, there was a large flooding area inland (Figure 3.6a). The spring tide further enhanced this blocking effect and created a larger flooding area.

The largest compound effect, resulting from the interaction between upstream discharge and storm surge, occurred near October 9th at 14:00 when the storm surge reached the coast of this region. It is worth noting that the blocking effect of storm surge started right after its arrival at the coast and caused some river flooding upstream along the river channel (Figure 3.6b). Along the coastline, there was no additional flooding. The peak value of storm surge was similar to the spring tide sea level. In general, the storm surge cannot cause serious flooding if it occurs alone, considering the relatively steady environment that interacts with the tide every day. There was no more compound flooding after October 9th, which was due to the low level of upstream discharge when the storm surge arrived. As a result, not much water from upstream could be blocked in this region, and the river flooding caused by storm surge was not as severe as that caused by the spring tide. However, the compound flooding resulting from the interaction between upstream discharge and storm surge was larger in percentage than that caused by the interaction between upstream discharge and tide (Table 3.1).

The compound effect caused by the interaction between tide and storm surge was not only along the coastline but also along the river channel (Figure 3.6c). This compound effect-caused flooding was larger compared to any other two-factor combinations. Approximately 62% more flooding area was caused by the interactively coupled compound effect near October 7th at 20:00 when sea level reached its peak in this

flooding event. This larger sea level caused compound flooding both along the river channel and coastline. Even though the environment was relatively steady, it was sensitive to slight changes in natural factors (Figure 2.4). Among all factors, the tide seemed to be the most important. This is mainly due to the tide-induced sea level variation, which occurs semi-diurnally and diurnally, allowing the tide to interact with other natural factors more frequently. For example, during this Hurricane Matthew event, the tide interacted with the storm surge around October 8th and with the peak of upstream discharge around October 18th. From this perspective, tide is the nexus for coastal compound flooding.

The interaction between local rainfall and other factors caused a nearly zero compound effect. This is mainly due to the flooding areas associated with local rainfall being spatially scattered and away from both the coastline and the river channel. The rainfall-induced flash flooding was isolated in space, inferring that local rainfall had fewer chances to interact with upstream discharge, tide, and storm surge.

It is important to note that the compound effect is not always positive. A negative compound effect (Figure 3.6b) indicates that, at times, the flooding area in the coupled model was smaller than that in the linear combination. The water level at the seaside can either be positive (rising) or negative (falling). When the sea level is positive, more flooding could be produced by the blocking effect. However, when the sea level is negative, the decrease in flooding in the coupled model is greater than in the linear combination. This leads to a negative compound effect. Thus, the compound effect exhibits more complex characteristics in both spatial distribution and temporal variation.

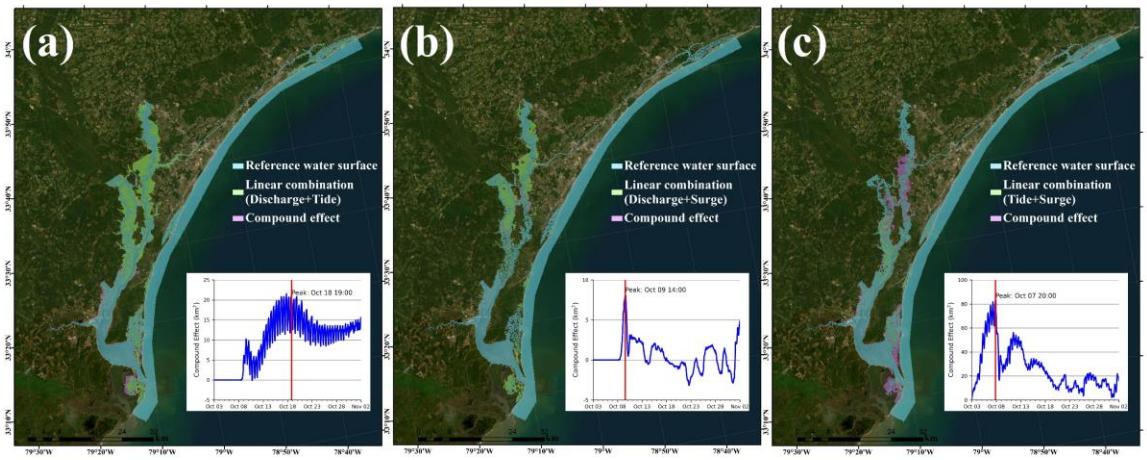

Figure 3.6 Flooding area comparison between model result and linear combination when the compound effect reached its peak. (a) Keep upstream discharge and tide (EXP8) at time Oct 18 19:00, (b) Keep upstream and storm surge (EXP9) at time Oct 09 14:00, (c) Keep tide and storm surge (EXP12) at time Oct 7 20:00. The linear combination (green) means that the flooding area appeared in both compound modeling result and linear combination of each individual factor result. Compound effect (red) means that the flooding area was caused by the interaction between two factors.

In summary, the compound effect caused by upstream discharge, tide, and storm surge increased the flooding area by approximately 62% (Table 3.1, Figure 3.7). It is important to note that this 62% increase, attributed to the compound effect, was limited to the Hurricane Matthew event. For other events, the compound effect may have different contributions to coastal flooding, which will be explored in future studies.

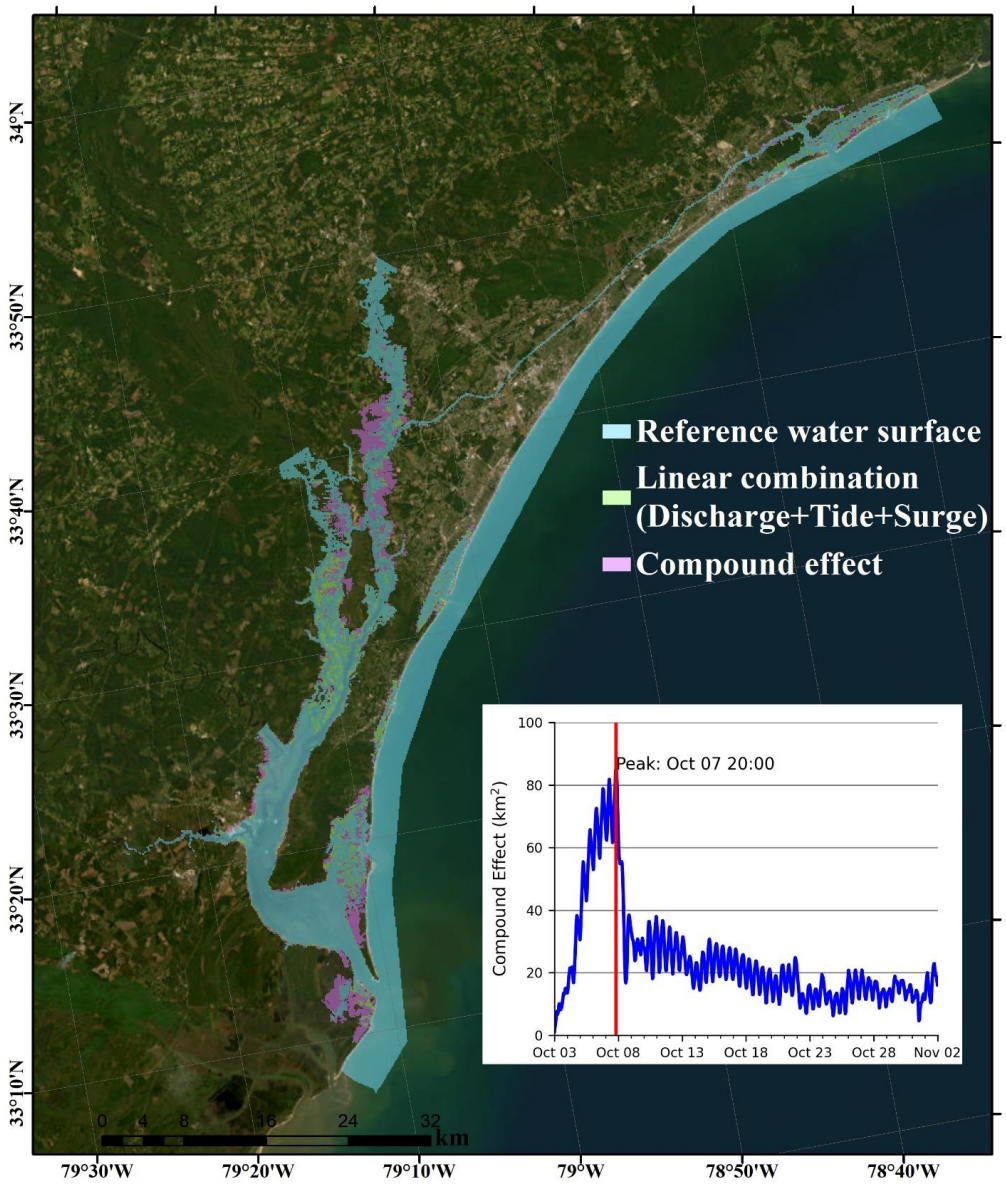

Figure 3.7. Flooding area comparison between model result and linear combination when the compound effect reaches its peak for keeping upstream discharge, local rainfall, tide, and storm surge (EXP1). The time is Oct 7 20:00. The linear combination (green) means the flooding area appeared in both compound modeling result and linear combination of each individual factor result. Compound flooding (red) means the flooding area appear only in compound modeling result, which means the compound flooding caused by the interaction between each two factors.

3.1.5 Compound effect in water volume

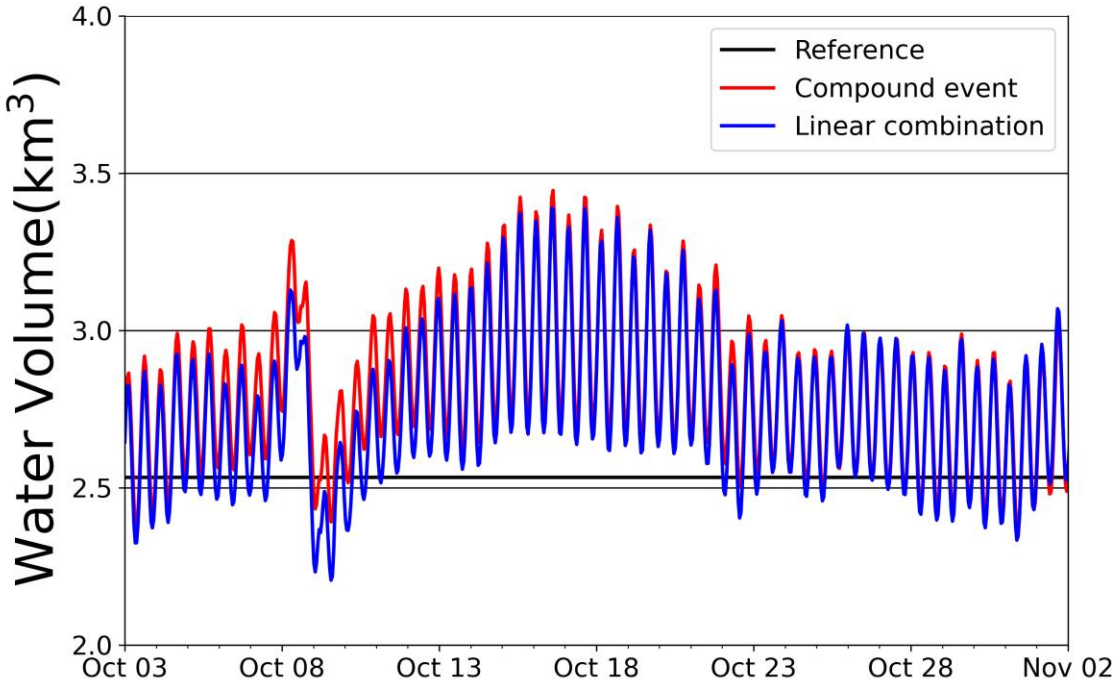

Figure 3.8. Water volume comparison between Hurricane Matthew case (control run) and linear combination of water volume result from only one factor including upstream discharge, local rainfall, tide, and storm surge (EXP3-EXP6). Since constant upstream discharge was considered in local rainfall, tide, and storm surge only simulations, three times of water volume result from reference run was removed from the linear combination.

The compound effect, caused by different factors, also influenced the timing of the total water volume that remained in the study area. Figure 3.8 shows the water volume comparison between coupled modeling and the linear combination of four natural factors (upstream discharge, storm surge, tide, and local rainfall) individual simulation. Since constant upstream discharge was considered in local rainfall, tide, and storm surge

individual simulations, three times of water volume resulting from the reference run was removed from the linear combination. The total water volume caused by the passage of Hurricane Matthew had a higher water volume than the linear combination of water volume. This suggests that compound coastal flooding contributed to retaining the water volume in the domain. This portion of the water volume that stayed in the domain could increase the overall flood duration and, consequently, enhance the flooding process.

3.1.6 EOF analysis about compound effect

To further explore the interactions between different factors and their contribution to compound effects, Empirical Orthogonal Function (EOF) analysis was employed. EOF is a technique used in signal processing, statistics, and climate science to analyze the spatiotemporal variability of a dataset. It is a mathematical technique for extracting the dominant patterns of variability (modes), which can be helpful in understanding the underlying dynamics of the system. Basically, EOF analysis decomposes a matrix into a set of orthogonal basis functions (EOFs) and corresponding principal components (PCs) that capture the dominant patterns of variability in the data. The PCs and EOFs represent the time series of the dominant patterns and the spatial patterns of the dominant modes of variability, respectively.

The following steps were taken to apply EOF analysis in the thesis:

1) A threshold of 1 cm, consistent with previous analysis, was applied to calculate the wet grid over the entire domain. The entire wet grid (water surface), instead of the flooding area, was used for EOF analysis. The rationale for this selection is that the inclusion of reference run data introduces more uncertainties into the

EOF analysis process, making subsequent steps more complicated.

2) For each time step, we calculated the difference grid between the coupled model and linear combination. The value of cells in this difference grid should be 1, 0, or -1. The combination of every time step's difference grid formed the matrix input for EOF analysis.
3) Lastly, the correlation coefficient between the first three PCs and three natural factors (upstream discharge, storm surge, and tide) was calculated. Local rainfall had a minimal effect on the spatial distribution of the flooding area, as analyzed previously. Therefore, EOF analysis was not employed to study local rainfall in the thesis.

Figure 3.9 displays the EOF analysis results for the interaction between upstream discharge and storm surge. The 1st EOF exhibits a negative pattern in coastal regions and a positive pattern inland. The temporal variation of the 1st PC indicates that after the storm surge peak arrived (around October 8th), compound flooding in inland regions increased, caused by the interaction between upstream discharge and downstream storm surge through the blocking effect, while coastal flood inundation in the coastal region decreased. Overall, the spatial and temporal patterns align with the positive and negative compound effects discussed in Section 3.1.4. Additionally, the 1st PC has a relatively high negative correlation with sea level (storm surge), which implies that sea level rise (storm surge in this case) variation dominated the difference in inland and coastal compound effects.

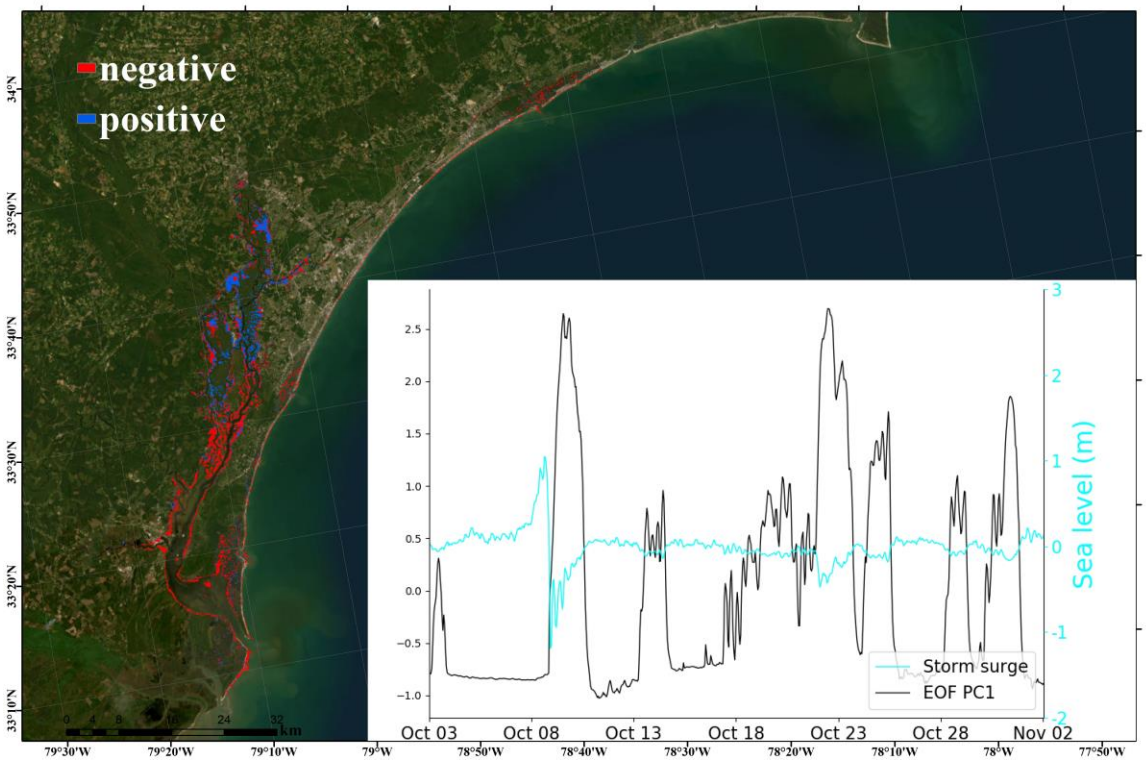

Figure 3.9. EOF analysis for the interaction between upstream discharge and storm surge. 1st orthogonal basis functions (EOF) and its corresponding principal component (PC). Its contribution for total variation is about 29%. The correlation coefficient of this PC with storm surge is -0.66.

Figure 3.10 and Figure 3.11 display the EOF analysis results for the interaction between upstream discharge and tide. The 1st EOF exhibits a positive pattern in coastal regions and a positive pattern inland. Considering the temporal variation of the 1st PC, it is evident that the spatial pattern was highly related to upstream discharge, primarily from the Pee Dee and Waccamaw rivers. The peak of the 1st PC aligned with the variation in peak upstream discharge from the Pee Dee and Waccamaw rivers (high correlation coefficient). When the upstream discharge peak arrived around October 18th, an increase in compound flooding occurred in inland regions, due to the blocking effect. The seawater

slowed down the river channel discharge from inland to the ocean. Meanwhile, at coastal regions, the large amount of inland river discharge caused more coastal flooding due to the compound effect. The 2nd EOF and its corresponding PC exhibit an opposite spatial change pattern in compound effect, increasing and decreasing. The variation of the 2nd PC is related to the tide process.

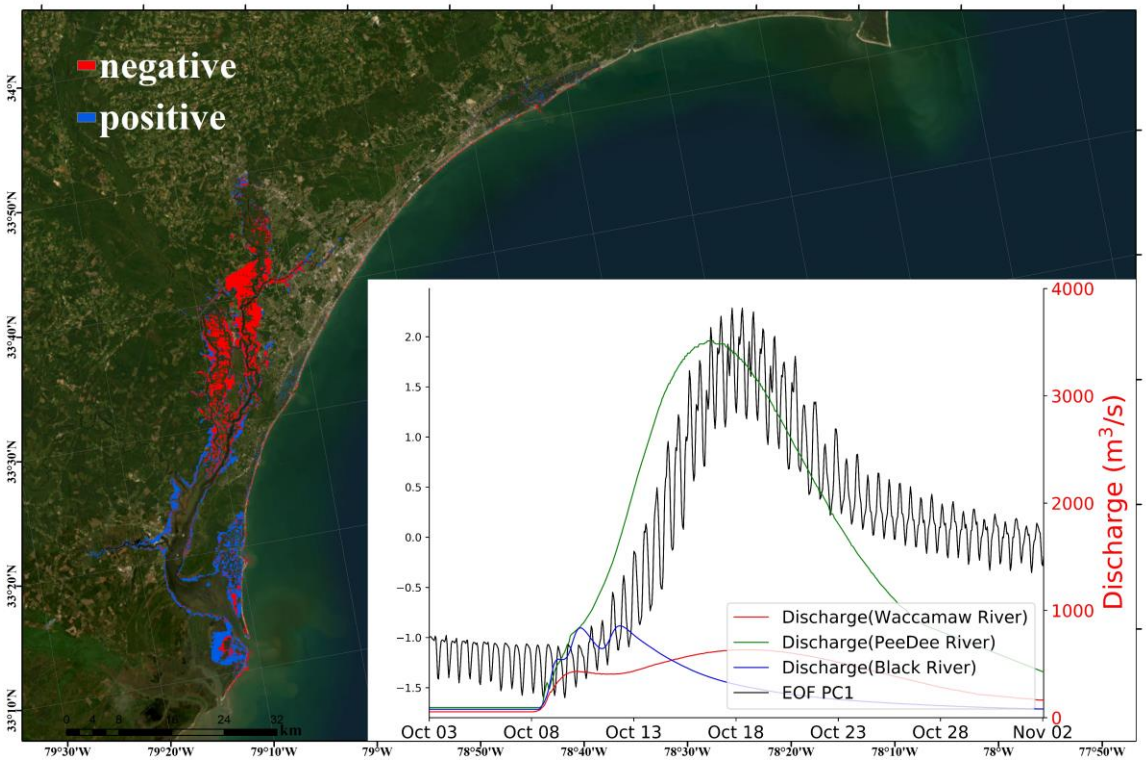

Figure 3.10. EOF analysis for interaction between upstream discharge and tide. 1st orthogonal basis functions (EOF) and its corresponding principal component (PC). Its contribution for total variation is about 18%. The correlation coefficients of this PC with three upstream discharge are 0.76, 0.79, and -0.09 for Waccamaw, PeeDee, and Black rivers respectively.

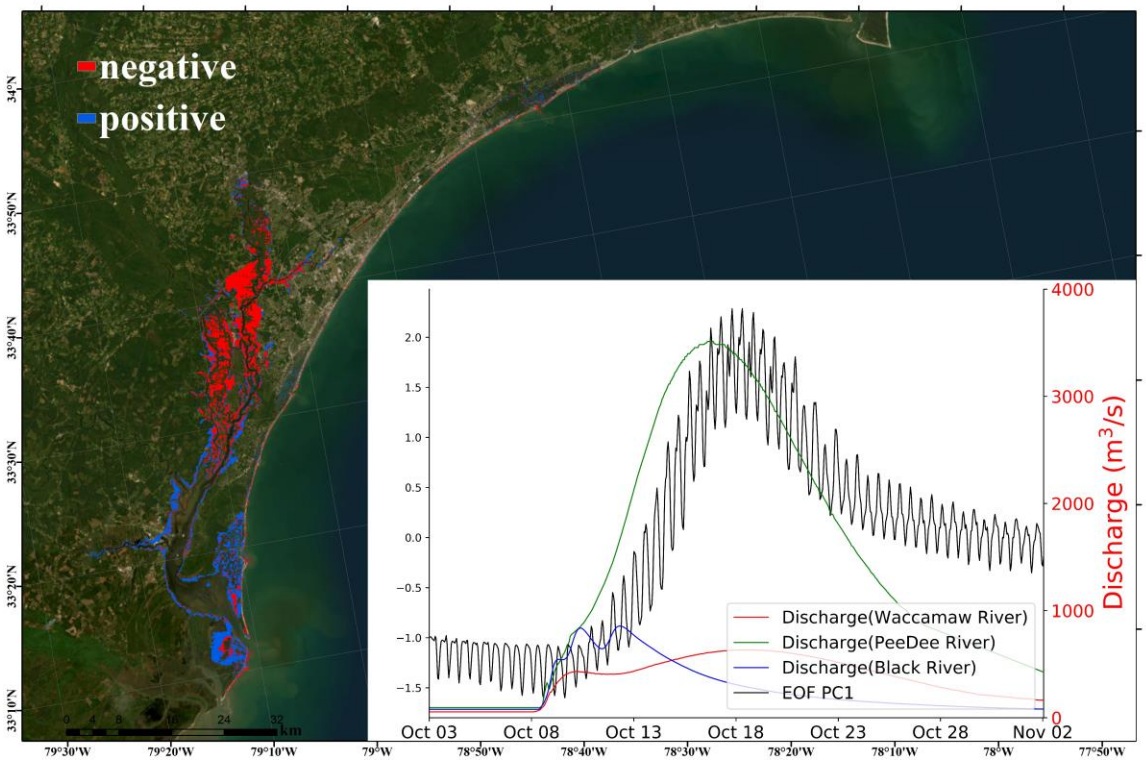

Figure 3.11. EOF analysis for interaction between upstream discharge and tide. 2nd orthogonal basis functions (EOF) and its corresponding principal component (PC). Its contribution for total variation is about 14%. The correlation coefficient of this PC with tide is -0.64.

Figure 3.12 displays the EOF analysis results for the interaction between storm surge and tide. The 1st EOF exhibits a negative pattern in some inland regions and a positive pattern in nearly all coastal and inland regions. With the negative pattern at the beginning of the 1st PC time series, it can be inferred that the early storm surge caused significant compound flooding both inland and along the coast through the blocking effect. The 1st PC is more closely related to storm surge, with a correlation coefficient of -0.43.

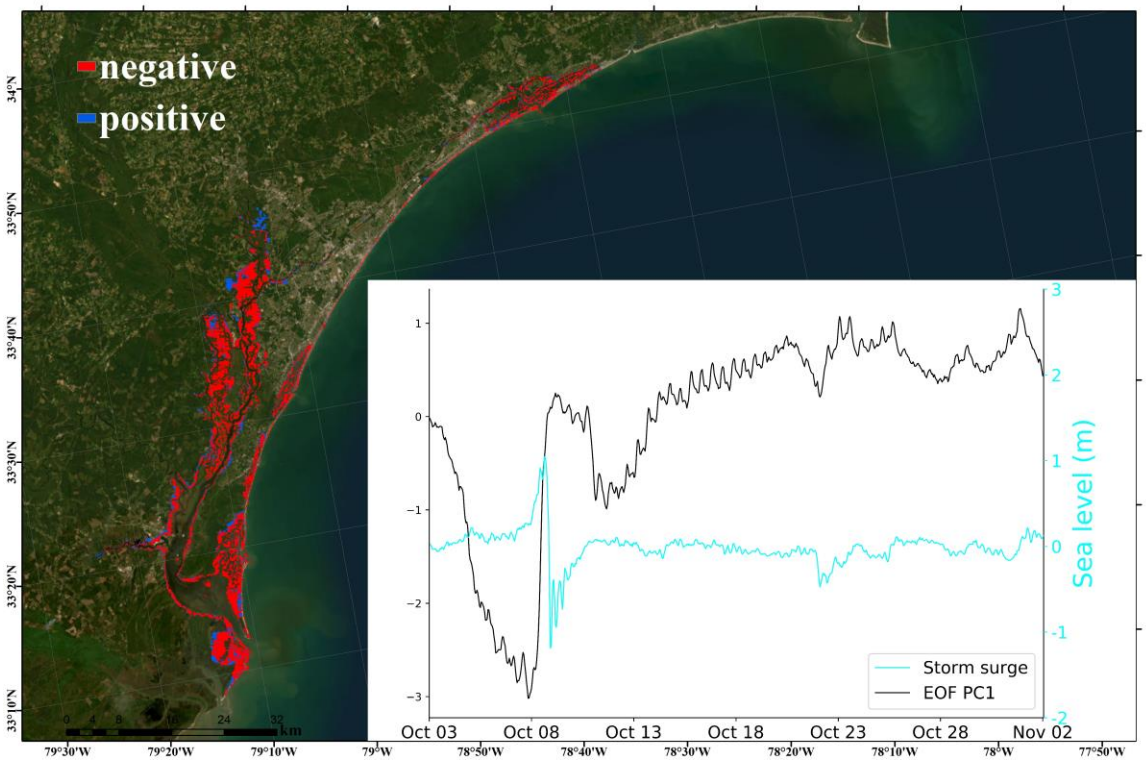

Figure 3.12. EOF analysis for interaction between storm surge and tide. 1st orthogonal basis functions (EOF) and its corresponding principal component (PC). Its contribution for total variation is about 12%. The correlation coefficient of this PC with surge is -0.43.

3.1.7 Summary about coastal compound flooding

In summary, the characteristics of coastal compound flooding can be described as follows:

1) Interactions between different natural factors can lead to more severe flooding (long-lasting water and increased water retention in the basin). The compound effect, caused by the combination of multiple factors, was quantified using numerical modeling. The blocking effect between downstream water levels (including tide and storm surge) and upstream discharge was the main reason for the compound effect in coastal flooding phenomena.
2) Interactions between different factors can change the timing of flooding area,

river discharge, and total water volume variation in the basin. The evolution of different factors is significant for the occurrence of coastal compound flooding. As coastal compound flooding is coincidental, the coastal region is greatly impacted once this coincidence occurs.

3) Local rainfall influences coastal flooding only by causing limited flash flooding. Due to the limitations of modeling, the analysis about local rainfall contains a great deal of uncertainty. There is no doubt that the current inundation model needs improvement. Nevertheless, numerical modeling is proposed as an important and efficient way to analyze coastal compound flooding.

3.2 Flood risk sensitivity tests

3.2.1 Natural factors

The entire calculation of flood risk included the population density grid and GDP per capita for all years from 2000 to 2020. In this section, we only compare natural factors. Therefore, only the flood risk calculations based on the population grid and GDP per capita in 2016 are shown here (Table 3.2). In the following discussion, data from the World Bank was mainly used. The time of flooding area grid used to calculate flood risk was the maximum flooding risk time instead of the maximum flooding area time since flooding and flood risk may not peak at same time.

Table 3.2. Flood Risk calculation for different environment settings based on population grid and GDP per capita at 2016. The unit is as billion 2020 US$.

	Upstream Discharge	Storm Surge	Sea level Rise	Flood Risk (unit: billion 2020 US$)
Sen_EXP001	1%	1%	0m	3.68
Sen_EXP002	1%	1%	0.43m	3.93

Sen_EXP003	1%	1%	0.55m	4.11
Sen_EXP004	1%	1%	0.84m	4.36
Sen_EXP005	1%	2%	0m	3.58
Sen_EXP006	1%	2%	0.43m	3.82
Sen_EXP007	1%	2%	0.55m	3.90
Sen_EXP008	1%	2%	0.84m	4.23
Sen_EXP009	1%	5%	0m	3.49
Sen_EXP010	1%	5%	0.43m	3.71
Sen_EXP011	1%	5%	0.55m	3.77
Sen_EXP012	1%	5%	0.84m	3.98
Sen_EXP013	1%	10%	0m	3.43
Sen_EXP014	1%	10%	0.43m	3.65
Sen_EXP015	1%	10%	0.55m	3.71
Sen_EXP016	1%	10%	0.84m	3.87
Sen_EXP017	2%	1%	0m	3.57
Sen_EXP018	2%	1%	0.43m	3.85
Sen_EXP019	2%	1%	0.55m	3.97
Sen_EXP020	2%	1%	0.84m	4.32
Sen_EXP021	2%	2%	0m	3.47
Sen_EXP022	2%	2%	0.43m	3.72
Sen_EXP023	2%	2%	0.55m	3.82
Sen_EXP024	2%	2%	0.84m	4.13
Sen_EXP025	2%	5%	0m	3.37
Sen_EXP026	2%	5%	0.43m	3.61
Sen_EXP027	2%	5%	0.55m	3.67
Sen_EXP028	2%	5%	0.84m	3.88
Sen_EXP029	2%	10%	0m	3.31
Sen_EXP030	2%	10%	0.43m	3.54
Sen_EXP031	2%	10%	0.55m	3.61
Sen_EXP032	2%	10%	0.84m	3.79
Sen_EXP033	5%	1%	0m	3.50
Sen_EXP034	5%	1%	0.43m	3.80
Sen_EXP035	5%	1%	0.55m	3.91
Sen_EXP036	5%	1%	0.84m	4.25
Sen_EXP037	5%	2%	0m	3.38
Sen_EXP038	5%	2%	0.43m	3.66
Sen_EXP039	5%	2%	0.55m	3.76
Sen_EXP040	5%	2%	0.84m	4.07
Sen_EXP041	5%	5%	0m	3.26
Sen_EXP042	5%	5%	0.43m	3.54
Sen_EXP043	5%	5%	0.55m	3.61
Sen_EXP044	5%	5%	0.84m	3.83
Sen_EXP045	5%	10%	0m	3.08

Sen_EXP046	5%	10%	0.43m	3.45
Sen_EXP047	5%	10%	0.55m	3.53
Sen_EXP048	5%	10%	0.84m	3.72
Sen_EXP049	10%	1%	0m	3.46
Sen_EXP050	10%	1%	0.43m	3.76
Sen_EXP051	10%	1%	0.55m	3.86
Sen_EXP052	10%	1%	0.84m	4.20
Sen_EXP053	10%	2%	0m	3.35
Sen_EXP054	10%	2%	0.43m	3.64
Sen_EXP055	10%	2%	0.55m	3.73
Sen_EXP056	10%	2%	0.84m	4.02
Sen_EXP057	10%	5%	0m	3.19
Sen_EXP058	10%	5%	0.43m	3.51
Sen_EXP059	10%	5%	0.55m	3.58
Sen_EXP060	10%	5%	0.84m	3.79
Sen_EXP061	10%	10%	0m	3.03
Sen_EXP062	10%	10%	0.43m	3.41
Sen_EXP063	10%	10%	0.55m	3.51
Sen_EXP064	10%	10%	0.84m	3.70

By comparing Sen_EXP001, Sen_EXP002, Sen_EXP003, and Sen_EXP004 in Table 3.2, we can identify the increased flood risk caused by sea level rise. For coastal flooding caused by a 1% annual chance upstream discharge and a 1% annual chance storm surge, the flood risk increased by 6.94%, 11.85%, and 18.50% with 0.43m, 0.55m, and 0.84m sea level rise by the end of this century, respectively. For different upstream discharge and storm surge settings, sea level rise could increase flood risk at different rates, as shown in Table 3.3. For example, for flooding caused by 1% upstream discharge + 1% storm surge, the increase in flood risk due to sea level rise from 0 to 0.43m is about 6.94%. For a smaller flood event caused by 2% upstream discharge + 2% storm surge, the flood risk increase is 7.03%. Similarly, the increases in flood risk are 8.82% and 12.63% for 5% upstream discharge + 5% storm surge and 10% upstream discharge + 10% storm surge. It suggests

that long-term sea level rise could make low-intensity coastal floods more dangerous by increasing flood risk. A similar pattern was also found in sea level rise from 0 to 0.55m and from 0 to 0.84m. However, this general pattern does not always work. Comparing 1% upstream discharge + 1% storm surge and 1% upstream discharge + 2% storm surge flood events, the flood risk increase due to sea level rise from 0 to 0.43m is larger in the former event, which is a larger flood event. The complexity in change pattern is mainly due to the complexity of coastal compound flooding. Additionally, an increase in upstream discharge and storm surge may not cause the flooding area to increase simultaneously.

Table 3.3. Flood Risk increase rate by different SLR scenarios.

Upstream Discharge	Storm Surge	Sea level Rise (0 m to 0.43m)	Sea level Rise (0 m to 0.55m)	Sea level Rise (0 m to 0.84m)
1%	1%	6.94%	11.85%	18.50%
1%	2%	6.82%	8.90%	18.10%
1%	5%	6.38%	7.90%	13.98%
1%	10%	6.19%	8.05%	13.00%
2%	1%	7.74%	11.31%	21.13%
2%	2%	7.03%	9.79%	18.96%
2%	5%	6.60%	8.81%	14.78%
2%	10%	7.07%	9.00%	14.79%
5%	1%	8.81%	11.85%	21.58%
5%	2%	8.49%	11.32%	20.44%
5%	5%	8.82%	10.78%	17.65%
5%	10%	12.07%	14.48%	20.69%
10%	1%	8.59%	11.66%	21.17%
10%	2%	8.57%	11.43%	20.00%
10%	5%	10.00%	12.33%	19.00%
10%	10%	12.63%	15.79%	22.11%

By comparing Sen_EXP001, Sen_EXP017, Sen_EXP033, and Sen_EXP049 in Table 3.2, we can identify the increased flood risk caused by changes in upstream discharge. For environmental settings with 0m sea level rise and a 1% annual chance storm surge, the

flood risk increased by 0.92%, 3.07%, and 6.13% when the upstream discharge magnitude changed from a 10% to a 5%, 2%, and 1% annual chance, respectively. The flood risk changed along with multiple upstream discharge scenarios for different sea level rise and storm surge settings, as shown in Table 3.4. The largest sea level setting is 1% storm surge + 0.84m sea level rise, while the smallest sea level setting is 10% storm surge + 0m sea level rise. The increase of flood risk due to upstream discharge is lower in the largest sea level setting and higher in the smallest sea level setting. This indicates that when the sea level remains relatively high, the importance of upstream discharge in contributing to coastal flood risk decreases.

Table 3.4. Flood Risk increase rate by upstream discharge with different annual chance.

Storm Surge	Sea level Rise	Upstream Discharge (10% to 5%)	Upstream Discharge (10% to 2%)	Upstream Discharge (10% to 1%)
1%	0m	0.92%	3.07%	6.13%
1%	0.43m	1.13%	2.26%	4.52%
1%	0.55m	1.10%	2.75%	6.32%
1%	0.84m	1.27%	3.04%	3.80%
2%	0m	0.95%	3.81%	6.98%
2%	0.43m	0.88%	2.34%	5.26%
2%	0.55m	0.85%	2.28%	4.56%
2%	0.84m	1.32%	2.91%	5.29%
5%	0m	2.00%	6.00%	9.67%
5%	0.43m	0.91%	2.73%	6.06%
5%	0.55m	0.59%	2.67%	5.34%
5%	0.84m	0.84%	2.24%	5.04%
10%	0m	1.75%	9.12%	13.33%
10%	0.43m	1.25%	3.74%	6.85%
10%	0.55m	0.61%	2.73%	5.76%
10%	0.84m	0.57%	2.59%	4.89%

Table 3.5. Flood Risk increase rate by storm surge with different annual chance.

Upstream Discharge	Sea level Rise	Storm Surge (10% to 5%)	Storm Surge (10% to 2%)	Storm Surge (10% to 1%)
1%	0m	1.86%	4.33%	7.12%
1%	0.43m	2.04%	4.96%	7.87%
1%	0.55m	1.72%	5.16%	10.89%
1%	0.84m	2.74%	9.04%	12.33%
2%	0m	2.25%	5.14%	8.04%
2%	0.43m	1.80%	5.11%	8.71%
2%	0.55m	2.06%	5.90%	10.32%
2%	0.84m	2.24%	8.96%	14.01%
5%	0m	5.52%	9.66%	13.45%
5%	0.43m	2.46%	6.15%	10.15%
5%	0.55m	2.11%	6.63%	10.84%
5%	0.84m	2.86%	9.43%	14.29%
10%	0m	5.26%	10.53%	14.39%
10%	0.43m	2.80%	6.54%	10.28%
10%	0.55m	2.12%	6.36%	10.30%
10%	0.84m	2.59%	8.62%	13.51%

By comparing Sen_EXP001, Sen_EXP005, Sen_EXP009, and Sen_EXP013 in Table 3.2, we can identify the increased flood risk caused by changes in storm surge magnitude. For environmental settings with 0m sea level rise and a 1% annual chance upstream discharge, the flood risk increased by 1.86%, 4.33%, and 7.12% with the storm surge magnitude changing from a 10% to a 5%, 2%, and 1% annual chance, respectively. The flood risk changed along with different storm surge scenarios for various sea level rise and upstream settings, as shown in Table 3.5. The general pattern of storm surge in changing flood risk is more complicated. On the one hand, as upstream discharge magnitude decreased, storm surge magnitude change enhanced the flood risk increase. On the other hand, as sea level rise increased, the increase of flood risk caused by storm surge magnitude change also increased. This illustrates that when the discharge decreases, the

importance of storm surge in contributing to flood risk increases. Meanwhile, sea level rise enhances the contribution of storm surge in flood risk calculation. This general pattern agrees with most of the data but not all.

In summary, the flood risk increase due to sea level rise is larger than due to the magnitude change of upstream discharge and storm surge. Basically, larger upstream discharge, storm surge, and sea level rise lead to more flood risk. There are some special patterns of changing flood risk due to different factors:

1) Long-term sea level rise makes low-intensity coastal floods more dangerous by increasing flood risk.
2) The higher the sea level setting, including both storm surge and long-term sea level rise, the lower the flood risk increase due to upstream discharge change.
3) As upstream discharge magnitude decreases, the influence of storm surge magnitude change on flood risk increases becomes stronger.
4) The increases in sea level rise enhance flood risk increases caused by storm surge magnitude change.

3.2.2 Human factors

In this section, we focus solely on human factors. The flood risk calculations based on a specific flood event with a 1% annual chance upstream discharge and a 1% annual chance storm surge are shown here. The entire calculation used the population grid and GDP per capita from 2000 to 2020. For a simplified comparison, we display results only for the years 2000, 2005, 2010, 2015, and 2020. Different sea level rise scenarios are shown separately in Tables 3.6, 3.7, 3.8 and 3.9.

Here is a simple instruction for understanding the information in the tables:

1) At the center of each table, the flood risk (in billion 2020 US$) was calculated based on different combinations of population grid and GDP per capita.
2) The last column shows the flood risk increase rate due to population growth annually (along columns).
3) The last row shows the flood risk increase rate resulting from GDP increase annually (along rows).
4) The last cell is the flood risk increase rate caused by both population growth and GDP increase (along diagonal).

Table 3.6. Flood Risk calculation by different population and GDP per capita settings, with 0 m sea level rise (Unit: billion 2020 US$). The last column shows the flood risk increase rate along population growth annually (along columns). The last row shows the flood risk increase rate along GDP increase annually (along rows). The last cell is the flood risk increase rate along both population growth and GDP increase (along diagonal).

GDP per capita / Population	2000	2005	2010	2015	2020	Population growth annually rate
2000	2.07	2.24	2.24	2.41	2.48	
2005	2.41	2.61	2.61	2.81	2.89	3.08%
2010	2.74	2.98	2.97	3.21	3.29	2.67%
2015	3.08	3.34	3.34	3.60	3.70	2.36%
2020	3.42	3.71	3.71	4.00	4.11	2.11%
GDP increase annually rate		1.63%	0.00%	1.51%	0.54%	3.49%

Table 3.7. Similar with Table 3.7 but with 0.43 m sea level rise.

GDP per capita / Population	2000	2005	2010	2015	2020	Population growth annually rate
2000	2.21	2.40	2.40	2.58	2.65	
2005	2.57	2.79	2.79	3.01	3.09	3.08%
2010	2.94	3.18	3.18	3.43	3.52	2.67%
2015	3.30	3.58	3.57	3.85	3.96	2.35%
2020	3.66	3.97	3.97	4.28	4.39	2.11%
GDP increase annually rate		1.63%	0.00%	1.51%	0.54%	3.49%

Table 3.8. Similar with Table 3.7 but with 0.55 m sea level rise.

GDP per capita / Population	2000	2005	2010	2015	2020	Population growth annually rate
2000	2.32	2.52	2.52	2.71	2.78	
2005	2.70	2.92	2.92	3.15	3.23	3.04%
2010	3.07	3.33	3.33	3.59	3.69	2.64%
2015	3.45	3.74	3.74	4.03	4.14	2.33%
2020	3.82	4.14	4.14	4.46	4.59	2.09%
GDP increase annually rate		1.63%	0.00%	1.51%	0.54%	3.46%

Table 3.9 Similar with Table 3.7 but with 0.84 m sea level rise.

GDP per capita / Population	2000	2005	2010	2015	2020	Population growth annually rate
2000	2.47	2.68	2.67	2.88	2.96	
2005	2.86	3.11	3.10	3.35	3.44	3.02%
2010	3.26	3.54	3.53	3.81	3.91	2.63%
2015	3.66	3.97	3.96	4.27	4.39	2.32%
2020	4.05	4.40	4.39	4.73	4.86	2.08%
GDP increase annually rate		1.63%	0.00%	1.51%	0.54%	3.45%

Under various sea level rise scenarios, the flood risk increases from 3.45% to 3.49% due

to human factors, including population growth and GDP increase. By comparison, the population growth had relatively large effects on the annual flood risk increase than GDP increase. The annual GDP increase rate from 2005 to 2010 is negative, which means that the estimated flood risk has slightly decrease if only considering GDP change from 2005 to 2010.

3.2.3 Comparison between natural and human factors

Table 3.10. Flood risk increase range related to specific factors.

Factor	Flood risk increase range	Detailed explanation
Upstream discharge	0.57% - 13.33%	Upstream discharge magnitude with certain annual chance
Storm surge	1.72% - 14.39%	Storm surge height with certain annual chance
Sea level rise	6.19% - 22.11%	Sea level rise prediction by the end of this century with different RCPs projection
Population growth	2.08% - 3.52%	Population growth rates every year
GDP increase	0.54% - 1.63%	GDP increase rates every year

Combining the data analyzed in the previous two sections, a comparison between natural and human factors can be established, highlighting the sensitivity of flood risk in response to the change of each factor separately (Table 3.10). In general, flood risk is more sensitive to changes in natural factors than changes in human factors, as indicated by the largest increase rate for each factor. Based on Table 3.10, the overall importance (sensitivity) order, from largest to smallest, is: sea level rise, storm surge, upstream discharge, population growth, and GDP increase. It should be noted that the increase range of natural factors is much larger than human factors due to the fact that the effect (compound effect) of one natural factor on flood risk estimation is not independent. Depending on how other natural factors are set, one natural factor could either increase

or decrease the flood risk.

Time scale is a significant issue when describing the importance of factors contributing to flood risk. The actual factors compared in this study are explained in detail in Table 3.11, and they have different time scales. Sea level rise is a long-term issue with a near 100-year time scale. Upstream discharge and storm surge occur every year but with different periods for different magnitudes. Population growth and GDP increase are annual changes.

Therefore, the modified explanation of the importance order shown in the above table (Table 3.11) should be as follows: Compared to extreme flood events with different magnitudes, annual population growth and GDP increase, long-term sea level rise created more potential flood risk. If we consider the population growth and GDP increase in two decades (2000 to 2020), the flood risk increase caused by population growth and GDP increase could be around 63.8% and 19.6%, respectively. Thus, human factors are much more important than natural factors. Comparing the rare extreme flood events with extreme weather conditions, such as storms, hurricanes, and long-term sea level rise, rapid population growth and GDP increase related to urbanization bring more flood risk in the future. This agrees with empirical evidence suggesting that both population growth and GDP increase are associated with increased vulnerability to coastal flooding (Hallegatte et al., 2013; Neumann et al., 2015).

3.3 Historical flood event study

Figure 3.13 to Figure 3.19 display the model input for each historical flood event under examination. In general, the upstream discharges for Hurricane Bertha 2020, Hurricane

Florence and Michael 2018, and Hurricane Matthew 2016 were significantly larger than that of other events, suggesting an increasing trend in the magnitude of coastal floods in this region.

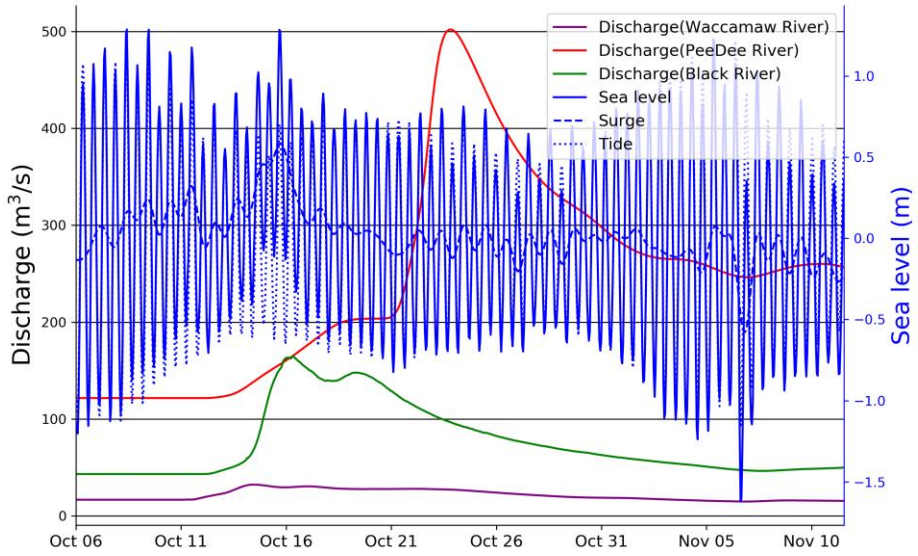

Figure 3.13. Model inputs for 2002 Hurricane Kyle event: River discharge from Waccamaw, PeeDee, and Black Rivers; sea level variation at seaside, tide and storm surge are plotted separately.

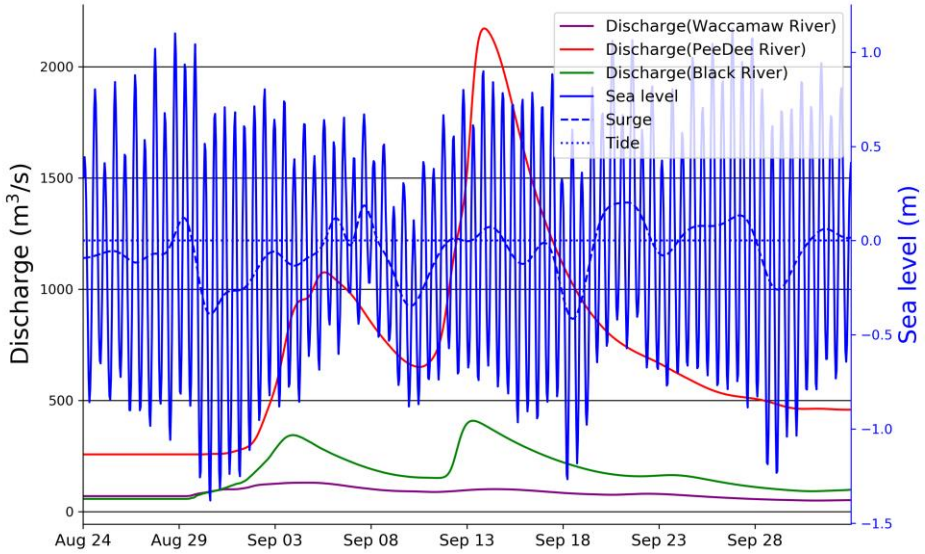

Figure 3.14. Model inputs for 2004 Hurricane Gaston and Ivan event: River discharge from Waccamaw, PeeDee, and Black Rivers; sea level variation at seaside, tide and storm surge are plotted separately.

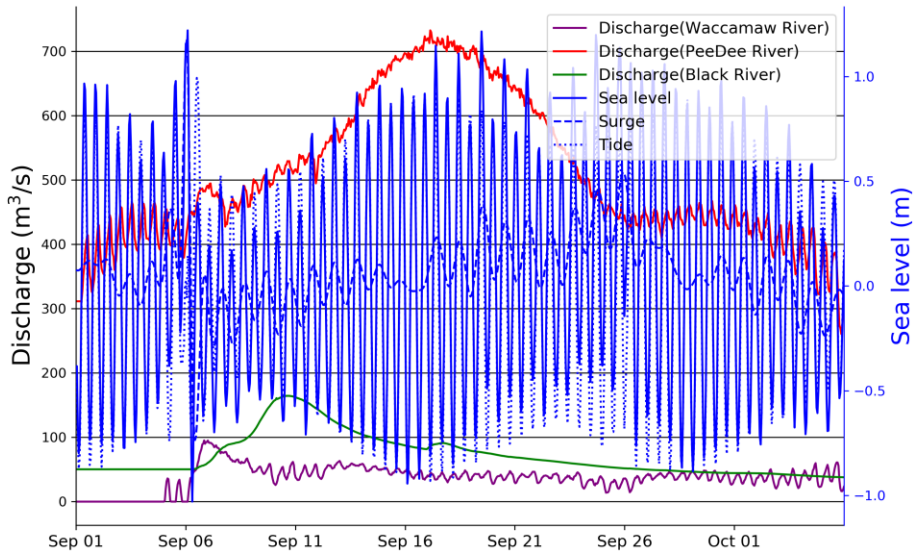

Figure 3.15. Model inputs for 2008 Hurricane Hanna event: River discharge from Waccamaw, PeeDee, and Black Rivers; sea level variation at seaside, tide and storm surge are plotted separately.

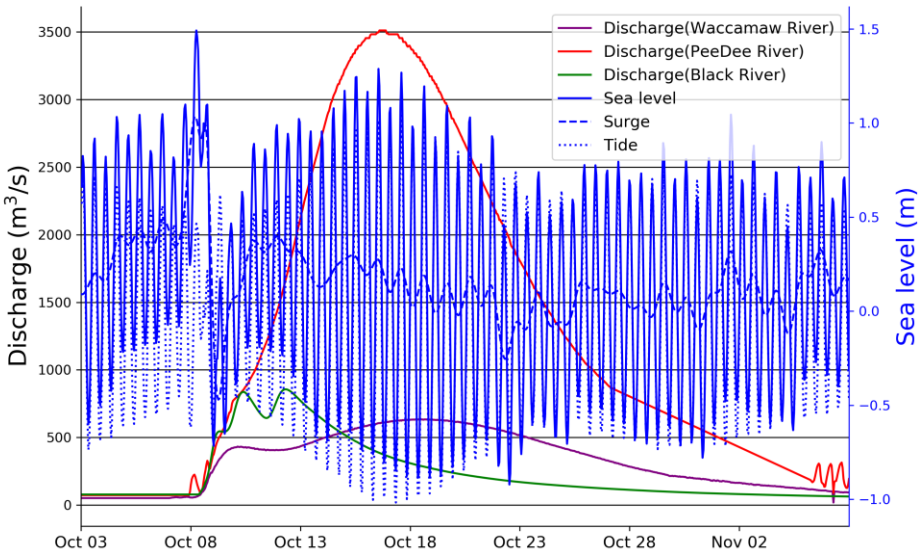

Figure 3.16. Model inputs for 2016 Hurricane Matthew event: River discharge from Waccamaw, PeeDee, and Black Rivers; sea level variation at seaside, tide and storm surge are plotted separately.

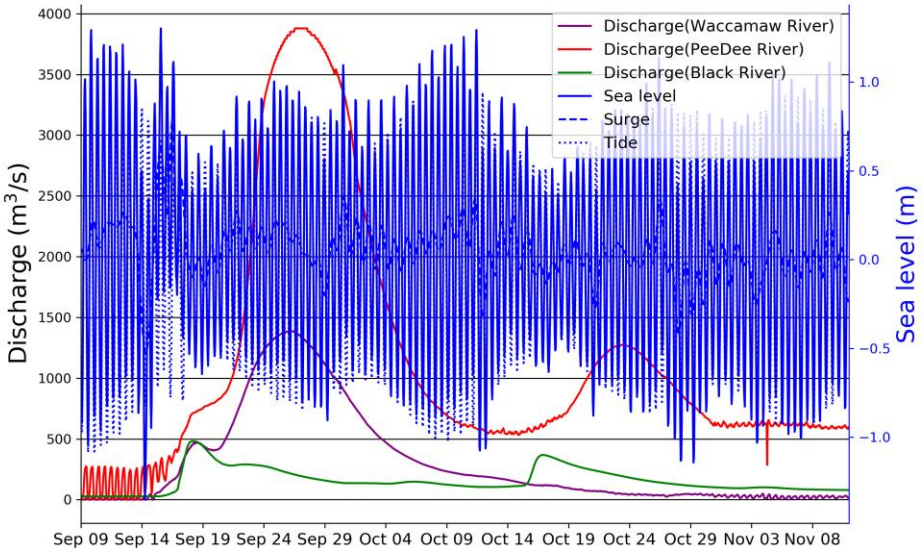

Figure 3.17. Model inputs for 2018 Hurricane Florence and Michael event: River discharge from Waccamaw, PeeDee, and Black Rivers; sea level variation at seaside, tide and storm surge are plotted separately.

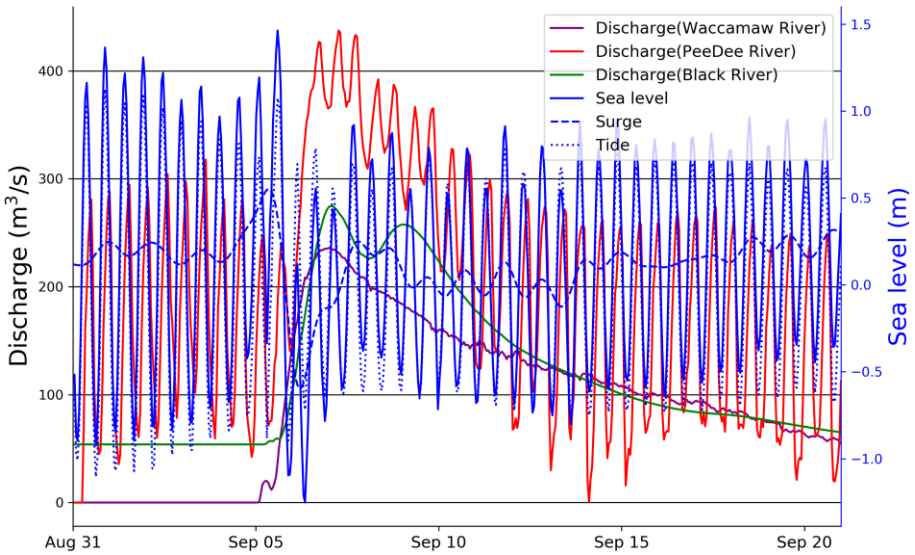

Figure 3.18. Model inputs for 2019 hurricane Dorian event: River discharge from Waccamaw, PeeDee, and Black Rivers; sea level variation at seaside, tide and storm surge are plotted separately.

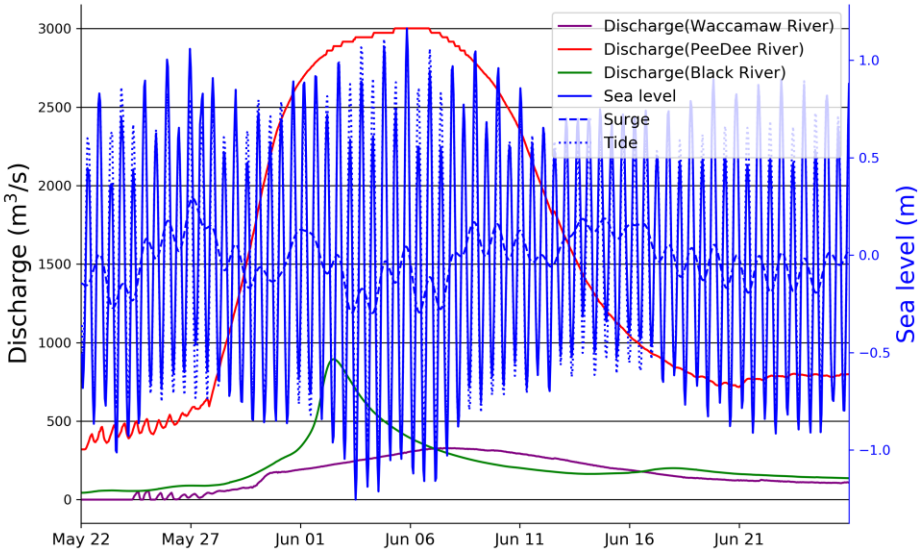

Figure 3.19. Model inputs for 2020 hurricane Bertha event: River discharge from Waccamaw, PeeDee, and Black Rivers; sea level variation at seaside, tide and storm surge are plotted separately.

Table 3.11 shows the maximum flooding area for historical coastal flood events with different upstream discharge, storm surge, and tide settings. Table 3.12 shows the flood risk calculated for historical coastal flood events with different upstream discharge, storm surge, and tide settings, based on the population grid and GDP per capita for each specific year. For example, the flood risk for Hurricane Kyle 2002 employed the population grid and GDP per capita in 2002.

Similar to the analysis based on upstream discharge from model input, the maximum flooding area shows an increasing trend from 2002 to 2020. Hurricane Bertha in 2020,

Hurricane Florence and Michael in 2018, and Hurricane Matthew in 2016 accounted for the three largest flooding area events. Notably, upstream discharge, storm surge, and tide contributed to different portions of the flooding area in various flood events (Table 3.12). For instance, in the Hurricane Matthew case, the storm surge had the greatest influence on the flooding area (762.64 km²), whereas in the Hurricane Florence and Michael cases, upstream discharge had the most significant impact on the flooding area (730.67 km²). The difference is due to the timing of how each natural factor interacts with one another, as discussed in the previous compound flooding section. Coastal flooding is a coincidental event that highly depends on timing.

Table 3.11. Wet area (include permanent water surface and flooding area) calculation for different upstream discharge, storm surge, and tide settings of historical flood events (unit: km2).

Event Name	Year	Upstream discharge only	Storm surge only	Tide only	Upstream discharge + Storm surge	Upstream discharge + Tide	Storm surge + Tide	Upstream discharge + Storm surge + Tide
KYLE	2002	617.76	675.1	697.85	684.75	729.77	741.54	751.73
GASTON & IVAN	2004	692.32	648.87	735.48	696.24	761.56	744.19	758.56
HANNA	2008	654.27	697.3	679.82	728.76	737.89	737.76	765.8
MATTHEW	2016	719.79	762.64	680.24	771.05	796.75	776.44	816.7
FLORENCE & MICHAEL	2018	730.67	649.75	629.33	758.81	797.3	681.43	812.94
DORIAN	2019	657.37	625.07	635.06	695.03	742.81	701.39	762.11
BERTHA	2020	710.3	617.16	697.56	721.68	798.66	696.51	798.11

The estimated flood risk for Hurricanes Florence and Michael in 2018 is higher than for Hurricane Matthew in 2016. The logical flow suggests that Hurricanes Florence and Michael in 2018 brought more upstream discharge to the study area. However, due to the interaction between the inland river system and the coastal ocean, the larger

discharge did not result in a larger flooding area. The stronger population growth and GDP increase in 2018 compared with 2016 (Table 3.13) lead to the higher estimated flood risk for Hurricanes Florence and Michael than for Hurricane Matthew. Even Hurricane Bertha in 2020, which has a lower upstream discharge and sea level change, has a larger estimated flood risk than Hurricane Matthew in 2016.

Table 3.12. Flood risk calculation for different upstream discharge, storm surge, and tide settings of historical flood events (unit: billion 2020 US $).

Event Name	Year	Upstream discharge only	Storm surge only	Tide only	Upstream discharge + Storm surge	Upstream discharge + Tide	Storm surge + Tide	Upstream discharge + Storm surge + Tide
KYLE	2002	1.09	1.25	1.32	1.27	1.4	1.36	1.42
GASTON & IVAN	2004	1.41	1.3	1.53	1.42	1.54	1.62	1.61
HANNA	2008	1.51	1.68	1.64	1.73	1.78	1.81	1.87
MATTHEW	2016	2.41	2.44	2.24	2.6	2.53	2.83	2.92
FLORENCE & MICHAEL	2018	2.78	2.27	2.26	2.94	2.39	3.15	3.19
DORIAN	2019	2.3	2.23	2.37	2.45	2.6	2.67	2.75
BERTHA	2020	2.58	2.05	2.43	2.65	2.43	3.08	3.07

4 Conclusion

This study seeks to investigate the proposition that human influences can significantly affect current and future coastal flooding risks for coastal communities, on par with natural factors. The research contributed to a deeper understanding of coastal compound flood hazards. To accomplish these objectives, we created a holistic approach for assessing coastal flood risk, incorporating both natural processes and human-related factors (e.g., GDP per capita and population density). This analysis shed light on the respective roles and consequences of these factors in shaping coastal flood risk.

Coastal compound flooding, as a natural process, encompasses several key characteristics:

1) The interplay among the natural factors (tide, storm surge, upstream discharge, and sea level rise) could alter the timing of inundated areas, river discharge, and overall water volume fluctuations in the basin.

2) The interactions between different natural factors lead to more severe flooding with long-lasting water and increased water retention in the basin.

3) The blocking effect between downstream water levels and upstream discharge is the main reason for the compound effect in coastal flooding.

4) Local rainfall plays a limited role in coastal flooding.

Coastal flood risk, as a human-related concern, is influenced by the severity of coastal

flood hazards which depend on the interplay of natural factors and their compounded effects, as well as the vulnerability stemming from population growth and economic development. The importance of each factor varies with timescale:

1) For a flooding event, the magnitude of natural factor (storm surge and discharge) holds greater significance compared with human factors.

2) On a daily timescale, tides affect both inland and coastal areas through their interaction with upstream discharge.

3) Over the course of decades, population and GDP remain the primary factors shaping flood risk assessments by increase the vulnerability of coastal communities to flooding.

4) In discussions of potential flood risk toward the end of the century, long-term sea level rise is an essential factor that must be considered.

For coastal flooding along the northeastern South Carolina coast, the interaction between sea level rise and upstream discharge considerably increases compound coastal flooding, which heightens the potential coastal flood hazards in the future. Over the past 20 years, the flood risk has continually increased due to the growing vulnerability of coastal communities to coastal floods.

The current study faces certain limitations regarding the modeling of rainfall process and the representation of economic factors, which warrant further exploration.

Firstly, the current modeling settings lack three essential hydrological processes: exfiltration, baseflow, and evapotranspiration. This limitation negatively affects the rainfall representation in the study. To overcome this issue, it is necessary to address the conflicts between the hydrological model and the inundation model. Additionally, further

research should focus on developing improved model coupling strategies.

Secondly, the representation of economic factors in coastal flood risk assessments could be refined. Presently, the study mainly focuses on population growth and GDP as indicators of vulnerability. While these factors are indeed important, a more comprehensive economic representation should also consider other dimensions, such as infrastructure investments, land use policies, and adaptive capacity of coastal communities. Incorporating these additional factors would provide a more nuanced understanding of how economic aspects influence coastal flood risk and vulnerability. This, in turn, could inform more targeted and effective strategies for managing and reducing flood risk in coastal areas.

By addressing these limitations and expanding the scope of the study, future research can contribute to a more robust and comprehensive understanding of coastal flood risk, which is essential for developing effective mitigation and adaptation measures to protect vulnerable coastal communities.

Overall, coastal flooding is a common phenomenon in coastal regions. However, due to the combined effects of climate change and coastal urbanization, the likelihood of daily coastal floods escalating into extreme coastal flood hazards has increased. Compared to the increased flood risk resulting from the compound effect of various natural factors, the heightened vulnerability caused by population growth and economic development also contributes significantly to the overall flood risk.

List of References

Anthes, R. A., Corell, R. W., Holland, G., Hurrell, J. W., MacCracken, M. C., & Trenberth, K. E. (2006). Hurricanes and global warming—Potential linkages and consequences. *Bulletin of the American Meteorological Society*, *87*(5), 623–628.

Bakhtyar, R., Maitaria, K., Velissariou, P., Trimble, B., Mashriqui, H., Moghimi, S., Abdolali, A., Van der Westhuysen, A. J., Ma, Z., Clark, E. P., & Flowers, T. (2020). A New 1D/2D Coupled Modeling Approach for a Riverine-Estuarine System Under Storm Events: Application to Delaware River Basin. *Journal of Geophysical Research: Oceans*, *125*(9), e2019JC015822. https://doi.org/10.1029/2019JC015822

Baky, M. A. A., Islam, M., & Paul, S. (2020). Flood hazard, vulnerability and risk assessment for different land use classes using a flow model. *Earth Systems and Environment*, *4*(1), 225–244. https://doi.org/10.1007/s41748-019-00141-w

Baldwin, W. E., Morton, R. A., Putney, T. R., Katuna, M. P., Harris, M. S., Gayes, P. T., Driscoll, N. W., Denny, J. F., & Schwab, W. C. (2006). Migration of the Pee Dee River system inferred from ancestral paleochannels underlying the South Carolina Grand Strand and Long Bay inner shelf. *Geological Society of America Bulletin*, *118*(5–6), 533–549. https://doi.org/10.1130/B25856.1

Barnes, S. L., & Newton, C. W. (1986). Thunderstorms in the synoptic setting. *Thunderstorm Morphology and Dynamics*, *1*, 2.

Barnhardt, W. A., Schwab, W. C., Gayes, P. T., Morton, R. A., Driscoll, N. W., Baldwin, W. E., & Wright, E. E. (2008). *Coastal change along the shore of Northeastern South Carolina: The South Carolina coastal erosion study* (No. 1206; US Geological Survey

Open File Report).

Bevacqua, E., Vousdoukas, M. I., Shepherd, T. G., & Vrac, M. (2020). Brief communication: The role of using precipitation or river discharge data when assessing global coastal compound flooding. *Natural Hazards and Earth System Sciences*, *20*(6), 1765–1782. https://doi.org/10.5194/nhess-20-1765-2020

Brakenridge, G. R. (2010). *Global active archive of large flood events*. Dartmouth Flood Observatory; University of Colorado. https://floodobservatory.colorado.edu/Archives/index.html

Brunner, G. (2022). *HEC-RAS 2D User's Manual*.

Cao, Q., Gershunov, A., Shulgina, T., Ralph, F. M., Sun, N., & Lettenmaier, D. P. (2020). Floods due to Atmospheric Rivers along the U.S. West Coast: The Role of Antecedent Soil Moisture in a Warming Climate. *Journal of Hydrometeorology*, *21*(8), 1827–1845. https://doi.org/10.1175/JHM-D-19-0242.1

Center For International Earth Science Information Network-CIESIN-Columbia University. (2018). *Documentation for the gridded population of the world, Version 4 (GPWv4), Revision 11 Data Sets*. https://doi.org/10.7927/H45Q4T5F

Chan, J. C. L., & Shi, J. (1996). Long-term trends and interannual variability in tropical cyclone activity over the western North Pacific. *Geophysical Research Letters*, *23*(20), 2765–2767. https://doi.org/10.1029/96GL02637

Changnon, D. (1994). Regional and temporal variations in heavy precipitation in south carolina. *International Journal of Climatology*, *14*(2), 165–177. https://doi.org/10.1002/joc.3370140204

Chow, V. T., Maidment, D. R., & Mays, L. W. (1988). *Applied hydrology*. McGraw-Hill.

Colgan, C. S. (2003). *Measurement of the ocean and coastal economy: Theory and method*.

Crossett, K., Ache, B., Pacheco, P., & Haber, K. (2013). *National coastal population report, population trends from 1970 to 2020* (NOAA State of the Coast Report Series,). US Department of Commerce.

Cry, G. W. (1967). *Effects of tropical cyclone rainfall on the distribution of precipitation over the eastern and southern United States* (Vol. 1). US Department of Commerce, Environmental Science Services Administration.

Delgado, J. M., Apel, H., & Merz, B. (2010). Flood trends and variability in the Mekong river. *Hydrology and Earth System Sciences*, 12.

Dresback, K. M., Fleming, J. G., Blanton, B. O., Kaiser, C., Gourley, J. J., Tromble, E. M., Luettich, R. A., Kolar, R. L., Hong, Y., Van Cooten, S., Vergara, H. J., Flamig, Z. L., Lander, H. M., Kelleher, K. E., & Nemunaitis-Monroe, K. L. (2013). Skill assessment of a real-time forecast system utilizing a coupled hydrologic and coastal hydrodynamic model during Hurricane Irene (2011). *Continental Shelf Research*, *71*, 78–94. https://doi.org/10.1016/j.csr.2013.10.007

Emanuel, K. (2005). Increasing destructiveness of tropical cyclones over the past 30 years. *Nature*, *436*(7051), 686–688. https://doi.org/10.1038/nature03906

Emanuel, K. A. (1987). *The dependence of hurricane intensity on climate*. 3.

Ezer, T., & Atkinson, L. P. (2014). Accelerated flooding along the U.S. east coast: On the impact of sea-level rise, tides, storms, the Gulf Stream, and the North Atlantic Oscillations. *Earth's Future*, *2*(8), 362–382.

https://doi.org/10.1002/2014EF000252

Field, C. B., Barros, V., Stocker, T. F., & Dahe, Q. (Eds.). (2012). *Managing the risks of extreme events and disasters to advance climate change adaptation: Special report of the Intergovernmental Panel on Climate Change*. Cambridge University Press. https://doi.org/10.1017/CBO9781139177245

Gochis, D. J., Yu, W., & Yates, D. N. (2015). *The WRF-Hydro model technical description and user's guide, version 3.0, NCAR Technical Document*.

Gori, A., Lin, N., & Smith, J. (2020). Assessing compound flooding from landfalling tropical cyclones on the North Carolina Coast. *Water Resources Research*, e2019WR026788.

Guha-Sapir, D. (2017). EM-DAT: The emergency events database. *Universite Catholique de Louvain (UCL)—CRED. Belgium: July*.

Hallegatte, S., Green, C., Nicholls, R. J., & Corfee-Morlot, J. (2013). Future flood losses in major coastal cities. *Nature Climate Change*, *3*(9), 802–806. https://doi.org/10.1038/nclimate1979

Henderson-Sellers, A., Zhang, H., Berz, G., Emanuel, K., Gray, W., Landsea, C., Holland, G., Lighthill, J., Shieh, S.-L., & Webster, P. (1998). Tropical cyclones and global climate change: A post-IPCC assessment. *Bulletin of the American Meteorological Society*, *79*(1), 19–38.

Hirabayashi, Y., Kanae, S., Emori, S., Oki, T., & Kimoto, M. (2008). Global projections of changing risks of floods and droughts in a changing climate. *Hydrological Sciences Journal*, *53*(4), 754–772. https://doi.org/10.1623/hysj.53.4.754

Hirabayashi, Y., Mahendran, R., Koirala, S., Konoshima, L., Yamazaki, D., Watanabe, S., Kim, H., & Kanae, S. (2013). Global flood risk under climate change. *Nature Climate Change*, *3*(9), 816–821. https://doi.org/10.1038/nclimate1911

HL-RDHM User Manual v. 3.0.0. (2009). https://www.cbrfc.noaa.gov/present/rdhm/RDHM_3_0_0_User_Manual.pdf

Homer, C., Dewitz, J., Jin, S., Xian, G., Costello, C., Danielson, P., Gass, L., Funk, M., Wickham, J., & Stehman, S. (2020). Conterminous United States land cover change patterns 2001–2016 from the 2016 National Land Cover Database. *ISPRS Journal of Photogrammetry and Remote Sensing*, *162*, 184–199.

Hong, Y., & Adler, R. F. (2008). Estimation of global SCS curve numbers using satellite remote sensing and geospatial data. *International Journal of Remote Sensing*, *29*(2), 471–477. https://doi.org/10.1080/01431160701264292

Horton, R., Herweijer, C., Rosenzweig, C., Liu, J., Gornitz, V., & Ruane, A. C. (2008). Sea level rise projections for current generation CGCMs based on the semi-empirical method. *Geophysical Research Letters*, *35*(2). https://doi.org/10.1029/2007GL032486

Ibrahim, N. F., Zardari, N. H., Shirazi, S. M., Mohd Haniffah, M. R., Mat Talib, S., Yusop, Z., & Mohd Yusoff, S. M. A. (2017). Identification of vulnerable areas to floods in Kelantan River sub-basins by using flood vulnerability index. *International Journal of GEOMATE*, *12*(29), 107–114.

IPCC. (2001). *Climate change 2001: Synthesis report* . Cambridge University Press.

IPCC. (2008). *Climate change 2007: Synthesis report*. Intergovernmental Panel on Climate

Change.

IPCC. (2015). *Climate change 2014: Synthesis report*. Intergovernmental Panel on Climate Change. Geneva, Szwitzerland.

IPCC. (2019). *Special report on the ocean and cryosphere in a changing climate*. Intergovernmental Panel on Climate Change.

Jevrejeva, S., Jackson, L. P., Grinsted, A., Lincke, D., & Marzeion, B. (2018). Flood damage costs under the sea level rise with warming of 1.5 °C and 2 °C. *Environmental Research Letters*, *13*(7), 074014. https://doi.org/10.1088/1748-9326/aacc76

Jevrejeva, S., Jackson, L., Riva, R., Grinsted, A., & Moore, J. (2017). *Coastal sea level rise with warming above 2 degree*. *EGU General Assembly Conference Abstracts*, 3514.

Jongman, B., Ward, P. J., & Aerts, J. C. J. H. (2012). Global exposure to river and coastal flooding: Long term trends and changes. *Global Environmental Change*, *22*(4), 823–835. https://doi.org/10.1016/j.gloenvcha.2012.07.004

Knutson, T. R., McBride, J. L., Chan, J., Emanuel, K., Holland, G., Landsea, C., Held, I., Kossin, J. P., Srivastava, A. K., & Sugi, M. (2010). Tropical cyclones and climate change. *Nature Geoscience*, *3*(3), 157–163. https://doi.org/10.1038/ngeo779

Knutson, T. R., & Tuleya, R. E. (2004). Impact of CO2-induced warming on simulated hurricane intensity and precipitation: Sensitivity to the choice of climate model and convective parameterization. *Journal of Climate*, *17*, 19.

Lambeck, K., & Chappell, J. (2001). Sea level change through the last glacial cycle. *Science*, *292*(5517), 679–686. https://doi.org/10.1126/science.1059549

Landsea, C. W., & Franklin, J. L. (2013). Atlantic hurricane database uncertainty and

presentation of a new database format. *Monthly Weather Review*, *141*(10), 3576–3592. https://doi.org/10.1175/MWR-D-12-00254.1

Landsea, C. W., Nicholls, N., Gray, W. M., & Avila, L. A. (1996). Downward trends in the frequency of intense at Atlantic Hurricanes during the past five decades. *Geophysical Research Letters*, *23*(13), 1697–1700. https://doi.org/10.1029/96GL01029

Lawrence, M. B. (1996). *Hurricane Bertha* (Tropical Cyclone Report). National Hurricane Center. https://www.nhc.noaa.gov/data/tcr/AL021996_Bertha.pdf

Lin, N., & Emanuel, K. (2016). Grey swan tropical cyclones. *Nature Climate Change*, *6*(1), 106–111. https://doi.org/10.1038/nclimate2777

Lin, Y. (2011). *GCIP/EOP Surface: Precipitation NCEP/EMC 4KM Gridded Data (GRIB) Stage IV Data. Version 1.0. UCAR/NCAR-Earth Observing Laboratory*. Boulder, Colo.

Maddox, R. A., Chappell, C. F., & Hoxit, L. R. (1979). Synoptic and meso-α scale aspects of flash flood events. *Bulletin of the American Meteorological Society*, *60*(2), 115–123.

Marshall, S. J., & Clarke, G. K. C. (1999). Modeling North American freshwater runoff through the last glacial cycle. *Quaternary Research*, *52*(3), 300–315. https://doi.org/10.1006/qres.1999.2079

Mayfield, M. (1996a). *Hurricane Fran* (Tropical Cyclone Report). National Hurricane Center.

Mayfield, M. (1996b). *Tropical Storm Arthur* (Tropical Cyclone Report). National Hurricane Center. https://www.nhc.noaa.gov/data/tcr/AL011996_Arthur.pdf

McGranahan, G., Balk, D., & Anderson, B. (2007). The rising tide: Assessing the risks of climate change and human settlements in low elevation coastal zones. *Environment and Urbanization*, *19*(1), 17–37. https://doi.org/10.1177/0956247807076960

Milly, P. C. D., Wetherald, R. T., Dunne, K. A., & Delworth, T. L. (2002). Increasing risk of great floods in a changing climate. *Nature*, *415*(6871), 514–517.

Moftakhari, H. R., Salvadori, G., AghaKouchak, A., Sanders, B. F., & Matthew, R. A. (2017). Compounding effects of sea level rise and fluvial flooding. *Proceedings of the National Academy of Sciences*, *114*(37), 9785–9790. https://doi.org/10.1073/pnas.1620325114

Moran, J. M. (1989). *Meteorology; the Atmosphere and the Science of Weather*.

Mousavi, M. E., Irish, J. L., Frey, A. E., Olivera, F., & Edge, B. L. (2011). Global warming and hurricanes: The potential impact of hurricane intensification and sea level rise on coastal flooding. *Climatic Change*, *104*(3–4), 575–597. https://doi.org/10.1007/s10584-009-9790-0

Muñoz, D. F., Yin, D., Bakhtyar, R., Moftakhari, H., Xue, Z., Mandli, K., & Ferreira, C. (2022). Inter-Model Comparison of Delft3D-FM and 2D HEC-RAS for Total Water Level Prediction in Coastal to Inland Transition Zones. *JAWRA Journal of the American Water Resources Association*, *58*(1), 34–49. https://doi.org/10.1111/1752-1688.12952

Neumann, B., Vafeidis, A. T., Zimmermann, J., & Nicholls, R. J. (2015). Future coastal population growth and exposure to sea-level rise and coastal flooding—A global

assessment. *PLOS ONE*, *10*(3), e0118571. https://doi.org/10.1371/journal.pone.0118571

Nicholls, R. J., & Cazenave, A. (2010). Sea-level rise and its impact on coastal zones. *Science*, *328*(5985), 1517–1520. https://doi.org/10.1126/science.1185782

Niu, G.-Y., Yang, Z.-L., Mitchell, K. E., Chen, F., Ek, M. B., Barlage, M., Kumar, A., Manning, K., Niyogi, D., Rosero, E., Tewari, M., & Xia, Y. (2011). The community Noah land surface model with multiparameterization options (Noah-MP): 1. Model description and evaluation with local-scale measurements. *Journal of Geophysical Research*, *116*(D12), D12109. https://doi.org/10.1029/2010JD015139

NOAA. (2017). *Socioeconomic Data Summary*. NOAA Office for Coastal Management. https://coast.noaa.gov/data/digitalcoast/pdf/socioecon-pocket-guide.pdf

Oppenheimer, M., Little, C. M., & Cooke, R. M. (2016). Expert judgement and uncertainty quantification for climate change. *Nature Climate Change*, *6*(5), 445–451. https://doi.org/10.1038/nclimate2959

Pielke Jr, R. A., Landsea, C., Mayfield, M., Layer, J., & Pasch, R. (2005). Hurricanes and global warming. *Bulletin of the American Meteorological Society*, *86*(11), 1571–1576.

Pietrafesa, L. J., Zhang, H., Bao, S., Gayes, P. T., & Hallstrom, J. O. (2019). Coastal flooding and inundation and inland flooding due to downstream blocking. *Journal of Marine Science and Engineering*, *7*(10), 336.

Reidmiller, D. R., Avery, C. W., Easterling, D. R., Kunkel, K. E., Lewis, K. L. M., Maycock, T. K., & Stewart, B. C. (2018). *Impacts, risks, and adaptation in the United States: The*

fourth national climate assessment, Volume II. U.S. Global Change Research Program. https://doi.org/10.7930/NCA4.2018

Santamaría-Gómez, A., Gravelle, M., Dangendorf, S., Marcos, M., Spada, G., & Wöppelmann, G. (2017). Uncertainty of the 20th century sea-level rise due to vertical land motion errors. *Earth and Planetary Science Letters*, *473*, 24–32. https://doi.org/10.1016/j.epsl.2017.05.038

Schmocker-Fackel, P., & Naef, F. (2010). More frequent flooding? Changes in flood frequency in Switzerland since 1850. *Journal of Hydrology*, *381*(1–2), 1–8. https://doi.org/10.1016/j.jhydrol.2009.09.022

Severinghaus, J. P., & Brook, E. J. (1999). Abrupt climate change at the end of the last glacial period inferred from trapped air in polar ice. *Science*, *286*(5441), 930–934. https://doi.org/10.1126/science.286.5441.930

Small, C., & Nicholls, R. J. (2003). A global analysis of human settlement in coastal zones. *Journal of Coastal Research*, 584–599.

Sweet, W. V., & Park, J. (2014). From the extreme to the mean: Acceleration and tipping points of coastal inundation from sea level rise: SWEET AND PARK. *Earth's Future*, *2*(12), 579–600. https://doi.org/10.1002/2014EF000272

UNISDR, U. N. I. S. for D. (2009). *UNISDR terminology on disaster risk reduction*. UNISDR Geneva.

U.S. Global Change Research Program (Ed.). (2009). *Global climate change impacts in the United States: A state of knowledge report*. Cambridge University Press.

van den Hurk, B., van Meijgaard, E., de Valk, P., van Heeringen, K.-J., & Gooijer, J. (2015).

Analysis of a compounding surge and precipitation event in the Netherlands. *Environmental Research Letters*, *10*(3), 035001. https://doi.org/10.1088/1748-9326/10/3/035001

van Vuuren, D. P., Edmonds, J., Kainuma, M., Riahi, K., Thomson, A., Hibbard, K., Hurtt, G. C., Kram, T., Krey, V., Lamarque, J.-F., Masui, T., Meinshausen, M., Nakicenovic, N., Smith, S. J., & Rose, S. K. (2011). The representative concentration pathways: An overview. *Climatic Change*, *109*(1–2), 5–31. https://doi.org/10.1007/s10584-011-0148-z

Vitousek, S., Barnard, P. L., Fletcher, C. H., Frazer, N., Erikson, L., & Storlazzi, C. D. (2017). Doubling of coastal flooding frequency within decades due to sea-level rise. *Scientific Reports*, *7*(1), 1399. https://doi.org/10.1038/s41598-017-01362-7

Wahl, T., Jain, S., Bender, J., Meyers, S. D., & Luther, M. E. (2015). Increasing risk of compound flooding from storm surge and rainfall for major US cities. *Nature Climate Change*, *5*(12), 1093–1097. https://doi.org/10.1038/nclimate2736

Walsh, K. (2004). Tropical cyclones and climate change: Unresolved issues. *Climate Research*, *27*(1), 77–83.

Walsh, K. J. E., McBride, J. L., Klotzbach, P. J., Balachandran, S., Camargo, S. J., Holland, G., Knutson, T. R., Kossin, J. P., Lee, T., Sobel, A., & Sugi, M. (2016). Tropical cyclones and climate change. *WIREs Climate Change*, *7*(1), 65–89. https://doi.org/10.1002/wcc.371

Ward, R. C. (1978). Floods- a geographical perspective. *Macmillan*.

Wdowinski, S., Bray, R., Kirtman, B. P., & Wu, Z. (2016). Increasing flooding hazard in

coastal communities due to rising sea level: Case study of Miami Beach, Florida. *Ocean & Coastal Management*, *126*, 1–8. https://doi.org/10.1016/j.ocecoaman.2016.03.002

Webster, P. J., Holland, G. J., Curry, J. A., & Chang, H.-R. (2005). Changes in tropical cyclone number, duration, and intensity in a warming environment. *Science*, *309*(5742), 1844–1846. https://doi.org/10.1126/science.1116448

Woodruff, J. D., Irish, J. L., & Camargo, S. J. (2013). Coastal flooding by tropical cyclones and sea-level rise. *Nature*, *504*(7478), 44–52. https://doi.org/10.1038/nature12855

Xu, H., Xu, K., Lian, J., & Ma, C. (2019). Compound effects of rainfall and storm tides on coastal flooding risk. *Stochastic Environmental Research and Risk Assessment*, *33*(7), 1249–1261. https://doi.org/10.1007/s00477-019-01695-x

Ye, F., Zhang, Y. J., Yu, H., Sun, W., Moghimi, S., Myers, E., Nunez, K., Zhang, R., Wang, H. V., Roland, A., Martins, K., Bertin, X., Du, J., & Liu, Z. (2020). Simulating storm surge and compound flooding events with a creek-to-ocean model: Importance of baroclinic effects. *Ocean Modelling*, *145*, 101526. https://doi.org/10.1016/j.ocemod.2019.101526

Zscheischler, J., Westra, S., van den Hurk, B. J. J. M., Seneviratne, S. I., Ward, P. J., Pitman, A., AghaKouchak, A., Bresch, D. N., Leonard, M., Wahl, T., & Zhang, X. (2018). Future climate risk from compound events. *Nature Climate Change*, *8*(6), 469–477. https://doi.org/10.1038/s41558-018-0156-3